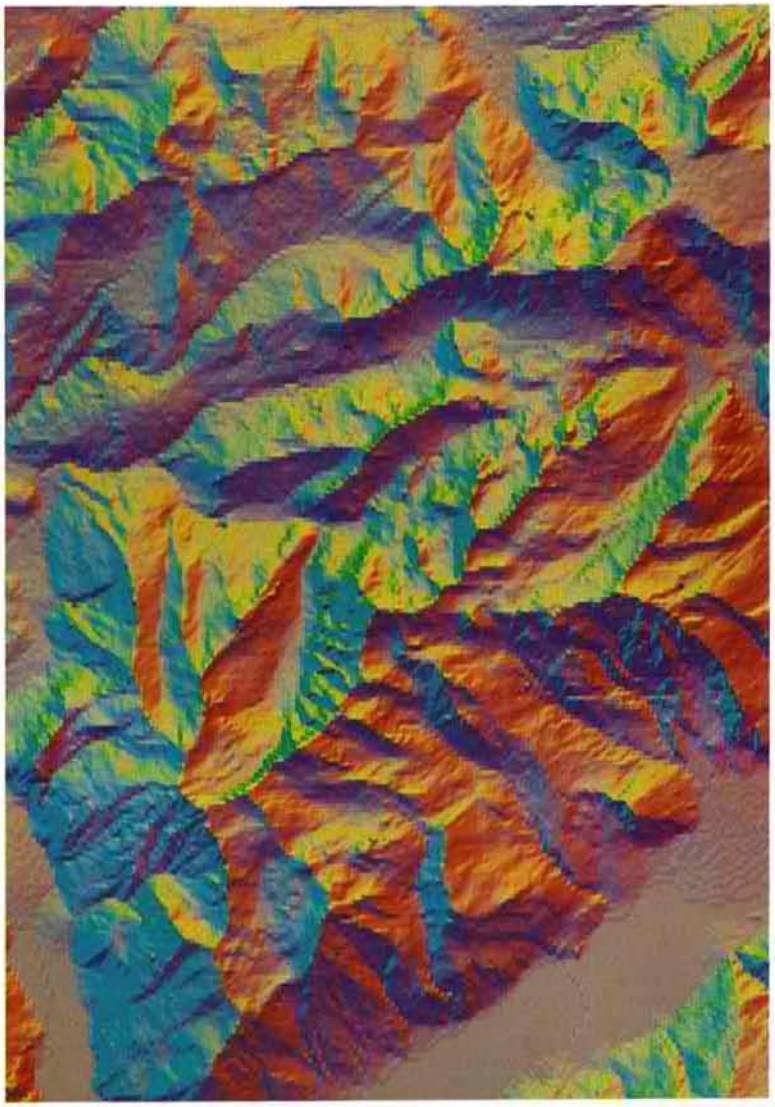

Colored hill-shading view of terrain illuminated by colored lights, located in three different directions.

Geo-Processing, 2(1982)65—146
Elsevier Scientific Publishing Company, Amsterdam — Printed in The Netherlands

HILL SHADING AND THE REFLECTANCE MAP

BERTHOLD K.P. HORN

Artificial Intelligence Laboratory, Massachusetts Institute of Technology, Cambridge, Massachusetts 02139 (U.S.A.)

ABSTRACT

Horn, B.K.P., 1982. Hill shading and the reflectance map. Geo-Processing, 2: 65—146.

Shaded overlays for maps give the user an immediate appreciation for the surface topography since they appeal to an important visual depth cue. A brief review of the history of manual methods is followed by a discussion of a number of methods that have been proposed for the automatic generation of shaded overlays. These techniques are compared using the reflectance map as a common representation for the dependence of tone or gray level on the orientation of surface elements.

INTRODUCTION

Of the several ways of depicting surface form on maps, hill-shading has the most immediate appeal and provides for quick comprehension of the topography. In this sense, hill-shading is complementary to the use of contours, which provide accurate terrain elevations but require careful scrutiny if one is to ascertain the surface form. Shaded maps are most important when the interpreter's time is limited, as in aviation, for users that are not trained cartographers, and for small scale maps, where contours degenerate into messy tangles of lines.

Why then do we not see more shaded maps? One reason is the expense of present manual methods of production, which require skilled artists with good insight into cartography. Working from existing contour maps, ridge and stream lines extracted from such maps, and at times aided also by aerial photography, they wield airbrushes, in what is a slow, tedious, and imprecise operation. Different individuals called upon to create such images by manual methods will inevitably produce different results because of the inherent subjective judgement. The resulting differences in expression of the terrain characteristics of the same surface at the same scale provide a particular problem for a map series, where adjoining sheets should match in terms of hill-shading symbology. This justifies investigation of an objective system which makes the treatment of all terrain forms comparable and repeatable.

Attempts at automation began with the notion that the gray levels used in the shading should derive from a model of how light might be reflected from a surface. Ignoring shadowing and mutual illumination effects, it seems clear that the reflected intensity will be a function of the local surface inclination. The choice of a method for calculating the gray tone based on the orientation

0165-2273/82/0000—0000/$02.75

of each surface element has however been the subject of occasionally bitter controversy for almost two centuries. Much of the difficulty stems from a lack of a common representation that would allow comparison of methods which appear at first glance to be incomparable.

The recently developed reflectance map constitutes such a common denominator. It is a simple device developed originally for work in machine vision where one is interested in calculating surface shape from the gray levels in an image. This is clearly just the inverse of the problem of producing shaded pictures from a surface model. The reflectance map is a plot of apparent brightness versus two variables, namely the slope of the surface element in the west-to-east direction and the slope in the south-to-north direction. Producing a shaded overlay for a map then is simply a matter of calculating these two slopes for each surface element and looking up the appropriate gray level in the reflectance map (see Fig. 1). This is a very simple, local computation that can be carried out efficiently even on enormous databases. The resulting gray levels can then be fed to a graphic output device that will produce a continuous tone or halftone photographic transparency from the given stream of numbers.

What reflectance map is to be used? Careful comparison of more than a dozen proposed shading methods shows that some of the simplest provide a good impression of the shape of the surface. These experiments also show that the most commonly used assumptions about surface reflectance do not lead to the best results, while simple monotonic functions of the surface slope in the direction away from the assumed light source work admirably. What matters is the visual impression, not theoretical rules [1]. One goal of this paper is a review of various hillshading methods that have been proposed in the past. Much can be learned from these efforts when they are evaluated in terms of the corresponding reflectance maps.

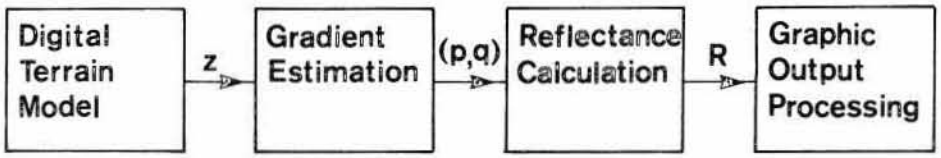

Figure 1: Block diagram of a system for the generation of relief shading. The gray-value is calculated by applying the reflectance map to the gradient estimate obtained by sampling neighboring points in the digital terrain model.

EARLY HISTORY OF HILL-SHADING

Chiaroscuro, the technique of using light and shade in pictorial representation of three dimensional shapes, has been used by artists for many centuries. Leonardo da Vinci put it to good effect in his maps of Toscana, drawn in 1502 and 1503, that contained oblique shaded views of relief forms illuminated from the left [1]. Woodcuts of the area around Zürich in Switzerland drawn half a century later by Murer use shaded sideviews as well. Overhead views using relief shading appear for the first time in maps of the same area drawn a century after that by Gygers, but these then gave way to less desirable forms [1].

The choice of the representation for relief forms depend to a great extent on the available reproduction technology. Woodcuts and engraving methods lend themselves to linear forms, where brightness of an area in the reproduction is controlled by the spacing and width of darkened lines. Useful directional, textural effects can be generated by orienting these line fragments, or hachures (Schraffuren), along lines of steepest descent. Crowding of such lines in steep areas may have given rise to notions of "steeper implies darker".

Lehmann proposed the first rigorous relationships [2],[3] between surface slopes and quantities measurable on the printed map. In 1799, when his method (Böschungsschraffen) was published anonymously, the techniques for measuring the surface accurately at a large enough number of points did not exist. Results of this first method of illustrating shape are in some ways analogous to those one might obtain by illuminating a model of the surface from above, an arrangement that gives rise to images that are difficult to interpret.

Partly as a result of this, an alternate form (Schattenschraffen) evolved [4]–[6], in which the line thickness is varied according to the orientation of the local surface patch with respect to a light source, usually assumed to be near the top left of the map when it is oriented properly for viewing. For maps with north at the top this corresponds to north-west. Surface patches sloping downward in that direction are portrayed with a light tone, while those sloping upward in that direction get a dark tone. Since flat areas have no lines of descent, they remain white. Aside from this defect, this method produces an image similar to one obtained by obliquely illuminating a diffusely reflecting model of the surface. Having flat areas appear white makes maps produced by this method a little difficult to interpret. They are nevertheless superior to those made by the earlier method, as evidenced for example by the "Dufourkarte" of Switzerland made between 1842 and 1864 using this approach [1]. These methods for portraying surface shape preceded the widespread use of contours [7], in part because the latter require detailed surface measurements that were not available before the advent of photogrammetry.

While lithography was invented by Alois Senefelder in 1796, it found little application in cartography until around 1850. It permitted the production of multicolored maps, but more importantly, led to the use of halftones, destined to ultimately replace lines as a means of modulating the average reflectance in the printed map. W. H. Fox Talbot invented a photomechanical halftone process in 1852, but commerical success came only years after the patenting of the halftone screen by Frederick von Egloffstein in 1865, and the crossline screen of William A. Leggo in 1869.

Having access to these new reproduction schemes, Wiechel [8] developed shading methods (Schräglichtschummerung) to replace the use of hachures as described above. His fundamental paper, based in part on work by Burmester [9] on shaded pictures of *regular* surfaces, placed the field of hill-shading on a sound foundation. Wiechel discovered the error regarding flat surfaces, for example, and developed a graphic method for determining the gray value from contour interval and direction. Unfortunately, the means for controlled generation of halftones as a function of surface orientation did not then exist and his work was ignored for a long time.

HILL-SHADING IN THIS CENTURY

Two methods based on lines, this time contours instead of lines of steepest descent, were explored by Kitirô Tanaka in the 1930's. His first method used the lines of intersection of the terrain surface with uniformly spaced, parallel, inclined planes [10],[11]. Tanaka's initiative gave rise to considerable discussion [12]–[19], partly in the form of an acrimonious debate [20]–[23]. His other method was based on portrayal of a terraced model of the terrain [24]–[26], an approach that had been used previously, unguided by his careful analysis [27]–[29]. While line-based methods give rise to beautiful, easy to interpret maps, they cannot show the fine detail of surface topography possible with halftones and must be based on smoothed, generalized information such as contours. These lines also tend to interfere with others used to portray planimetric information.

A shaded overlay can also be produced by photographing an appropriately illuminated scaled model of the surface. If this model has a matte or diffusely reflecting surface, a map overlay of high quality will result provided attention is paid to the projection geometry. While this was an approach taken early on [27], it really only became practical in the 1950's with the introduction of milling machines that allow an operator to carve a model by tracing contours on an existing map [30]–[37]. This is still an expensive, slow process however, in part because of the manual work required to smooth out the resulting "terraced" model.

The Swiss school of cartography improved on earlier forms [28]–[30],[38],[39] and developed shading to a fine art, producing numerous outstanding maps in this time [40]–[48]. Imhof argues that automated methods, such as relief model photography, cannot produce results nearly as impressive, since the cartographer cannot easily influence the process [1]. The manual shading method is however slow and expensive, and consequently has not been used except for small areas and those of particular interest or military importance. One cannot expect, with significant areas of the world still not mapped at large scales, and the rising cost of labor, that shaded overlays produced this way will be used in many maps.

Yoëli [49]–[57] saw the potential of the digital computer in dealing with this dilemma. It is possible to implement Wiechel's method based on oblique illumination of a diffusely reflecting surface if terrain elevations can be read into a computer and suitable continuous tone output devices are available. Yoëli was hampered by the lack of such devices at that time. Blachut and Marsik tried to simplify the required calculations to the point where a computer might not even be required [58],[59]. Peucker helped popularize the whole idea of computer-based cartography [19],[60]–[62], and found a piecewise linear approximation to the equation for the brightness of a diffuse reflector that works well [61]. Many other interesting reports appeared during this time on the subject of hill-shading, too numerous to mention individually [63]–[70].

Brassel [71]–[74] took Imhof's admonitions seriously and tried to implement as much as had been formalized of the "Swiss manner". With the output devices available to him at that time it was not easy to judge whether the added complexity was worth the effort. All of these computer based methods require detailed digital terrain models. The storage capacity and techniques for handling this kind of information now exist [32],[75]–[81]. as do the photographic output devices needed. There has been significant progress, too, in the automatic generation of digital terrain models directly from aerial photographs [81]–[87], partly as a byproduct of work on orthophoto

generation [88]−[91]. More compact and appropriate representations for these terrain models are under investigation [92]−[95], as are alternate methods for relief protrayal such as block diagrams [96]−[102].

Considerable progress has been made recently in the computer graphics area in the portrayal of regular objects with simple surfaces [103]−[116]. Early models for the reflection of light from matte surfaces [117]−[120] are being elaborated, including some for the material on the lunar surface [121]−130]. In this context, work on models of the microstructure of surfaces is relevant [131]−[136]. In a recent effort in the machine vision area, a method was developed for portraying the dependence of brightness on surface orientation using the so-called reflectance map [137]−[141]. The reflectance map can be determined if the detailed geometric dependence of reflection from the surface [142],[143] and the distribution of light sources are known. Alternatively, it can be found empirically, or derived directly by analyzing the interaction of light rays with the surface microstructure.

As a result of the development of the reflectance map, the availability of detailed digital terrain data, small computers able to perform the simple calculations required, and geometrically accurate gray-level output devices, we may say that automatic hill-shading has come of age.

DIGITAL TERRAIN MODELS

For many applications of cartographic data it is useful to have machine-readable surface representations. Such terrain models are used for example in the design of roads and in order to determine the region irradiated by a radio frequency antenna. Initially, digital terrain models were generated manually by interpolation from existing contour maps. This is a tedious, error-prone process producing a digitized version of the surface represented by the contours, which in turn is a smoothed, generalized version of the real surface.

The contour information on topographic maps is produced by manual scanning of stereo pairs of aerial photographs. Today, fortunately, stereo-comparators often come equipped with coordinate readouts that allow the extraction of information needed for the generation of digital terrain models [144]. Conveniently taken during orthophoto generation [88]−[91], the data tends to be accurate and detailed. Even more exciting is the prospect for machines that achieve stereo fusion without human help [81]−[87], since they will lead to the automatic production of digital terrain models. In the past such machines had difficulties dealing with uniform surfaces such as lakes, featureless surfaces, large slopes, and depth discontinuities, as well as broken surfaces, such as forest canopies. This is apparently still true when aerial photographs are used with disparities large enough to ensure high accuracy.

Various representations can be chosen for the surface elevation information. Series expansion, a weighted sum of mathematical functions such as polynomials, Gaussian hills or periodic functions may be used. These tend to be expensive to evaluate however and not accurate in approximating surfaces that have slope discontinuities. This is important for many types of terrain, at all but the largest scales. Perhaps the simplest surface representation is an array of elevations, $\{z_{ij}\}$, based on a fixed grid, usually square. Determining the height at a particular point is simple and the interchange of terrain models between users is easy since the format is so

trivial. One disadvantage of this kind of surface representation is the high redundancy in areas where the surface is relatively smooth. The illustrations in this paper are based on digital terrain models consisting of arrays of elevation values.

Methods that achieve considerable data compression by covering the surface with panels stretched between specially chosen points have been developed [92]–[95]. These exploit the fact that real geographical surfaces are not arbitrary sets of elevations but have definite structure and regularity. Such representations may ultimately replace the simpler, more voluminous ones, if users can be persuaded to accept the greater programming complexities involved.

Digital terrain models may also be referred to as digital *elevation* models if they contain no information other than the elevation values.

THE REFLECTANCE MAP

The human visual system has a remarkable ability to determine the distance to objects viewed, as well as their shape, using a variety of depth cues. One such cue is shading, the dependence of apparent brightness of a surface element on its orientation with respect to the light source(s) and the viewer. Without this particular depth cue we would be hard pressed to interpret pictures of smooth, opaque objects such as people, since other cues like stereo disparity and motion parallax are absent in a flat, still photograph. It can be shown that shading contains enough information to allow the observer to recover the shape. In fact, a computer program has been developed that can do this using a single digitized image [137].

Such work in the area of machine vision has led to a need to model the image-forming process more carefully [138]. The input to the visual sensing system is image irradiance, which is proportional to scene radiance (here loosely called apparent brightness) [140]. Scene radiance in turn can be related to the underlying geometric dependence of reflectance of the surface material and the distribution of light sources [142],[143]. Here we concentrate on the dependence of scene radiance on the orientation of the surface element. Shaded overlays for maps are interpreted by the viewer using the same mechanism normally employed to determine the shape of three-dimensional surfaces from the shading found in their images. Thus shaded overlays should be produced in a way that emulates the image-forming process, one in which brightness depends on surface orientation. This is why the reflectance map, which captures this dependence, is useful in this endeavor.

Consider a surface $z(x, y)$ viewed from a great distance above (see Fig. 2). Let the x-axis point to the east, the y-axis north and the z-axis straight up. The orientation of a surface element can be specified simply by giving its slope p in the x (west-to-east) direction and its slope q in the y (south-to-north) direction. The slopes p and q are the components of the gradient vector, (p, q). The apparent brightness of a surface element $R(p, q)$ depends on its orientation, or equivalently, the local gradient. It is convenient to illustrate this dependence by plotting contours of constant apparent brightness on a graph with axes p and q. This reflectance map [138] provides a graphic illustration of the dependence of apparent brightness on surface orientation. The pq-plane, in which the reflectance map is drawn, is called the gradient space, because each point in it corresponds to a particular gradient.

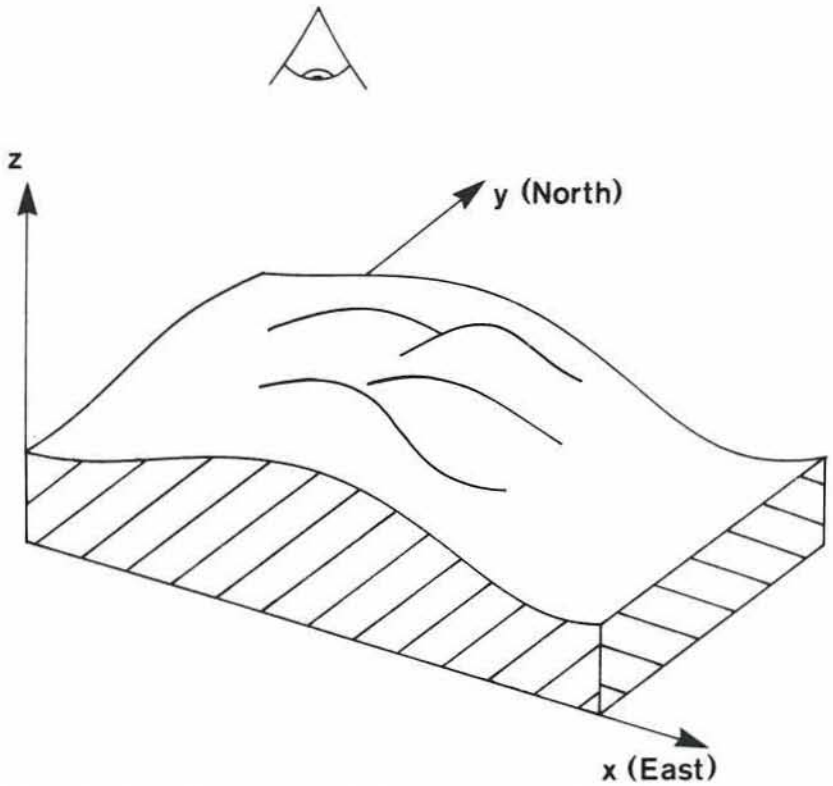

Figure 2: Coordinate system and viewing geometry. The viewer is actually at a great distance above the terrain so that the projection is orthographic.

Surface orientation has two degrees of freedom. We have chosen here to specify the orientation of a surface element by the two components of the gradient. Another useful way of specifying surface orientation is to find the intersection of the surface normal with the unit sphere. Each point on the surface of this Gaussian sphere again corresponds uniquely to a particular surface orientation. If the terrain is single-valued, with no overhangs, all surface normals will point more or less upwards and pierce the Gaussian sphere in a hemisphere lying above an equator corresponding to the horizontal plane. Gradient space happens to be the projection of this hemisphere from the center of the sphere onto a plane tangent at the upper pole.

While we will not use this representation in the calculation of relief shading, it is helpful in understanding previous attempts at graphical portrayal of the dependence of apparent brightness on surface orientation. The first such method was developed by Wiechel more than a century ago [8]. His brilliant analysis appears to have been largely ignored partly because it depended on mathematical manipulations that may have been inaccessible to many of the intended users. Later, Kitirô Tanaka invented another method showing the variation of apparent brightness with surface gradient [10],[11],[24],[25]. This second precursor of the reflectance map also appears to have found little following.

POSITION DEPENDENT EFFECTS

Since the reflectance map gives apparent brightness as a function of local surface gradient only, it does not take into account effects dependent on the *position* of the surface element. One such effect is illumination of one surface element by another. Fortunately this mutual illumination effect is small unless surface reflectance is quite high [138]. It is not known whether mutual illumination effects aid or hinder the perception of surface shape. They are difficult to calculate and so have not been emulated in work on hill-shading.

Another position dependent effect on apparent brightness is the blocking of light by one portion of the surface before it reaches another. Cast shadows can be calculated by determining which surface elements are not visible from the point of view of the light source [139]. Shadows cast by one complicated shape on another are hard to interpret however and apparently detract from the visual quality of shaded overlays [1],[35],[36]. They are thus rarely included.

Scattering of light by air molecules and aerosol particles changes the apparent brightness of a surface element viewed through the atmosphere. The brightness is shifted towards a background value equal to the brightness of an infinitely thick layer of air. The difference between the brightness and the background value decreases with the thickness of the gaseous layer through which the surface is viewed [145]. The resulting reduction in contrast as a function of distance is referred to as aerial perspective and can be a useful depth cue, although there is no general agreement that it aids the perception of surface shape. It has been used at times by map-makers and can be modeled easily [1],[71],[73],[74]. The effect has not been added to any of the hill-shading schemes presented here in order to simplify comparisons.

WHERE DO REFLECTANCE MAPS COME FROM?

A reflectance map may be based on experimental data. One can mount a sample of the surface in question on a goniometer stage and measure its apparent brightness from a fixed viewpoint under fixed lighting conditions while varying its orientation. Instead, one can take a picture of a test object of known shape and calculate the orientation of the corresponding surface element for each point in the image. The reflectance map is then obtained by reading off the measured brightness there.

Alternatively, one may use even more detailed information about light reflection from the surface. The bidirectional reflectance distribution function (BRDF) describes how bright a surface will appear viewed from one specified direction when illuminated from another specified direction [142],[143]. By integrating over the given light source distribution one can calculate the reflectance map from this information [140]. Crudely speaking, the reflectance map is like a "convolution" of the BRDF and the source-radiance distribution.

Most commonly, reflectance maps are based on phenomenological models, rather than physical reality. The so called Lambertian surface, or perfect diffuser, for example, has the property that it appears equally bright from all viewing directions. It also reflects all light, absorbing none. It turns out that these two constraints are sufficient to determine uniquely the BRDF of such a surface, and from it the reflectance map, provided the positions of the light

sources are also given. Some reflectance maps are based on mathematical models of the interaction of light with the surface. Such models tend to be either too complex to allow analytic solution or too simple to represent real surfaces effectively. Nevertheless some have come quite close to predicting the observed behavior of particular surfaces [134]–[136].

Here, new reflectance maps will be determined, based on proposed methods for producing shaded overlays for maps. Their derivation will not depend on an understanding of the image-formation process or the physics of light reflection. Instead, they will require an analysis of how the brightness of a point in the overlay depends on the gradient of the underlying geographical surface.

Which reflectance map should be used? The answer to this question must depend on the quality of the impression a viewer gets of the shape of the surface portrayed. Various methods for producing shaded overlays can be compared by evaluating sample products and classified according to the corresponding reflectance maps. It will become apparent that in this way general conclusions can be drawn about a new method just by inspecting its reflectance map.

NORMALIZATION OF GRAY TONE

A picture made by applying varying amounts of light absorbing substances, such as ink, to an opaque, diffusely reflecting material like paper, has a limited dynamic range. Reflectance is limited at the low end by the properties of the ink and at the high end by the paper, which will at most reflect all the light incident upon it, unless it fluoresces. The diffuse reflectance is thus always less than or equal to one. Similarly, if absorbing substances are used on a transparent substrate, a limit applies, since transparency cannot be larger than one.

The problem of fitting a given image into the available dynamic range is fundamental to all methods of reproduction. A normalization is applied so that the maximum apparent brightness to be reproduced is represented by a reflectance of one (or whatever the maximum is for the paper being used). This scaling will have to be applied whenever relief shading is based on models of image-formation by light reflected from the terrain surface.

GRADIENT ESTIMATION

The apparent brightness of a surface element depends on its orientation with respect to the viewer and the light source. The orientation of the surface element is described fully by a surface normal, or equivalently by the gradient. The components of the gradient are the slopes p (in the west-to-east direction) and q (in the south-to-north direction). These slopes have to be estimated from the array of terrain elevations. It is convenient to use a short-hand here for elevations in the neighborhood of a particular point (see Fig. 3). In the context of a single point at discrete coordinate (i,j), we will denote the elevation at that point by z_{oo}, while elevations of the adjacent grid points to the west and east will be called z_{-o} and z_{+o} respectively. Similarly, elevations at the points to the south and north will be denoted z_{o-} and z_{o+}.

z_{-+} z_{o+} z_{++}

z_{-o} z_{oo} z_{+o}

z_{--} z_{o-} z_{+-}

Figure 3: Short-hand notation for elevations of neighboring points.

The simplest estimates for the slope p might be

$$p_+ = \frac{z_{+o} - z_{oo}}{\Delta x} \quad \text{and} \quad p_- = \frac{z_{oo} - z_{-o}}{\Delta x}, \tag{1}$$

where Δx is the grid interval in the west-to-east direction, expressed in the same units as the terrain elevations. These estimates are biased, actually estimating the slope half a grid interval to the right and left of the central point, respectively. Their average however, the central difference, is unbiased,

$$p_c = \frac{z_{+o} - z_{-o}}{2\,\Delta x} \tag{2}$$

Numerical analysis [146]–[149] teaches us that for certain classes of surfaces an even better estimate is obtained using a weighted average of three such central differences,

$$p_w = \frac{(z_{++} + 2\,z_{+o} + z_{+-}) - (z_{-+} + 2\,z_{-o} + z_{--})}{8\,\Delta x} \tag{3}$$

Symmetrically, one can estimate the south-to-north slope,

$$q_w = \frac{(z_{++} + 2\,z_{o+} + z_{-+}) - (z_{+-} + 2\,z_{o-} + z_{--})}{8\,\Delta y} \tag{4}$$

These expressions produce excellent estimates for the components of the gradient of the central point. The results depend on elevations in a 3×3 neighborhood, with individual elevation values weighted less than they are in the simpler expression for the central difference. This has the advantage that local errors in terrain elevation tend not to contribute as heavily to error in slope. At the same time, more calculations are required and three rows of the digital terrain model have to be available at one time.

Care has to be taken to avoid corruption of the slope estimates by quantization noise in the elevation values. Numerical problems due to the division of small integers may result when a terrain model is too finely interpolated, with limited vertical resolution. If it is necessary to generate many pixels in the output, it is better to interpolate the gray values produced by the shading algorithm.

GRADIENT SMOOTHING EFFECTS

More complicated slope estimators than the ones described tend to introduce a *smoothing effect*, as can be seen by applying them near points of discontinuity in slope. To illustrate this more clearly, consider two horizontal smoothing operations **H**+ and **H**− that modify the terrain model as follows,

$$\mathbf{H}+:\ z'_{oo} := \frac{z_{oo} + z_{+o}}{2} \quad \text{and} \quad \mathbf{H}-:\ z'_{oo} := \frac{z_{-o} + z_{oo}}{2}. \tag{5}$$

It can now be seen that the central difference slope estimate p_c on the original terrain model, equals the biased estimate p_+, calculated from the terrain model smoothed using **H**−, or, equivalently, the biased estimate p_-, calculated from the terrain model smoothed using **H**+. Next consider two vertical smoothing operation **V**+ and **V**− in which the terrain model is modified as follows

$$\mathbf{V}+:\ z'_{oo} := \frac{z_{oo} + z_{o+}}{2} \quad \text{and} \quad \mathbf{V}-:\ z'_{oo} := \frac{z_{o-} + z_{oo}}{2}. \tag{6}$$

The complicated slope estimate p_w can be shown to produce the same result as the first difference p_+ calculated from a terrain model smoothed by applying **H**−, **V**+, and **V**−. Similarly the slope estimate q_w equals q_+ calculated from a terrain model smoothed by applying **V**−, **H**+, and **H**− (actually, since all of these operations are linear, their order can be arbitrarily rearranged). Perhaps any "smoothing" desired should be done as a separate editing operation, combined with the removal of "glitches" from the digital elevation model, rather than as part of the slope estimation. Also for terrain models of relatively limited size this smoothing may be undesirable. Some other slope estimators are simpler and introduce less smoothing. For example one can combine two biased estimates of the slope to get,

$$p_{1/2} = \frac{(z_{++} + z_{+o}) - (z_{o+} + z_{oo})}{2\,\Delta x} \quad \text{and} \quad q_{1/2} = \frac{(z_{++} + z_{o+}) - (z_{+o} + z_{oo})}{2\,\Delta y} \tag{7}$$

Here the average gradient in the top-right quadrant, (z_{oc}, z_{+o}, z_{++}, z_{o+}), rather than at the central point is being estimated, using elevations in a 2×2 neighborhood only. For the graphic illustrations presented here, the expressions for $p_{1/2}$ and $q_{1/2}$ were used to estimate the gradient.

At this time some terrain models are still produced by hand and have rather limited size. Rather than smoothing the terrain, one may wish to increase apparent resolution by some means. This can be done quite effectively by combining biased slope estimates (see Fig. 4). For every point in the terrain model, *four* gray values are produced corresponding to the four quadrants around it. Each is based on a different combination of the slope estimates (p_- or p_+) and (q_- or q_+) as appropriate for that quadrant. No miracles should be anticipated; this method cannot create information where there is none, but it can stretch what is available to its limits.

More complicated slope estimators than those discussed here do not seem called for, since the simple ones shown produce excellent results. Furthermore, estimators having wider support, while

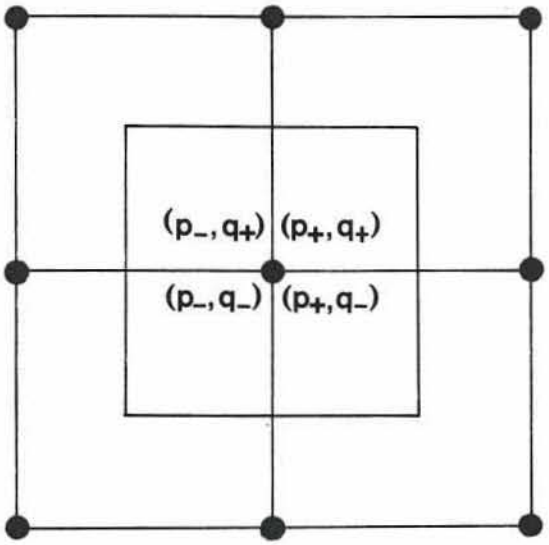

Figure 4: Combinations of biased slope estimates can be used to plot four times as many gray-tones as there are elevation values in the terrain model. The limited amount of data in a small terrain model may be stretched this way to produce reasonably detailed hill-shading output.

known to be more accurate for certain classes of functions such as polynomials, may perform worse on typical terrain with its discontinuities in slope along ridge and stream lines.

It has been cartographic practice to assume a light source in the northwest at a 45° elevation above the horizon. It is helpful in this case to introduce a rotated coordinate system as described in Appendix A.

EXAGGERATION OF TERRAIN ELEVATIONS

Compared to objects of a size that allow for easy manipulation by a human observer, the surface of the earth is in many places, though not everywhere, rather flat. The range of slopes is often so small as to cause disappointment with correctly proportioned models, so that height is often exaggerated in physical models. Similarly, shading based on models of light reflection from a surface tends to have undesirably low contrast. Here too terrain elevations may be exaggerated for all but the most mountainous regions. This is equivalent to multiplication of the components of the gradient by a constant factor, and corresponds to a simple transformation of the reflectance map. For reflectance maps based on reflection of light originating from an assumed source, a similar effect can often be achieved by a decrease in the elevation of the source. For flat surfaces the source may be lowered to a mere 10° or 20° above the horizon, where normally it might be at 45°.

PRODUCING SHADED OVERLAYS

The generation of shaded images from a digital terrain model using the reflectance map is straightforward (see Fig. 1). For each point in the terrain model the local gradient (p, q) is found. The reflectance map then provides the appropriate brightness $R(p, q)$, to be plotted on a suitable gray-level output device. All computations are local and can be accomplished in a single pass through the image.

To illustrate these ideas a simple program is shown (see Fig. 5) that does not incorporate any of the elaborations described later on. Two arrays are used, Z to store the terrain elevations and B to store the calculated brightness values. The latter has one row and one column fewer, since its entries correspond to points lying *between* those in the elevation array (the formulas for $p_{1/2}$ and $q_{1/2}$ are used). The spacing of the underlying grid is DX in the west-to-east direction and DY in the south-to-north direction. The procedures PE(I,J) and QE(I,J) estimate the slopes, while the procedure RM(P,Q) calculates the corresponding brightness using a particularly simple reflectance map. The resulting values range from 0.0 (black) to 1.0 (white) and have to be scaled appropriately before they can be fed to a particular gray-level output device.

```
procedure SHADING(N, M, DX, DY); integer N, M; real DX, DY;

  begin array Z[0:N,0:M], B[0:N-1,0:M-1];

        real procedure PE(I, J); integer I, J;
        PE := (Z[I,J] + Z[I-1,J] - Z[I,J-1] - Z[I-1,J-1]) / (2.0 * DX);

        real procedure QE(I, J); integer I, J;
        QE := (Z[I,J] + Z[I,J-1] - Z[I-1,J] - Z[I-1,J-1]) / (2.0 * DY);

        real procedure R(P, Q); real P, Q;
        RM := MAX(0.0, MIN(1.0, (1.0 + P - Q) / 2.0));

        <read terrain elevations into array Z>

        for J := 1 step 1 until M-1 do
          for I := 1 step 1 until N-1 do
                B[I-1,J-1] := RM(PE(I, J), QE(I, J));

        <write brightness values from array B>

  end
```

Figure 5: Simple program to generate shaded output from a terrain model.

Typical terrain models are quite large and may exceed allowable array storage limits or even the address space of a computer. Fortunately only two (or three) rows of the terrain model are needed for the estimation of the local slopes. The program given can be easily modified to read the terrain model, and to write the calculated gray values, one line at a time. This makes it possible to deal with terrain models of essentially arbitrary size.

Next one should note that terrain models typically are stored using integer (fixed point) representation for elevations to achieve compactness and because elevations are only known with limited precision (an elevation may be given in meters as a 16-bit quantity for example). Similarly, gray values to be sent to a graphic output device are typically quantized to relatively few levels because of the limited ability of the human eye to discern small brightness differences and the limited ability of the device to accurately reproduce these (a typical output device may take values between 0 and 255.) The calculations can thus be carried out largely in integer (fixed point) arithmetic and even a simple computer is adequate.

USE OF LOOKUP TABLES

Some of the formulas for reflectance maps discussed later on are quite elaborate and it would seem that a lot of computation is required to produce shaded output using them. Fortunately it is possible to make the amount of computation equally small in all cases by implementing the reflectance map as a lookup table, which is computed only at the beginning.

Since elevations are quantized, so are the estimates of slope. It is therefore not necessary that one be able to determine the apparent brightness for all possible values of the gradient (p, q). Further, it is reasonable to place an upper limit on slope, so that only a finite number of possible values can occur (For example, if slopes between -1.55 and $+1.60$ are considered, in increments of 0.05, then there are only 64 possibilities for p and 64 for q, and a lookup table with 4096 entries can be used). A second justification for the use of a lookup table is the quantization of the gray values produced. It makes little sense to calculate the apparent brightness with very high precision only to coarsely quantize the result. A convenient rule of thumb is that the number of possible discrete values for each gradient component need not be more than the number of gray levels available from the output device. The final choice of quantization must take into account both of the above considerations.

One can separate the estimation of slope from the calculation of gray value, and produce an intermediate file of coded surface gradient values. This file need not be larger that the original terrain model if the gradient is quantized properly (if p and q can each take on 64 values, each gradient can be encoded as a 12 bit value). The code in the lookup table can be based on ways of expression surface orientation other than in terms of components of the surface gradient. In any case, a file of surface orientation codes can be fed through a lookup table procedure to produce the final output. In this fashion different reflectance maps, encoded as different lookup tables, can be applied to a terrain model easily, with little more effort than reading and writing a file. The illustrations here were produced this way.

Many gray-level raster displays have a translation table between the image memory and the digital-to-analog converter driving the cathode ray tube intensity control. The quantized, packed

reflectance map can be loaded into this lookup table, while the image memory is loaded with the coded slope matrix. This allows one to view the same terrain with a variety of assumed reflectance properties simply by reloading the translation table, which is small compared to the image memory.

TAXONOMY OF REFLECTANCE MAPS

Here we have discussed some of the issues one is likely to encounter when developing a program that produces shaded output. In the remainder of this paper we will analyze a number of proposed hill-shading methods in terms of their equivalent reflectance maps. Notational tools will be introduced as they are needed. Rather than proceed in strict historic order, we will discuss relief shading methods in the following groups:

1) Rotationally symmetric reflectance maps – gray tone depends on slope only;

2) Methods based on varying line spacing or thickness to modulate average reflectance;

3) Ideal diffuse reflectance and various approximations thereto;

4) Gray tone depends only on the slope of the surface in the direction away from the assumed light source;

5) Methods depending on more elaborate models of diffuse reflectance from porous material, such as that covering the lunar surface;

6) Models for gloss and lustrous reflection - smooth surface, extended source and rough surface, point source.

AVERAGE REFLECTANCE OF EVENLY SPACED DARK LINES

Some early methods for hill-shading achieve the desired control of gray tone by varying the spacing between printed lines. One advantage of this approach is the ease with which such information can be printed, since it is not necessary to first screen a continuous tone image. One disadvantage is the confusion created when the lines used for this purpose are layed on top of others portraying planimetric information. While the directional textural effects of the lines are important in conveying information about shape, we concentrate here on the average reflectance.

Consider inked lines with reflectance r_b covering an area of paper with reflectance r_w (see Fig. 6). The ratio of the area covered by ink to the area not covered is the same as the ratio of the width of the lines to the width of the uninked spaces. This in turn equals b/w, where b is the width of the inked line and w the width of the uninked space measured along any direction not parallel to

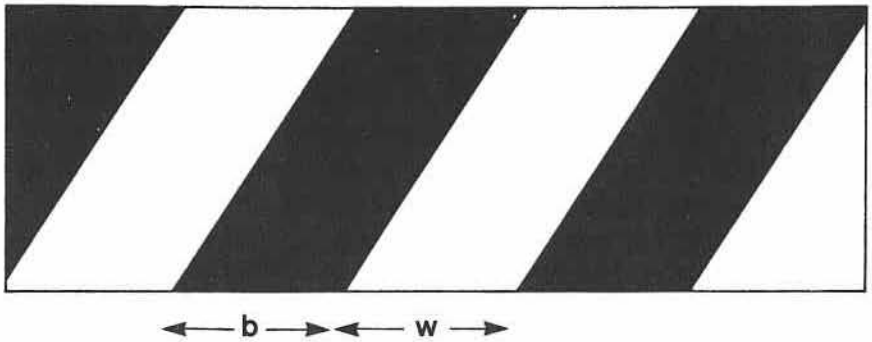

Figure 6: Magnified portion of surface covered with lines. The average tone depends on the fractional area covered by the lines, as well as the reflectance of the paper and the ink.

the lines. If we ignore diffusion of light in the paper, then the average reflectance of the surface is

$$R = \frac{w\,r_w + b\,r_b}{w + b}, \tag{8}$$

or,

$$R = r_w - \frac{b}{w + b}(r_w - r_b) \tag{9}$$

If, for example, the paper reflects all the incident light, and the ink none, then $r_w=1$ and $r_b=0$, so that $R = 1 - b/(w + b)$.

SLOPE OF THE SURFACE IN AN ARBITRARY DIRECTION

In the calculation of gray value produced by some methods of hill-shading it is necessary to know the slope of the surface in an arbitrary direction, given the slope p in the west-to-east direction and the slope q in the south-to-north direction. Note that p and q are the first partial derivatives of the elevation z with respect to x and y, respectively. Consider taking an infinitesimal step dx in the x direction and an infinitesimal step dy in the y direction. The change in elevation dz is given by

$$dz = p\,dx + q\,dy \tag{10}$$

Along a contour line for example, the elevation is constant, so that for a small step $dx = a\,ds$ and $dy = b\,ds$, we can write:

$$(p, q) \cdot (a, b)\,ds = 0 \tag{11}$$

where "•" denotes the dot-product. The local direction of the contours, (a, b) is of course perpendicular to the local gradient (p, q).

Now consider taking a small step in an arbitrary direction, (p_0, q_0) say. That is let $dx = p_0\, ds$ and $dy = q_0\, ds$. The length of the step, measured in the xy-plane is,

$$\sqrt{p_0^2 + q_0^2}\, ds. \tag{12}$$

While the change in elevation is,

$$dz = (p_0\, p + q_0\, q)\, ds \tag{13}$$

Consequently the slope, change in elevation divided by length of the step, is,

$$s = \frac{p_0\, p + q_0\, q}{\sqrt{p_0^2 + q_0^2}} \tag{14}$$

If we let α be the angle between the vector (p_0, q_0) and the x-axis, then, the above can also be written,

$$s = p \cos \alpha + q \sin \alpha \tag{15}$$

The direction in the xy-plane in which the slope is maximal can be found by differentiating with respect to α. The direction of steepest ascent is (p, q) and the maximum slope equals

$$\sqrt{p^2 + q^2}\,. \tag{16}$$

Lehmann's Böschungsschraffen

One of the earliest methods for depicting surface shape using a form of shading is that of Lehmann [2,3]. Illustrations based on *ad hoc* scales of increasing darkness as a function of slope ("Schwärzegradscalen") had been published before, but there was no systematic analysis of this approach until the appearance of an anonymous publication attributed to Lehmann. In his method, short lines in the direction of steepest descent, called hachures, are drawn with spacing and thickness specified by rules that ensure that the fractional area darkened is proportional to the angle of inclination of the surface, θ. That is, steeper implies darker. The lines merge, producing a continuous black area, when θ exceeds some maximum value θ_0, typically 45° or 60°. The slope of the surface equals the tangent of the angle of inclination or "dip". Using the expression for the slope in the direction of steepest ascent, we get,

$$\tan \theta = \sqrt{p^2 + q^2}\,. \tag{17}$$

Consequently, the average reflectance is,

$$R(p, q) = r_w - (r_w - r_b)\ \frac{\tan^{-1}\sqrt{p^2 + q^2}}{\theta_0}\,. \tag{18}$$

When the angle of inclination exceeds the maximum, the lines coalesce and $R(p, q) = r_b$. We can also write the above in another form,

$$R'(\theta,\varphi) = r_w - (r_w - r_b)\frac{\theta}{\theta_o}. \tag{19}$$

Here, φ, the azimuth of the direction of steepest descent, does not appear in the formula on the right, since apparent brightness in this case depends only on the magnitude of the slope. The direction *and* magnitude of the surface gradient can be found from a map prepared according to Lehmann's rules. The direction of steepest descent lies along the hachures, while the slope is directly related to the average tone that results from the width and spacing of these lines. In analyzing his method we have concentrated on calculating the average reflectance produced in the printed product. It should be pointed out that this method also gives rise to textural effects that will not be discussed.

Another interesting aspect of Lehmann's method is that the lines or hachures were drawn starting on one contour and ending on the next. This greatly contributed to the later development of the contour representation (Isohypsen) for terrain surfaces, that was to ultimately replace most of these early attempts at portraying surface shape [7].

Contour Density

Another method is based on the observation that lines on a contour map are more crowded in steep areas and that this crowding leads to darkening of tone or average gray value. This side effect may be helpful in visually conveying information about the nature of the surface. In order to calculate the dependence of the average local reflectance on the gradient, (p, q), we have to determine the spacing of contour lines on the map. We assume that the surface is locally smooth

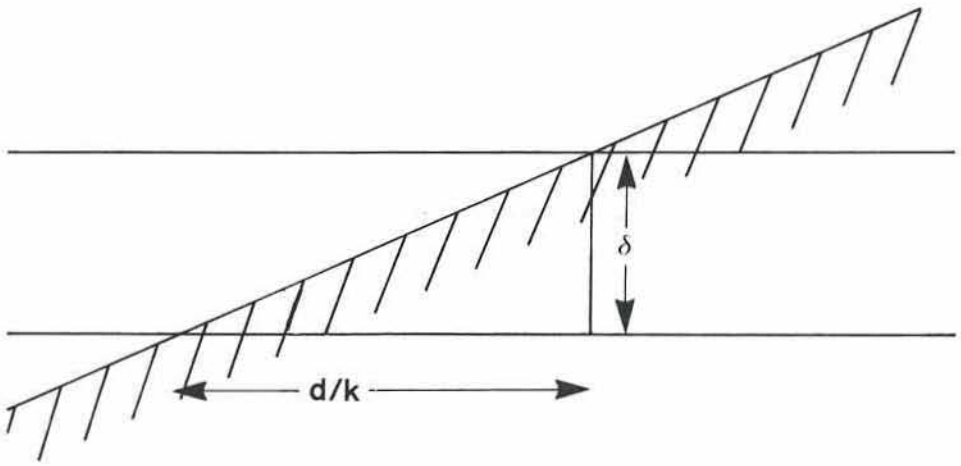

Figure 7: Spacing between successive contour lines along a given direction on the topographic map.

and can be approximated by a plane, at least on the scale of the spacing between contour lines (If this is not the case, aliasing, or undersampling problems occur in any case).

Consider a portion of the surface with slope s in some direction not parallel to the contour lines (see Fig. 7). Assume that the map scale is k and the vertical contour interval δ. Then it is clear that the spacing between contours on the map d can be obtained from the formula for slope,

$$s = \frac{\delta}{d/k}. \tag{20}$$

If we take the crosssection of the surface in the direction of steepest ascent, then $s = \sqrt{p^2 + q^2}$. As a result we can write,

$$d = \frac{k\delta}{\sqrt{p^2 + q^2}}. \tag{21}$$

On the map, $d=b+w$. That is, the spacing between contours is the sum of the width of the contour lines and the width of the blank spaces between them. The average reflectance then is,

$$R(p, q) = r_w - \frac{b}{k\delta}(r_w - r_b)\sqrt{p^2 + q^2}. \tag{22}$$

The result can also be expressed as,

$$R'(\theta,\varphi) = r_w - \frac{b}{k\delta}(r_w - r_b)\tan\theta, \tag{23}$$

where θ is the inclination of the surface. The above expressions only hold if w is not negative. When the slope is too steep, contour lines overlap, and the average reflectance is simply equal to r_b. In the special case that $r_w=1$ and $r_b=0$, the above simplifies to,

$$R(p, q) = 1 - \frac{b}{k\delta}\sqrt{p^2 + q^2}. \tag{24}$$

Typically $b/(k\delta)$ may equal 1 or $1/\sqrt{3}$.

Diffuse Surface under Vertical Illumination

The methods discussed so far produce tones that depend on the magnitude of the gradient only, not its direction. This is similar to the effect one would obtain if a physical model of the terrain was illuminated vertically, with the light source placed near the viewer. An ideal diffusing surface has an apparent brightness that is proportional to the cosine of the incident angle i as discussed later. This is the angle between the direction of the incident rays and the local normal, which, in the case of vertical illumination, is just θ. Therefore,

$$R'(\theta,\varphi) = \cos\theta, \tag{25}$$

or,

$$R(p, q) = \frac{1}{\sqrt{1 + p^2 + q^2}}. \tag{26}$$

Instead of illumination from a point source, one may consider the effect of a distributed source. A uniform hemispherical source illuminating a diffusely reflecting surface leads to a result of the following form [140],

$$R'(\theta,\varphi) = \cos^2(\theta/2) = \tfrac{1}{2}(1 + \cos\theta), \tag{27}$$

or,

$$R(p, q) = \frac{1}{2} + \frac{1}{2}\,\frac{1}{\sqrt{1 + p^2 + q^2}}. \tag{28}$$

This reflectance map leads to flatter, even less interpretable pictures, since the range of reflectances has been halved and all reflectances have been shifted upwards by a half. In the derivation of the formula above, reflection from the surrounding terrain surface is ignored. If the terrain surface diffusely reflects a fraction ρ of the incident light, the constant term in the above expression is increased from ½ to ½(1 + ρ), while the coefficient of cos θ decreases from ½ to ½(1 − ρ). It is at times suggested that a component of surface brightness due to distributed illumination from the sky be added to that resulting from oblique illumination. This however typically detracts from the shaded result, rather than improving it.

The methods discussed so far give rise to rotationally symmetric reflectance maps, that can be described adequately by a single cross-section, showing tone versus slope [1],[35],[36]. This representation has sometimes been misused for asymmetric reflectance maps, where it does *not* apply. Rotationally symmetric reflectance maps produce shaded images that are difficult to interpret. Moving the assumed light source away from the overhead position gives rise to better shaded map overlays, but forces us to introduce some new concepts.

The Surface Normal

The surface normal is a vector perpendicular to the local tangent plane. The direction of the surface normal **n** can be found by taking the cross-product of any two vectors parallel to lines locally tangent to the surface (as long as they are not parallel to each other). We can find two such vectors by remembering that the change in elevation when one takes a small step dx in the x-direction is just $dz = p\,dx$, while the change in elevation corresponding to a step dy in the y-direction is $dz = q\,dy$. The two vectors, $(1, 0, p)\,dx$ and $(0, 1, q)\,dy$, are, therefore, parallel to lines tangent to the surface and so their cross-product is a surface normal.

$$\mathbf{n} = (1, 0, p) \times (0, 1, q) = (-p, -q, 1). \tag{29}$$

Note that the gradient (p, q) is just the (negative) projection of this vector on the xy-plane. A unit surface normal N can be obtained by dividing the vector **n** by its magnitude

$$N = \sqrt{1 + p^2 + q^2}. \tag{30}$$

While it is convenient to specify directions as vectors, it is at times helpful to use spherical coordinates instead. A direction can then be given as an azimuth angle, φ, measured anti-clockwise from the x-axis, and a polar or zenith angle θ (see Fig. 8). (In navigation, the

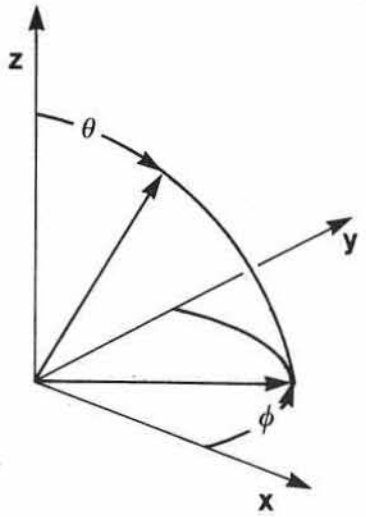

Figure 8: Definition of the azimuth angle, φ, and the zenith angle, θ. Here, azimuth is measured counter-clockwise from the x-axis in the xy-plane, while the zenith angle is measured from the z-axis.

azimuth angle is usually measured clockwise from north, and the elevation angle is given instead of the zenith angle. These are just the complements of the angles used here.) The unit vector in the direction so defined equals,

$$N = (\cos\varphi \sin\theta, \sin\varphi \sin\theta, \cos\theta)\,. \tag{31}$$

To find the azimuth and zenith angle of the surface normal we identify components of corresponding unit vectors. Then,

$$\sin\varphi = -\frac{q}{\sqrt{p^2+q^2}} \quad \text{and} \quad \cos\varphi = -\frac{p}{\sqrt{p^2+q^2}}\,, \tag{32}$$

while,

$$\sin\theta = \frac{\sqrt{p^2+q^2}}{\sqrt{1+p^2+q^2}} \quad \text{and} \quad \cos\theta = \frac{1}{\sqrt{1+p^2+q^2}}\,. \tag{33}$$

Conversely,

$$p = -\cos\varphi \tan\theta \quad \text{and} \quad q = -\sin\varphi \tan\theta\,. \tag{34}$$

We will find it convenient to use both vector and spherical coordinate notation to specify direction.

Position Of The Light Source

The reflectance maps discussed so far are rotationally symmetric about the origin, only the magnitude of the gradient, not its direction affecting the resulting gray value. This corresponds to a situation where the light source is at the viewing position. Most hill-shading methods have the assumed light source in some other position, typically in the north-west, with a zenith angle of around 45° ($\theta_0 = 45°$, $\varphi_0 = 135°$). The unit vector,

$$S = (\cos\varphi_0 \sin\theta_0,\ \sin\varphi_0 \sin\theta_0,\ \cos\theta_0) \tag{35}$$

points directly at the light source. A surface element will be illuminated maximally when the rays from the light source strike it perpendicularly, that is, when the surface normal points at the light source. By identifying components in the expression for the surface normal $\mathbf{n}_0 = (-p_0, -q_0, 1)$ with those in the expression for the vector pointing at the source one finds that the components of the gradient of such a surface element are,

$$p_0 = -\cos\varphi_0 \tan\theta_0 \quad \text{and} \quad q_0 = -\sin\varphi_0 \tan\theta_0 . \tag{36}$$

When the source is in the standard cartographic position, this means,

$$p_0 = 1/\sqrt{2} \quad \text{and} \quad q_0 = -1/\sqrt{2} . \tag{37}$$

This standard position for the assumed light source was probably chosen because we are used to viewing objects lighted from that direction [1]. When we look at nearby objects in front of us, our body blocks the light arriving from behind us. Further, when writing on a horizontal surface, many of us find our right hand blocking light coming from that direction. We thus often arrange for light sources to be to the left, in front of us. While we can certainly interpret shading in pictures where the light source is not in this standard position, there seems to be a larger possibility of depth reversal in that case, particularly if the object has a complex, unfamiliar shape.

Returning now to the specification of the position of the light source, we find two identities that will be helpful later:

$$\cos(\varphi - \varphi_0) = \frac{p_0 p + q_0 q}{\sqrt{p^2+q^2}\ \sqrt{p_0^2+q_0^2}} \tag{38}$$

and,

$$p_0 p + q_0 q = \tan\theta \tan\theta_0 \cos(\varphi - \varphi_0) . \tag{39}$$

It also follows that the slope of the surface in the direction, (p_0, q_0), away from the light source is,

$$s = \tan\theta \cos(\varphi - \varphi_0) . \tag{40}$$

Tanaka's Orthographical Relief Method

A method proposed by Kitirô Tanaka in 1930 [10],[11], involves drawing the lines of intersection of the surface with evenly spaced *inclined* planes. These planes are oriented so that

their common normal points towards an equivalent light source (see Fig. 9). Thus slopes tilted away from this direction have contours spaced closely, giving rise to heavier shading than that on horizontal surfaces, while surfaces lying parallel to the inclined planes are lightest. As in Lehmann's method, some information may be conveyed by the directional texture of the contours. Here we concentrate on the average reflectance only.

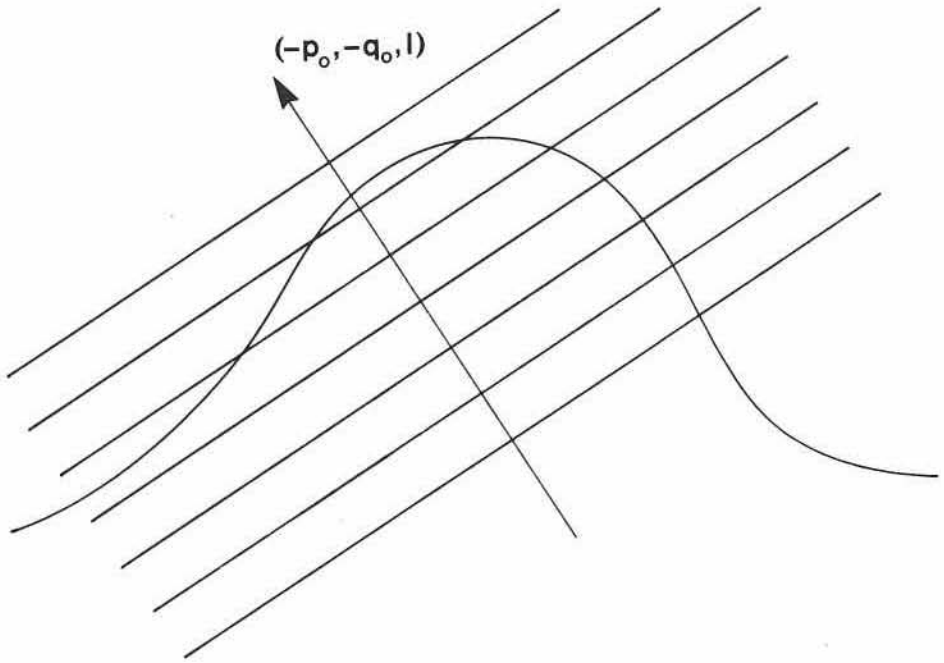

Figure 9: Side-view of a hill cut by inclined planes. Viewed from above, the lines of intersection crowd together where the surface slopes away from the equivalent source. Conversely, there are no lines where the terrain surface is parallel to the inclined planes.

A contour is the intersection of the terrain's surface $z=z(x, y)$ with a plane. The equation $z=z_0$ applies to a horizontal plane appropriate for ordinary contours. For "inclined contours" an inclined plane is used with an equation of the form

$$\frac{(-p_o, -q_o, 1) \bullet (x, y, z)}{\sqrt{1+p_o^2+q_o^2}} = z_o'. \tag{41}$$

The vector $(-p_o, -q_o, 1)$ is perpendicular to the inclined planes. Ordinary contours represent the locus of the solution of $z(x, y)=z_o$, while inclined contours are the loci of solutions of the equation,

$$\frac{1}{\sqrt{1+p_o^2+q_o^2}} [z(x, y)-p_o x-q_o y] = z_o'. \tag{42}$$

We can now apply our analysis of the contour density model to the modified surface, $z'(x, y)$, defined by the left hand side of this equation! All we need are the slopes of this new surface. Differentiating the above expression with respect to x and y, we get,

$$p' = \frac{p - p_o}{\sqrt{1+p_o^2+q_o^2}} \quad \text{and} \quad q' = \frac{q - q_o}{\sqrt{1+p_o^2+q_o^2}}. \tag{43}$$

Finally then,

$$R(p, q) = r_w - \frac{b}{k\delta}(r_w - r_b)\frac{\sqrt{(p-p_o)^2 + (q-q_o)^2}}{\sqrt{1+p_o^2+q_o^2}}. \tag{44}$$

We obtain the expression for contour density, derived earlier, when $p_o = q_o = 0$. Also, in the special case that $r_b = 0$, $r_w = 1$, $p_o = 1/\sqrt{2}$, and $q_o = -1/\sqrt{2}$,

$$R(p, q) = 1 - \frac{b}{k\delta}\frac{\sqrt{(p-1/\sqrt{2})^2 + (q+1/\sqrt{2})^2}}{\sqrt{2}}. \tag{45}$$

It is sometimes useful to express the apparent brightness as a function of the azimuth φ and zenith angle θ of the surface normal. If we let φ_o be the azimuth and θ_o the zenith angle of the normal to the inclined planes, then the formula can be rewritten as follows,

$$R'(\theta,\varphi) = r_w - \frac{b}{k\delta}(r_w - r_b)\cos\theta_o \sqrt{\tan^2\theta - 2\tan\theta\tan\theta_o\cos(\varphi-\varphi_o) + \tan^2\theta_o}. \tag{46}$$

When $\theta_o = 45°$, $r_b = 0$ and $r_w = 1$, then, as Tanaka showed [10],[11],

$$R'(\theta,\varphi) = 1 - \frac{b}{k\delta}\frac{\sqrt{1 - \sin 2\theta\cos(\varphi-\varphi_o)}}{\sqrt{2}\cos\theta}. \tag{47}$$

How does one choose the parameter $b/(k\delta)$? Tanaka felt that the shading produced by his method should match that seen on a surface covered with an ideal material called a perfect diffuser. The apparent brightness of such a surface varies with the cosine of the incident angle, between the surface normal and a vector pointing at the light source. He introduced a parameter called the line factor. It is the ratio of the width of the inked line, b, to, $k\delta/\sin\theta_o$, the interval between inclined contours for a horizontal surface. The line factor is just,

$$\frac{b}{k\delta}\frac{\sqrt{p_o^2+q_o^2}}{\sqrt{1+p_o^2+q_o^2}}. \tag{48}$$

Tanaka proposed varying the line width b in order to produce shading that matches that seen on a perfect diffuser, but realized the impracticality of this approach for all but polyhedral surfaces [10],[11]. Resigned to using a fixed line width, he chose to optimize the line factor by considering the brightness distribution on a spherical cap extending to 45° slope. With the source at 45° elevation, the least deviation from the brightness distribution one would see if the surface was a perfect diffuser is obtained when the line factor equals 0.3608. Consequently, $b/(k\delta) = 0.3608\sqrt{2}$. Finally then,

$$R(p, q) = 1 - 0.3608\sqrt{(p-1/\sqrt{2})^2 + (q+1/\sqrt{2})^2}. \tag{49}$$

It is unfortunate that this method later gave rise to some misunderstanding as well as a less rigorous hybridized form [15].

A common representation for relief form is the block diagram, an oblique view of a series of equally-spaced, vertical profiles [97]−[102]. The projection typically is orthographic, although at times a perspective projection is utilized. Surfaces not visible to the viewer are eliminated (see Fig.10). Shading can of course be applied to oblique views as may be done in sophisticated flight simulators of the future. We concentrate here on map forms that provide for superposition of planimetric information however, and digress only to point out that part of the appeal of block diagrams lies in their implicit shading, due to the variation in the spacing of lines.

Following the discussion in the last section, it is clear that the equivalent light-source position is in the horizontal plane at right angles to the vertical cutting surfaces. The analysis just presented then applies directly. Things are a little more difficult if the result is to be expressed in terms of the coordinate system of the surface rather than one oriented with respect to the viewer. Details may be found in appendices B & C, where contour density shading and Tanaka's inclined contour method are shown to be special cases of this more general situation.

Figure 10: "Block-diagram" representation of terrain surface. This is an isometric projection of a series of uniformly spaced vertical profiles of the surface viewed from the south-east. Note the shading effect due to the variation in line spacing.

Wiechel's Contour-Terrace Model

Imagine a three-dimensional model of the terrain built by stacking pieces of some material cut according to the shape of the contours on a topographic map [8]. If the thickness of the material is chosen correctly the model will be a scaled approximation of the terrain, looking a little like a tiered cake. Illuminating this construction with a distant point source will give rise to a form of shading since each contour "terrace" casts a shadow on the one beneath it (see Fig.11). Wiechel [8] was the first to analyze the reflectance properties of such a surface. In order to calculate the average brightness of a portion of the model, when viewed from above, we must determine the width of the shadow relative to the width of the terrace.

The width of the shadow, measured perpendicular to the contours, varies, depending on the orientation of contours relative to the direction of the rays from the source. For example, when measured this way, the width is zero where the contour is locally parallel to the projection of the rays on the xy-plane. Measured in a vertical plane containing the light source however, the width of the shadow is constant, since the terrace has a fixed height (see Fig.12). If the light source has a zenith angle θ_o, the contour interval is δ, and the map scale k, then,

$$\tan \theta_o = \frac{b}{k\delta} \tag{50}$$

but,

$$\tan \theta_o = \sqrt{p_o^2 + q_o^2}\,. \tag{51}$$

To calculate the average brightness we must know the width, d, of the terrace in the model, measured in the same vertical plane. The slope in this plane evidently is just

$$s = -\frac{k\delta}{d}\,. \tag{52}$$

We know that the slope of a surface in the direction (p_o,q_o) is,

$$s = \frac{p_o p + q_o q}{\sqrt{p_o^2 + q_o^2}}\,. \tag{53}$$

Solving for d from the last two equations and for b from the two before them, we get

$$\frac{b}{d} = -(p_o p + q_o q)\,. \tag{54}$$

For example, when the local surface normal, $(-p, -q, 1)$, is perpendicular to the direction to the source, $(-p_o, -q_o, 1)$, their dot-product is zero and $b/d = 1$. The terrace is then covered exactly by the shadow. In the above expression both the contour interval and the map scale have cancelled, as one might have predicted.

When $(p_o p + q_o q) < -1$, shadows coalesce and no further increase in b/d is possible. When, on the other hand, $(p_o p + q_o q) > 0$, the slope is facing *towards* the light source. This means that no shadow is cast. In this model, shading only occurs on slopes facing away from the source, while those facing towards it are all *uniformly* bright. This is certainly not what one would expect of a real surface and suggests that the contour-terrace model has some shortcomings. This is not

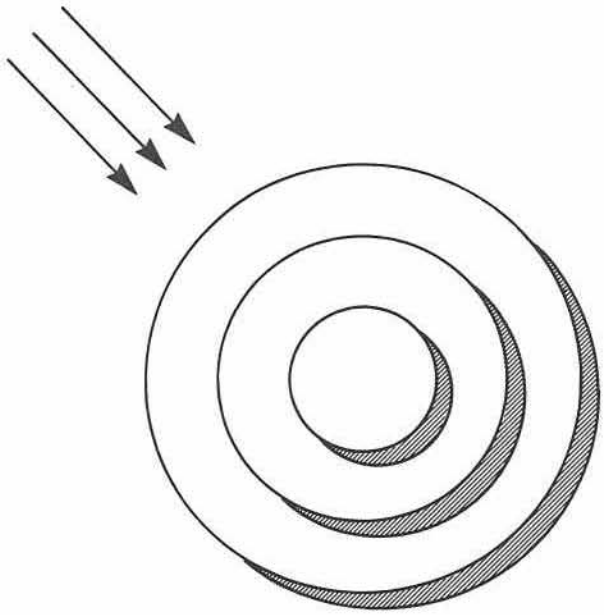

Figure 11: Shadows cast in the contour terrace model. The width of the shadows, measured perpendicular to the contours, varies with the direction of the contours relative to the direction of the incident rays.

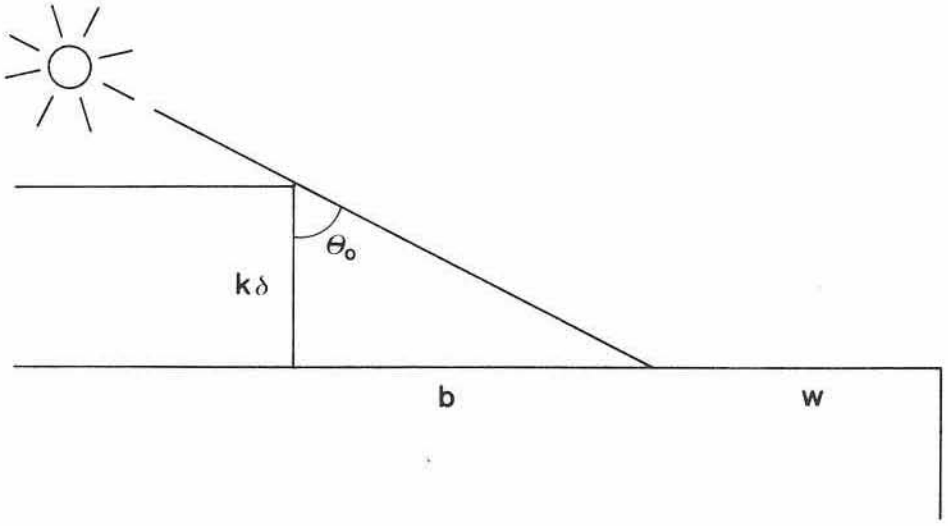

Figure 12: Section of the contour terrace model in a vertical plane containing the light-source. The width of the shadow, b, measured in this plane is constant, while the width of the terrace, $(b+w)$, depends on the slope of the surface in a direction parallel to the projection of the incident rays on the ground plane.

surprising since apparent brightness depends on surface orientation, not height, and while the model represents height with reasonable accuracy it does a poor job of modeling surface orientation. Indeed the surface of the model is mostly horizontal, with some narrow strips of a vertical orientation. The latter are not even visible from above.

Wiechel noted that light would be reflected from these vertical surfaces onto the terraces [8]. The surface thus appears brighter, viewed from above, near vertical surfaces facing towards the light source. He made the simplifying assumption that reflection produces *uniformly* bright patches with the same shape as shadows that would be cast were a source to be placed opposite the actual light source. This is not a reasonable assumption unless the vertical surfaces are made of narrow mirror facets, each oriented perpendicular to the direction of the incident light! In this case, surfaces illuminated by reflection as well as by direct light have a brightness twice that of those illuminated only by direct light. This version of the model is fortunately simple enough to be amenable to analysis. First note that, if we assume the surface to be an ideal diffuser, then the brightness of horizontal surfaces that are neither shadowed nor illuminated by reflection equals the cosine of the zenith angle of the source. Therefore, let $r_b=0$ and $r_w=\cos\theta_o$, where,

$$\cos\theta_o = \frac{1}{\sqrt{1+p_o^2+q_o^2}} \tag{55}$$

and so,

$$R(p, q) = \frac{1 + p_o p + q_o q}{\sqrt{1+p_o^2+q_o^2}} \tag{56}$$

or,

$$R'(\theta,\varphi) = [1 + \tan\theta \tan\theta_o \cos(\varphi-\varphi_o)] \cos\theta_o . \tag{57}$$

When the source is in the standard position (North-West at 45°) this becomes,

$$R(p, q) = \frac{1 + (p-q)/\sqrt{2}}{\sqrt{2}} . \tag{58}$$

Note that here apparent brightness already becomes equal to one when the angle of inclination is about 30.36° towards the light source. This may be contrasted with the case of the ideal diffuser, to be discussed later, where it reaches one only for an inclination of 45°. Wiechel used this model as the second approximation to the ideal diffuser (the first will be discussed later) and expressed his result as [8],

$$\frac{\cos i}{\cos e}, \tag{59}$$

where i is the incident angle, and e is the emittance angle, here equal to θ. These angles will play an important role in the discussion of more recent methods later on.

According to Raisz and Imhof [1],[27]–[29] terraced contour models were used in the late 1800's. An early example is an alpine excursion map published in 1865 that employed "contour shadows" [1]. The first attempts at photography of obliquely illuminated surfaces also used terraced terrain models [27]. Wiechel probably was influenced by these early efforts when he chose to develop this method for hill shading.

Wiechel's Helligkeitsmaassstab

Wiechel based his method for irregular surfaces on that developed earlier by Burmester for regular surfaces [9]. In order to make his approach practical he needed a graphical device for translating measurements of contour interval and direction of steepest descent into gray tones. The "Helligkeitsmaassstab" (his spelling) is arranged so that these measurements can be transferred directly, and the correct tone determined from a series of isophotes, contours of constant brightness. Steep slopes, with small contour intervals correspond to points near the origin of this diagram, while those of gentle slope map into points further away.

His diagram therefore is a sort of inside-out reflectance map! The main difference is that radial distance from the origin in gradient space is proportional to $\tan \theta$, while it is proportional to $\cot \theta$ in this early precursor. This corresponds to a conformal mapping operation referred to as inversion with respect to the unit circle. Wiechel showed that his diagram corresponded to the image of an appropriately illuminated logarithmoid made of the desired material. The equation of this surface is

$$z = -\log \sqrt{x^2 + y^2}. \tag{60}$$

The reflectance map, by the way, can be thought of as the image of a paraboloid [138].

It is indeed unfortunate that Wiechel's construction was ignored. Wiechel developed two shading methods that did not require this two-dimensional diagram. In each case apparent brightness depended only on the slope of the surface in the direction away from the light source. This property manifests itself in the reflectance map in the form of parallel straight-line contours. The effect is less apparent in Wiechel's diagram, where isophotes become nested circles through the origin, with centers along the line in the direction of the light source.

Tanaka's Relief Contour Method

Kitirô Tanaka, in 1939, developed an ingenious method [24]–[26] for drawing the shadows one would see if one looked at a contour-terrace model. His method is based on the observation that the length of the shadow, measured in the direction of the incident rays, is constant. Using a pen with a wide nib one can trace the contours, while maintaining the orientation of the nib parallel to the direction of the incident rays (as in roundhand writing). Only those portions of the contours are traced that correspond to slopes facing away from the assumed light source. Tanaka used black ink on gray paper for reasons that will become apparent. If the reflectance of this paper is r_g then,

$$R(p, q) = r_g + (r_g - r_b)(p_o p + q_o q) \tag{61}$$

provided $(p_o p + q_o q) < 0$, otherwise $R(p, q) = r_g$.

Tanaka also came up with a way of modulating the average reflectance of the paper in areas that corresponded to slopes facing *towards* the source. His approach is somewhat analogous to taking the negative of a picture of the contour-terrace model obtained by illuminating it from the

other side. Thus white "shadows" are cast in the opposite direction to the black shadows. These can be drawn with white ink on gray paper using the same method as before except that now the section of the contours that correspond to slopes facing towards the light source are traced. It is easy to see that the resulting average reflectance will be,

$$R(p, q) = r_g - (r_g - r_w)(p_o p + q_o q) \tag{62}$$

where r_w is the reflectance of the white ink. When $(p_o p + q_o q) < 0$, no "shadows" appear and $R(p, q) = r_g$. Tanaka combined the two methods, tracing contours using both white and black ink. The corresponding reflectance map $R(p, q)$ equals one of the expressions above depending on whether the slope locally faces away from or towards the assumed source.

He apparently also experimented with nibs of different width for white and black ink. This corresponds to changing the elevation of the assumed sources. If the width of the nib is b, then the relationship is,

$$\frac{b}{k\delta} = \tan\theta_o = \sqrt{p_o^2 + q_o^2}\,. \tag{63}$$

The results of this tedious manual method are most impressive [24]–[26]. One can write the above expressions in the alternate notation,

$$R'(\theta,\varphi) = r_g + (r_g - r_b)\tan\theta\tan\theta_o\cos(\varphi-\varphi_o), \quad \text{when} \quad \cos(\varphi-\varphi_o) < 0\,, \tag{64}$$

$$R'(\theta,\varphi) = r_g - (r_g - r_w)\tan\theta\tan\theta_o\cos(\varphi-\varphi_o), \quad \text{when} \quad \cos(\varphi-\varphi_o) > 0\,. \tag{65}$$

Tanaka preferred a reflectance for the gray background halfway between that of the black ink and the white ink. Placing the light source in the standard position we get,

$$R(p, q) = \tfrac{1}{2}\left[1 + \frac{p-q}{\sqrt{2}}\right], \tag{66}$$

or,

$$R'(\theta,\varphi) = \tfrac{1}{2}\left[1 + \tan\theta\cos(\varphi-\varphi_o)\right]. \tag{67}$$

This result can also be expressed as, $(\cos i \cos g) / \cos e$, where g is the phase angle, here equal to θ_o. Note that except for scaling by $\cos g$, this is the same result as that obtained by Wiechel for his contour-terrace model. One effect of this scaling is that apparent brightness rises to one only when the angle of inclination is 45°, on the other hand, horizontal surface now have a gray value of only 0.5.

Tanaka's Hemispherical Brightness Distribution

Tanaka needed a way to display the dependence of tone on surface orientation to permit comparison of the results produced by his two methods and what would be seen if the surface modeled were an ideal diffuser. He chose an oblique view of the brightness distribution on a spherical cap extending to 45° inclination [10],[11],[24]-[26]. If the cap is increased until it is a hemisphere, one obtains something like the reflectance map. One difference is that radial distance

from the origin in gradient space is proportional to $\tan\theta$, while here it is proportional to $\sin\theta$. Thus, while the reflectance map is a central projection of the Gaussian sphere onto a horizontal plane, this is a *parallel* projection. Put another way: we are dealing here with an image of a hemisphere, while the reflectance map is the image of a paraboloid.

Tanaka's oblique views of the distribution of brightness versus surface orientation do not provide the quantitative information available in a contour representation such as Wiechel's. His method is nevertheless very helpful and it is unfortunate that few seem to have paid any attention to it, judging by the continued use of inappropriate forms. It is not uncommon for example to see the dependence of tone on surface orientation shown as a curve depending on one variable, slope, when it clearly depends on two, slope and the direction of steepest descent, or equivalently, the two components of the gradient.

Lambertian Surfaces

We now turn from graphical methods using variation in line spacing and line thickness to those utilizing continuous tone or halftone techniques. These are often based on a model of what the terrain would look like were it made of some ideal material, illuminated from a predetermined direction. The result differs from an aerial photograph, since no account is taken here of varying terrain cover, the light source is often placed in a position that is astronomically impossible, and the terrain model has been smoothed and generalized. Not being like an aerial photograph is an advantage, since aerial photographs, taken with the sun fairly high in the sky, often do not provide for easy (monocular) comprehension of surface topography.

The amount of light captured by a surface patch will depend on its inclination relative to the incident beam. As seen from the source the surface is foreshortened, its apparent (or projected) area equal to its true area multiplied by the cosine of the incident angle. Thus the irradiance is proportional to $\cos i$. Strangely, it is commonly assumed that the *radiance* (apparent brightness) of the surface patch is also proportional to $\cos i$. This is generally not the case since light may be reflected differently in different directions, as can be seen by considering a specularly reflecting material.

One can however postulate an *ideal* surface that reflects all light incident on it and appears equally bright from all viewing directions. Such a surface is called an ideal diffuser or Lambertian reflector and has the property that its radiance equals the irradiance divided by π [142],[143]. In this special case the radiance is proportional to the cosine of the incident angle. No real surface behaves exactly like this, although pressed powders of highly transparent materials like barium sulfate and magnesium carbonate come close. Matte white paint, opal glass, and rough white paper are somewhat worse approximations, as is snow [131]. Most proposed schemes for automatic hill-shading are based on models of brightness distribution on ideally diffusing surfaces [8],[10],[11],[49]–[57],[71],[73],[74], even though there is no evidence that perception of surface shape is optimized by this choice of reflectance model. As we will see, reflectance calculations based on this model are not particularly simple either.

The cosine of the incident angle can be found by considering the appropriate spherical

triangle (see Fig.13) formed by the local normal N, the direction towards the source S, and the vertical V. One then finds as Wiechel already showed [8],

$$R'(\theta,\varphi) = \cos\theta_0 \cos\theta + \sin\theta_0 \sin\theta \cos(\varphi-\varphi_0)\,. \tag{68}$$

Alternatively one can simply take the dot-product of the unit vector N normal to the surface and the unit vector S pointing towards the source [138],[140]

$$\cos i = \frac{(-p,-q,1)\bullet(-p_0,-q_0,1)}{\sqrt{1+p^2+q^2}\,\sqrt{1+p_0^2+q_0^2}}\,. \tag{69}$$

The reflectance map (normalized so that its maximum is one) then is,

$$R(p,q) = \frac{1+p_0p+q_0q}{\sqrt{1+p^2+q^2}\,\sqrt{1+p_0^2+q_0^2}}\,. \tag{70}$$

When $(1+p_0p+q_0q) < 0$ the surface element is turned away from the source and is self-shadowed. In this case, $R(p,q)=0$.

In the case of a point source of light at 45° zenith angle in the north-west, the reflectance map becomes

$$R(p,q) = \frac{1+(p-q)/\sqrt{2}}{\sqrt{2}\,\sqrt{1+p^2+q^2}}\,. \tag{71}$$

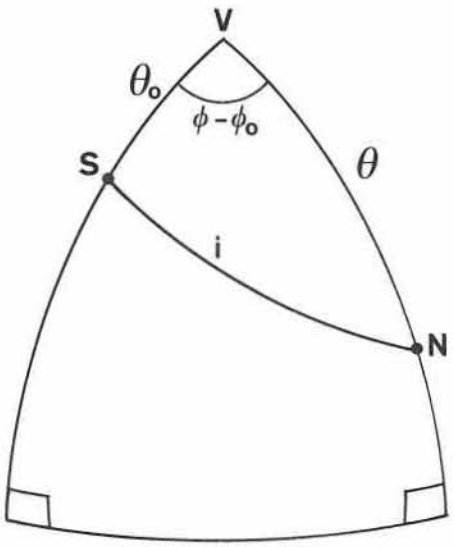

Figure 13: Spherical triangle used in calculating the incident angle, i, from the azimuth and elevation of the light-source and the azimuth and elevation of the surface normal. The direction towards the viewer is V, the direction to the source is S, while the surface normal is N.

Peucker's Piecewise Linear Approximation

The computation of gray value using the equation for the cosine of the incident angle is complicated and slow because of the appearance of the square root. Peucker [61] experimented with a number of approximations that are easier to compute. He found that an adequate, piecewise linear approximation for slopes less than one, is

$$0.3441\,p - 0.5129\,q + 0.6599, \quad \text{for} \quad p+q>0 \tag{72}$$

$$0.5129\,p - 0.3441\,q + 0.6599, \quad \text{for} \quad p+q<0 \tag{73}$$

or,

$$R(p, q) = 0.4285\,(p-q) - 0.0844\,|\,p+q\,| + 0.6599\,, \tag{74}$$

where $|\,p+q\,|$ denotes the absolute value of $(p+q)$. The above approximation produces excellent shaded overlays, that in fact seem easier to interpret that those produced using the exact equation for a perfectly diffusing surface.

Brassel's Adjustment Of Light Source Position

Perhaps the most outstanding examples of shaded maps come from Switzerland. Techniques for portraying the shape of the surface and integrating this information with planimetric detail have been perfected by a number of artists there [1],[40]−[47]. The results of automated methods as described here, cannot compete with the beauty of their products. Nevertheless, automated methods do provide a systematic, accurate way for generating shaded overlays. They will become of particular importance when good digital terrain models become easily available. Brassel attempted to incorporate as much as possible of the Swiss manner into his program [71]−[74]. He quickly realized two problems with methods based purely on Lambertian reflectance models.

The first effect is explained as follows. Surface elements sloping away from the source are dark, while those tilted towards the source are brighter. Brightest are those that have the light rays falling perpendicularly on the surface. Surface elements sloped more steeply, however, become *darker* again. This lack of monotonicity of brightness with slope is apparently disturbing and reduces the ability of the observer to correctly interpret the shape. Brassel ameliorated this effect by reducing the elevation of the light source in regions where this problem occurred.

If the zenith angle of the source θ_o is smaller than the zenith angle of the direction defined by the surface normal θ he moves the source to a new zenith angle θ_n that is a weighted average of θ_o and θ. To be precise,

$$\theta_n = \max\,[\theta_o,\, \alpha\,\theta + (1-\alpha)\theta_o]\,, \tag{75}$$

where

$$\theta = \tan^{-1}\sqrt{p^2+q^2}\,. \tag{76}$$

In his thesis [71], the weighting factor α was one, so that adjustment in elevation was complete. Curiously, this simple method has the effect of lowering the light source even for

surface elements tilted *away* from the source, as long as the slope is large enough. The above method can also be expressed directly in terms of the components of the gradient. When $(p^2+q^2) > (p_o^2+q_o^2)$,

$$p_n = p_o \frac{\sqrt{p^2+q^2}}{\sqrt{p_o^2+q_o^2}} \quad \text{and} \quad q_n = q_o \frac{\sqrt{p^2+q^2}}{\sqrt{p_o^2+q_o^2}}, \tag{77}$$

where p_n and q_n are the components of the gradient of a surface element oriented to be maximally illuminated by the adjusted light source. If there are no further adjustments of source position, the reflectance map in the specified region becomes,

$$R(p, q) = \frac{1 + (p_o p + q_o q)\,(\sqrt{p^2+q^2} \,/\, \sqrt{p_o^2+q_o^2})}{(1+p^2+q^2)}. \tag{78}$$

Adjustment of the Azimuth of the Source

Next, Brassel observed that ridge and stream lines become indistinct when their direction was more or less aligned with a direction toward the source. Opposite faces of a mountain or valley may end up with similar gray values when the cosine of the incident angle is similar for the two, even though they have quite different surface orientations. Maximum contrast occurs when a linear feature lies at right angles to the direction of the incident light, and Brassel therefore moves the light source in azimuth towards the local direction of steepest ascent or descent (whichever is closer).

The amount of adjustment depends on two parameters (see Fig.14). The maximum amount

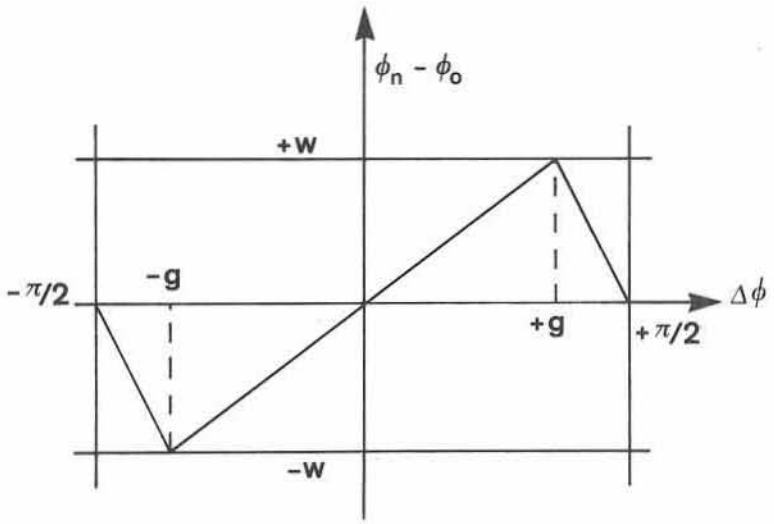

Figure 14: Sawtooth function giving adjustment of azimuth of the light source as a function of the angle between "regional" ridge and valley directions and the direction of the light source in Brassel's scheme.

of adjustment is specified by w (55° for example), while the azimuth difference at which this maximum occurs is specified by g (80° for example). The details of the computation are not very important but are given here for completeness. First, the azimuth of the direction of steepest ascent is computed using

$$\varphi = \text{atan}(-q,-p), \tag{79}$$

where atan(y,x) is the direction of the line from the origin to the point (x,y) measured counterclockwise from the x-axis. Next, the difference between φ and the azimuth of the source φ_0 is reduced to the range $-\pi/2$ to $+\pi/2$ by adding or subtracting integer multiples of π. Let the result be $\Delta\varphi$. The adjusted azimuth of the source is then calculated as follows,

$$\varphi_n = \varphi_0 + w\ \text{sign}(\Delta\varphi)\ \min\left[\frac{|\Delta\varphi|}{g},\ \frac{\pi/2-|\Delta\varphi|}{\pi/2-g}\right], \tag{80}$$

where sign $(\Delta\varphi)$ is $+1$ when $\Delta\varphi > 0$, and -1 when $\Delta\varphi < 0$. Now one can calculate the gradient (p_n, q_n) of the maximally illuminated surface element, or instead, use Wiechel's formula to get the cosine of the incident angle directly,

$$R'(\theta,\varphi) = \cos\theta_n \cos\theta + \sin\theta_n \sin\theta \cos(\varphi-\varphi_n). \tag{81}$$

Here it should be pointed out that in Brassel's scheme the gradient (p, q) used in the above formulas for adjusting the azimuth of the source is a *regional* value derived from ridge and stream lines in the area near a particular point. In this way the cartographer can influence the final appearance of the shaded overlay by altering these *manually* entered linear features. This method involves rather complicated global calculations that do not lend themselves to implementation in the straightforward way we have discussed. The apparent brightness of a surface element depends on both its orientation and some function of its surround.

A possible objection to this idea is that the distribution of light sources does not vary from place to place in a real imaging situation unless the sources are very close to the surface. It must be pointed out, however, that people seem to have little difficulty interpreting synthetic images where the assumed light source position varies. In fact, few notice such drastic changes in assumed light source position as are apparent in a recent map of the polar regions of Mars [150]. This may be related to the fact that our perception of shaded images does not give us a good appreciation for global differences in depth, instead giving us an excellent appreciation of local surface orientation patterns.

Whatever the merits of this argument, the above method can be modified to fit in with the notion of the reflectance map, as defined earlier, if one uses the *local* gradient (p, q) in the calculation of the adjusted source position. The illustration shown here uses this modified version. Note that in Brassel's scheme the adjustment in azimuth and zenith angle of the source are independent and can be carried out in either order.

Brassel also adjusted the apparent brightness according to the height of the terrain. This is a simple local computation that can be easily added to any of the basic methods presented here. It was not included here to simplify comparisons.

Alternate Light Source Adjustment Method

Brassel used a piecewise linear adjustment in azimuth. A similar effect can be achieved using a smoothly varying function like

$$\sin \delta\varphi = (\beta/2) \sin 2(\varphi - \varphi_0) = \beta \sin(\varphi - \varphi_0) \cos(\varphi - \varphi_0) . \tag{82}$$

That is,

$$\sin \delta\varphi = \beta \frac{(p_0 q - q_0 p)(p_0 p + q_0 q)}{(p^2 + q^2)(p_0^2 + q_0^2)} . \tag{83}$$

Adjusting the azimuth of the source by $\delta\varphi$ leads to a new position specified by,

$$p_S = p_0 \cos \delta\varphi - q_0 \sin \delta\varphi \quad \text{and} \quad q_S = p_0 \sin \delta\varphi + q_0 \cos \delta\varphi . \tag{84}$$

Adjustment is complete for small angles when $\beta = 1$. The use of trigonometric functions is avoided in the above calculation, since both the sine and the cosine of $\delta\varphi$ can be computed without them.

Next we turn to the adjustment in the elevation of the source. To avoid the peculiar phenomena of the lowering of the source even for surface elements turned *away* from it, we adjust the elevation according to the projection of the surface normal on a plane containing the source. When $(p_S p + q_S q) > (p_S^2 + q_S^2)$,

$$p_n = p_S \frac{p_S p + q_S q}{p_S^2 + q_S^2} \quad \text{and} \quad q_n = q_S \frac{p_S p + q_S q}{p_S^2 + q_S^2} . \tag{85}$$

In this region then the reflectance map becomes,

$$R(p, q) = \frac{\sqrt{1 + (p_S p + q_S q)^2 / (p_S^2 + q_S^2)}}{\sqrt{1 + p^2 + q^2}} , \tag{86}$$

otherwise it is calculated as before, that is, the cosine of the incident angle is

$$R(p, q) = \frac{1 + p_n p + q_n q}{\sqrt{1 + p^2 + q^2}\ \sqrt{1 + p_n^2 + q_n^2}} . \tag{87}$$

The advantage of the above method of adjustment is that simple calculations in terms of the components of the gradient replace trigonometric equations in terms of azimuth and zenith angles.

Wiechel's Projected Incident Angle

The first serious analysis of an approach based on the shading seen on the surface of an obliquely illuminated matte object is that of Wiechel [8]. He started by assuming a perfectly diffusing surface and proposed connecting points of equal apparent brightness by isophotes. He correctly determined the brightness of a perfect diffuser as already mentioned. In order to make calculations less unwieldy he also suggested three approximations, the second of these being the

contour-terrace model already discussed. His *first* method involved approximating the cosine of the incident angle, i, by the cosine of i', the projection of this angle onto a vertical plane lying parallel to the rays (see Fig.15). By applying the analogue formulas to the lower spherical triangle (see Fig.16) we get,

$$\sin i' \cos i = \cos i' \sin i \cos \chi . \tag{88}$$

Applying the analogue formulas next to the whole triangle we get

$$\sin i \cos \chi = \cos \theta \sin \theta_o - \sin \theta \cos\theta_o \cos (\varphi - \varphi_o) . \tag{89}$$

The second equation allows us to eliminate χ from the first and obtain an expression for $\tan i'$. Using the identity

$$\cos i' = \frac{1}{\sqrt{1 + \tan^2 i'}} , \tag{90}$$

we finally find,

$$R'(\theta,\varphi) = \frac{\cos i}{\cos \theta \sqrt{1 + \tan^2\theta \cos^2(\varphi-\varphi_o)}} , \tag{91}$$

where, using the cosine formula as before,

$$\cos i = \cos \theta \cos \theta_o + \sin\theta \sin \theta_o \cos(\varphi-\varphi_o) . \tag{92}$$

Alternatively one can project the vector $\mathbf{n}=(-p,-q,1)$ onto the plane with normal $\mathbf{s}=(q_o,-p_o,0)$. The result will equal,

$$\mathbf{n}' = \mathbf{n} - (\mathbf{n} \cdot \mathbf{s}) \frac{\mathbf{s}}{s^2} , \tag{93}$$

where s is the magnitude of the vector s. This projected vector will be perpendicular to the line in which a vertical plane including the light source cuts the surface:

$$\mathbf{n}' = \frac{1}{p_o^2+q_o^2} [-p_o(p_o p+q_o q) , -q_o(p_o p+q_o q) , p_o^2+q_o^2] . \tag{94}$$

Taking the dot-product of the projected vector and the vector pointing at the source, then dividing by their magnitudes we find,

$$R(p, q) = \frac{1+p_o p+q_o q}{\sqrt{1+p_o^2+q_o^2}\sqrt{1+(p_o p+q_o q)^2/(p_o^2+q_o^2)}} . \tag{95}$$

This matches the expression for perfectly diffuse reflection for values of (p, q) along the line from the origin to the source point (p_o, q_o). When the source is in the standard position the equation becomes

$$R(p, q) = \frac{1 + (p-q)/\sqrt{2}}{\sqrt{2}\sqrt{1 + (p-q)^2/2}} . \tag{96}$$

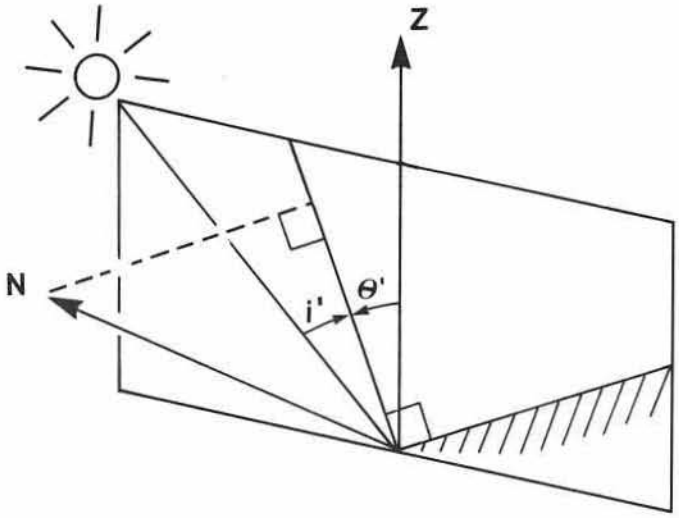

Figure 15: Projection of the surface normal on a vertical plane containing the assumed light-source. The projected normal is perpendicular to the line in which the plane cuts the terrain surface.

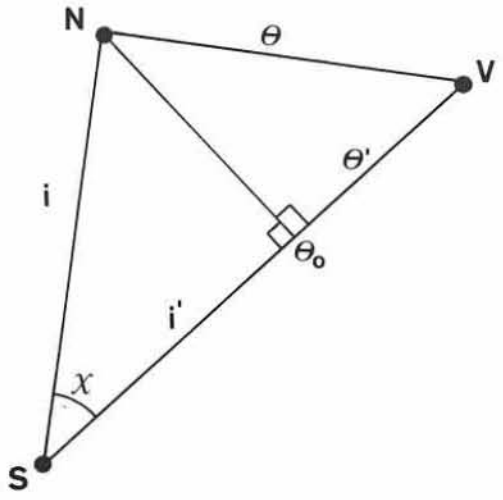

Figure 16: Spherical triangles used to calculate the projected incident angle, i', and the projected surface inclination, θ'. The direction towards the viewer is V, the direction to the source is S, while the surface normal is N.

While these equations are more complicated than the original equations for the cosine of the incident angle, i, it must be pointed out that the angle i' can be estimated graphically by measuring the contour interval in a direction parallel to the incident light rays. The same is true of Wiechel's second approximation introduced earlier. This greatly simplifies the manual construction of shaded maps from contour maps, and makes it possible to use a simple one-dimensional scale for brightness instead of Wiechel's more elaborate "Helligkeitsmaassstab". This property manifests itself in the reflectance map by the appearance of parallel straight line contours. It is also interesting to note that Wiechel's "approximations" produces results that seem better than those obtained using the equation for the perfect diffuser. Unfortunately, experimentation at his time was limited because of the lack of appropriate technology for systematically generating continuous tone patterns. Apparently no maps made by this method were ever published [1].

Wiechel's Modified Brightness

Finally, Wiechel postulated a material that would *not* appear equally bright from all viewing directions, but instead had brightness varying as the cosine of the emittance angle. This was used in part to discuss the relationship between the contour-terrace model and the original surface, but also put forward as a third, "modified brightness" model that might be used in calculating gray tone. In this case brightness varies in proportion to ($\cos i \cos e$). We can normalize his result here by dividing by the maximum of this product, $\cos^2(g/2)$, where g is the so-called phase angle, here equal to θ_0 (The term phase angle stems from work on lunar photometry, where this angle equals the phase of the moon). Then,

$$R(p, q) = 2\,\frac{\cos i \cos e}{1 + \cos g} \tag{97}$$

or,

$$R(p, q) = \frac{2\,(1+p_0 p+q_0 q)}{(1+\sqrt{1+p_0^2+q_0^2})\,(1+p^2+q^2)}\,. \tag{98}$$

Incidentally, this function does not satisfy Helmholtz's reciprocity law [124], and therefore cannot correspond to the reflectance of any real surface illuminated by a point source.

Marsik's Automatic Relief Shading

Blachut and Marsik further modified Wiechel's approximation, partly as a result of their dissatisfaction with the fact that a horizontal surface does not appear white when a perfectly diffusing material is assumed [58],[59]. This may have stemmed in part from early conventions in map-making where horizontal surfaces were portrayed without hachures [4]–[6]. Marsik also aimed for simpler calculations and considered the slope in the direction towards the source. For some reason, he proposed making the *density* of the printed result equal to the tangent of the projected slope angle θ' (see Fig. 15). Density is the logarithm (base 10) of the reciprocal of the

reflectance. Applying the analogue rule to the upper spherical triangle (see Fig. 16) one can show that,

$$0 = \cos\theta \sin\theta' - \sin\theta \cos\theta' \cos(\varphi - \varphi_0) . \tag{99}$$

Thus,
$$\tan\theta' = \tan\theta \cos(\varphi - \varphi_0), \tag{100}$$

and,
$$R'(\theta,\varphi) = 10^{\tan\theta \cos(\varphi - \varphi_0)} . \tag{101}$$

Using the expression for the projected normal $\mathbf{n}'$ developed in the last section, or, remembering the expression for the slope in the direction (p_0, q_0), one can also show,

$$R(p, q) = 10^{(p_0 p + q_0 q)/\sqrt{p_0^2 + q_0^2}} . \tag{102}$$

When $(p_0 p + q_0 q) > 0$, $R(p, q) > 1$ and so all surfaces facing towards the light source are white. No information is available to the viewer regarding surface shape in these areas. If the assumed light source is in the standard position we get the simple formula,

$$R(p, q) = 10^{(p-q)/\sqrt{2}} . \tag{103}$$

Marsik also limited the density to a maximum of 0.7 to avoid interference with planimetric information on the map.

Lommel-Seeliger Law

Many surfaces have reflectance properties that differ greatly from those of an ideal diffuser. The photometry of rocky planets and satellites has intrigued astronomers for many years [121]–[130]. Several models have been proposed to explain the observed behavior. One of the earliest, developed by Lommel [119] and modified by Seeliger [120], is based on an analysis of primary scattering in a porous surface [126],[128]. Their model consists of a random distribution of similar particles suspended in a transparent medium and results in a reflectance function that is given here in its simplest form,

$$\frac{1}{1 + (\cos e/\cos i)} , \tag{104}$$

unless $\cos i < 0$, when the surface is self shadowed. Here i is the incident angle, and e is the emittance angle, the angle between the local surface normal and the direction to the viewer, here equal to θ. The expression equals $1/(1+\cos g)$ when $i=0$, where g is the phase angle, here equal to θ_0. Using this value for normalization and remembering the expression for $\cos i$ one finds,

$$R'(\theta,\varphi) = \frac{1 + \cos\theta_0}{1 + \cos\theta/(\cos\theta\cos\theta_0 + \sin\theta\sin\theta_0\cos(\varphi - \varphi_0))} \tag{105}$$

or

$$R(p\,q) = \frac{1 + 1/\sqrt{1+p_o^2+q_o^2}}{1 + \sqrt{1+p_o^2+q_o^2}\,/\,(1+p_o p+q_o q)}, \tag{106}$$

unless $(1+p_o p+q_o q) < 0$, when $R(p, q)=0$. When the source is in the standard position,

$$R(p, q) = \frac{(1+1/\sqrt{2})\,[1 + (p-q)/\sqrt{2}]}{(1+\sqrt{2}) + (p-q)/\sqrt{2}}. \tag{107}$$

The Lommel-Seeliger law has been used in automated relief shading by Batson, Edwards and Eliason [70].

Based on detailed measurements and modeling, Fesenkov [123],[127] and later Hapke [128]−[130] further improved the equations for the reflectance of the material in the *maria* of the moon. Hapke imagined the surface as an open porous network into which light can penetrate freely from any direction. His result has three components: the Lommel-Seeliger formula for reflection from a surface layer containing many scattering points of low reflectance, Schönberg's formula [122] for reflection from a Lambertian sphere and a complicated factor resulting from mutual obscuration of the particles. The results of such investigations are often expressed in terms of angles other than the ones introduced so far. The Lommel-Seeliger law, for example, can be expressed in a way which simplifies the problem of calculating the shape of the lunar surface from shading in a single image [137],[138],[151]. The angles needed, luminance longitude and luminance latitude, are defined in Appendix D.

Minnaert's Reflectance Function

Minnaert discusses a large variety of models for the reflection of light from rough surfaces [126]. He also proposed a class of simple functions of the form,

$$\cos^{\kappa} i\, \cos^{\kappa-1} e \tag{108}$$

intended to fit observations of the radiance of lunar material while obeying the reciprocity law [124]. Here κ is a parameter to be chosen so that the best fit with experimental data is obtained. This parameter is meant to lie between zero and one, with the above expression becoming equal to that for the perfect diffuser when $\kappa=1$. We can normalize this expression so it equals one when $i=0$,

$$R(p, q) = \frac{\cos^{\kappa} i \cos^{\kappa-1} e}{\cos^{\kappa-1} g} \tag{109}$$

$$R(p, q) = \left[\frac{1+p_o p+q_o q}{1+p^2+q^2}\right]^{\kappa} \frac{\sqrt{1+p^2+q^2}}{\sqrt{1+p_o^2+q_o^2}}. \tag{110}$$

Particularly Simple Reflectance Maps

Several methods discussed here have reflectance depending only on the slope in the direction

away from the assumed light source, leading to parallel straight line contours in the reflectance map. These include Wiechel's first and second "approximation", Tanaka's relief contour method, the "law" of Lommel and Seeliger, Minnaert's formula when $\kappa = \frac{1}{2}$, as well as Marsik's automatic relief shading. These methods are quite effective in producing overlays that are easy to interpret. One can construct more such reflectance maps, including some that are even easier to calculate. One possibility, for example, is,

$$R(p, q) = \frac{1}{2}[1 + \frac{p' + a}{b}] \tag{111}$$

where,

$$p' = \frac{p_o p + q_o q}{\sqrt{p_o^2 + q_o^2}} \tag{112}$$

is the slope in the direction away from the source. Values less than or equal to zero correspond to black, while values greater than or equal to one correspond to white. The parameters a and b allow one to chose the gray value for horizontal surfaces and the rapidity with which the gray values changes with surface inclination. The simple program shown earlier (see Fig. 5) uses this form with $a=0$, $b=1/\sqrt{2}$ and $p_o = 1/\sqrt{2}$, $q_o = -1/\sqrt{2}$.

A simple alternative, where all possible slopes are mapped into the range from zero to one is,

$$R(p, q) = \frac{1}{2} + \frac{1}{2} \frac{p'+a}{\sqrt{b^2 + (p'+a)^2}}. \tag{113}$$

This has the advantage that the reflectance does not saturate for any finite slope and all changes of inclination in the vertical plane including the source translate into changes in gray level.

Another way to achieve this effect is the following, somewhat reminiscent of Lehmann's approach,

$$R(p, q) = \frac{1}{2} + \frac{1}{\pi} \tan^{-1}[\frac{\pi}{2} \frac{p' + a}{b}]. \tag{114}$$

These three formulas are given in a form where the rate at which the gray value changes with surface inclination is the same at $(p'+a)=0$.

Glossiness - The First Off-Specular Angle

Not all surfaces are matte. Some are perfectly specular or mirror-like. Since smooth, specularly reflecting surfaces form virtual images of the objects around them, patches of high brightness will appear when such a surface is illuminated by an extended source, like a fluorescent light fixture, or by light streaming in through a window. The size of the patches depends on the solid angle subtended by the source as well as the surface curvature, while the brightness distribution is that of the source.

To study reflection of an extended source in a specular surface, it is useful to introduce the "off-specular" angle s between the direction S to the center of the source and the direction S', of the point that is specularly reflected to the viewer (see Fig. 17). This, incidentally, is also the angle between the direction to the viewer V and the direction V' in which the rays from the center of the source are specularly reflected.

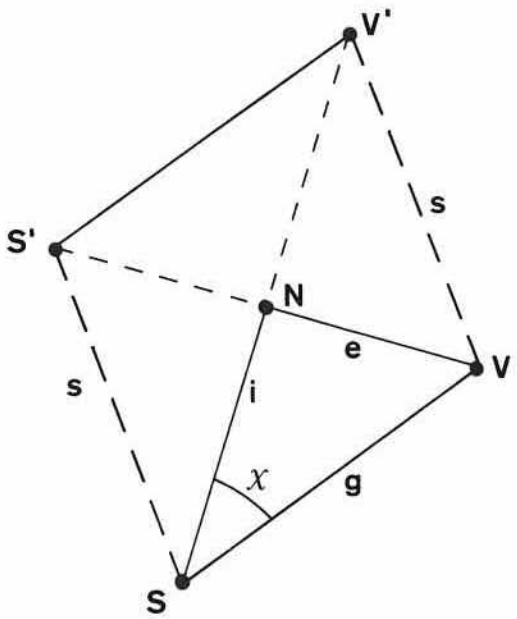

Figure 17: Spherical triangles used to calculate the first off-specular angle, s. It is the angle between S, the center of the source, and S', the direction from which light is specularly reflected towards the viewer. Equivalently, it is the angle between V, the direction of the viewer, and V', the direction in which light from the center of the source is specularly reflected.

We assume a circularly symmetric source, with brightness $L(s)$ at eccentricity s. This is the brightness the viewer observes in the specularly reflecting surface. Calculating the first off-specular angle s is simple using the appropriate spherical triangles:

$$\cos s = \cos 2i \cos g - \sin 2i \sin g \cos \chi , \tag{115}$$

$$\cos e = \cos i \cos g - \sin i \sin g \cos \chi . \tag{116}$$

Here, i is the incident angle, between the local normal and the direction to the source, $e=\theta$, is the emittance angle, between local normal and the direction to the viewer, while $g=\theta_o$ is the phase angle, between source and viewer. Eliminating χ from the two equations and expanding the sine and cosine of $2i$, one gets,

$$\cos s = 2 \cos i \cos e - \cos g . \tag{117}$$

Substituting expressions in p and q for $\cos i$, $\cos e$ and $\cos g$ one can rewrite this as,

$$\cos s = \frac{2\,(1+p_o p+q_o q)/(1+p^2+q^2) - 1}{\sqrt{1+p_o^2+q_o^2}} . \tag{118}$$

This result can also be obtained simply by finding the direction S' from which a ray must come to be specularly reflected to the viewer V, by a surface element with normal N.

$$S' = 2(V \cdot N)N - V \tag{119}$$

where $V=(0, 0, 1)$. The off-specular angle is the angle between S' and the center of the source S so

$$\cos s = S \cdot S' = 2(S \cdot N)(V \cdot N) - (S \cdot V). \tag{120}$$

Note that the cosine of the first off-specular angle can be calculated easily, without using trigonometric functions. The contours of constant $\cos s$ turn out to be nested circles in gradient space, with centers lying on the line from the origin to the point (p_0, q_0). This can be seen by noting that the locus of the point S', for constant s, is a circle about the point S and that circles on the Gaussian sphere give rise to circles in gradient space when projected stereographically [138].

The cosine of the off-specular angle s equals one when conditions are right for specular reflection, that is, when $e=i$ and $g=i+e$. This can be seen by setting $e=i=g/2$ in the trigonometric expression for $\cos s$.

Bui-Tuong's Formula - Specular Surface, Extended Source

Having seen how to calculate the off-specular angle s, we can now make a reflectance map, by assigning the distribution of source brightness $L(s)$. This function should be nonnegative monotonically decreasing with s, and equal to one when $s=0$. For ease of calculation one choice might be

$$L(s) = \cos^n (s/2) = [\tfrac{1}{2} (1 + \cos s)]^{n/2} \tag{121}$$

where n is a number that defines how compact the bright patch is (a useful value might be around 20). So far, we have developed the reflectance map for a specular surface and a circularly symmetric source. Many surfaces, such as glazed pottery or smooth plastic, have both glossy and diffuse components reflection. Specular reflection takes place at the smooth interface between two materials of different refractive index, while the matte component results from scattering of light that penetrates some distance into the surface layer.

We can combine these two components as follows

$$R(p, q) = [(1 - \alpha) + \alpha L(s)] \frac{\cos i}{\cos(g/2)} \tag{122}$$

where α determines how much of the incident light is reflected specularly. The expression is scaled so that its maximum is (approximately) equal to one. Here we have assumed the source, while distributed, is compact enough so that the diffuse reflection component can be approximated as $\cos i$. The above expression obeys the reciprocity law of Helmholtz [124] which applies to real surfaces illuminated by a point source. Bui-Tuong used a reflectance function

similar to the one derived above in his computer graphics work [113]. He apparently tried to model reflection from a surface that is not perfectly smooth. This requires a *different* off-specular angle however, as will be seen in the next section.

Luster - The Second Off-Specular Angle

Refulgency, gloss or shine can also appear when a point source is reflected in a surface that is not perfectly smooth. When a slightly uneven surface, of a material that gives rise to metallic or dielectric reflection, is illuminated by a point source, bright patches will be seen surrounding points where the local tangent plane is oriented correctly for specular reflection. The size of these patches will depend on the roughness of the surface and the surface curvature, while the distribution of brightness will depend to some extent on the texture of the microstructure of the surface.

In this case we will need to calculate the second off-specular angle s' between the local normal N and the normal N' oriented for specular reflection of rays from the source S towards the viewer V (see Fig. 18). By considering the appropriate spherical triangles one finds,

$$\cos s' = \cos i \cos(g/2) - \sin i \sin(g/2) \cos \chi , \tag{123}$$

$$\cos e = \cos i \cos g - \sin i \sin g \cos \chi . \tag{124}$$

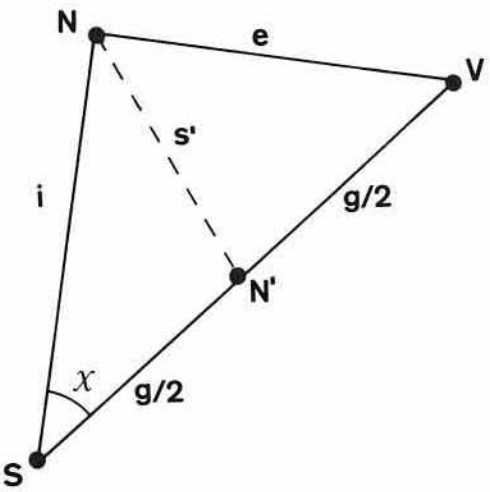

Figure 18: Spherical triangles used to calculate the second off-specular angle, s'. It is the angle between the actual surface normal, N, and a surface normal, N', oriented to specularly reflect rays from the source towards the viewer.

Eliminating χ from the two equations and expanding the sine and cosine of the phase angle g, one finds,

$$\cos s' = \frac{\cos i + \cos e}{2 \cos (g/2)} \tag{125}$$

or

$$\cos s' = \frac{\cos i + \cos e}{\sqrt{2}\sqrt{1 + \cos g}}. \tag{126}$$

This result can also be obtained by finding the vector N', normal to a surface element oriented to specularly reflect a ray from the source in the direction of the viewer V. That is,

$$N' = \frac{S + V}{|S + V|}. \tag{127}$$

The off-specular angle is the angle between the actual surface normal N, and the vector N'

$$\cos s' = N \cdot N' = \frac{(S \cdot N) + (V \cdot N)}{\sqrt{2}\sqrt{1 + (S \cdot V)}}. \tag{128}$$

The surface microstructure of an uneven surface can be modeled by many randomly disposed mirror-like facets, too small to be optically resolved, each turned a little from the average local surface orientation. One can define a distribution $P(s')$ describing what fraction of these microscopic facets are turned away from the average local normal by an angle s'. For ease of calculation one choice might be,

$$P(s') = \cos^n s'. \tag{129}$$

Blinn's Formula - Rough Surface, Point Source

One can use the fact that a normal N' oriented for specular reflection of the point source towards the viewer, lies in the direction $(-p_1, -q_1, 1)$, where

$$p_1 = -\cos \varphi_o \tan (\theta_o/2) \quad \text{and} \quad q_1 = -\sin \varphi_o \tan (\theta_o/2). \tag{130}$$

We can also find N' by normalizing the vector $(S+V)$, so that its third component equals 1:

$$p_1 = \frac{p_o}{1 + \sqrt{1+p_o^2+q_o^2}} \quad \text{and} \quad q_1 = \frac{q_o}{1 + \sqrt{1+p_o^2+q_o^2}}. \tag{131}$$

A surface with gradient (p_1, q_1) is oriented just right to specularly reflect a ray from the source to the viewer. This can be seen by noting that when $p=p_1$ and $q=q_1$, then

$$\cos i = \cos e = \frac{1}{\sqrt{1+p_1^2+q_1^2}} \tag{132}$$

and,

$$\cos g = \frac{2}{1+p_1^2+q_1^2} - 1. \tag{133}$$

In any case,

$$\cos s' = \frac{1+p_1 p+q_1 q}{\sqrt{1+p^2+q^2}\,\sqrt{1+p_1^2+q_1^2}}. \tag{134}$$

Note that s' will tend to be (roughly) half of s when both angles are small. Combining matte components of surface reflection with those from the rough outer surface we get,

$$R(p, q) = [(1-\alpha) + \alpha P(s')]\,\frac{\cos i}{\cos(g/2)}. \tag{135}$$

The above reflectance map also obeys Helmholtz's reciprocity law and is normalized so that its maximum is (approximately) equal to one. Blinn and Newell give a similar reflectance function, claiming it was what Bui-Tuong had proposed [114]. The two are not the same however since the two off-specular angles are different; in fact, the contours of constant s' are nested ellipses in gradient space, while, as mentioned earlier, the contours of constant s are nested circles. Indeed, Bui-Tuong's model corresponds to reflection of an extended, rotationally symmetric source in a specular surface, while the model presented in this section applies to reflection of a point source in a rough surface.

Blinn and Newell's Model for Specular Surfaces

One of the methods discribed by Blinn and Newell [114] assumes a perfectly specular surface in which the world surrounding the object is reflected. To make computations feasible, they imagine the surrounding objects at a distance great enough so that each part of the surround appears to lie in essentially the same direction from every point of the surface of the object. In this case one can imagine the brightness distribution of the surrounding objects projected onto the inside of a large sphere. The gray value used for a particular surface patch then is found by computing the direction S' from which a ray must come to be specularly reflected to the viewer V, by a patch with surface normal N. We have already seen that,

$$S' = 2\,(V \cdot N)\,N - V. \tag{136}$$

The appropriate gray value is then determined from the spherical distribution of brightness. In practice the sphere is mapped onto a plane by calculating the zenith angle, θ_0 and azimuth, φ_0 of S' [114]. The brightness distribution can be equally well specified in gradient space [138], since it is also a projection of the Gaussian sphere.

Surface models incorporating randomly dispersed mirror-like facets were first studied in the 1700's. This type of microstructure has been investigated extensively since then, despite the difficulties of reasoning about the three-dimensional nature of reflection from such surfaces. Recently, Torrance and Sparrow further elaborated on these models [134],[135] in order to match more closely experimental data showing maximum brightness for angles of reflection *larger* than the incident angle. They included in their considerations the effects of obstruction of the incident and emergent rays by facets near the one reflecting the ray. Blinn simplified and explained their calculations [115] and used them in producing shaded images of computer models of various

objects. The overall result can be broken into a product of three terms, one dependent on the distribution of facet orientations, the second being the formula for Fresnel reflection from a flat dielectric surface, while the third is the geometric attenuation factor accounting for partial occlusion of one facet by another. We will not discuss these models in any more detail here.

Models for glossy or lustrous reflection have been used with great success in computer graphics to increase the impression of realism the viewer has when confronted with a synthetic picture of objects represented in the computer. Unfortunately, these methods do not seem to improve the presentation of surface shape for cartographic purposes.

Colored Shading

It is often said that quantitative information about the surface cannot be obtained from relief shading [1]. Contour lines on the other hand do allow measurements of elevation and estimation of the gradient. Shading does provide *some* information about the gradient too, but cannot be used to determine both of its components locally, since only one measurement is available at each point. Since we can perceive the shape of objects portrayed by shaded pictures, it seems that these local constraints do lead to a *global* appreciation of shape, apparently based on our assumption that the surface is continuous and smooth.

If two shaded images, produced with the assumed light source in different positions, were available however, two measurements could be made at each point allowing one to determine the gradient *locally* [141]. It is inconvenient to work with two shaded overlays; fortunately though, they can be combined by printing them in different colors. In fact, yet another overlay can be added in a third color, but it adds no new information, since the two components of the gradient are already fully determined by the first two.

Colored shading corresponds to illumination by multiple sources, each of a different color. The exact color at each point in the printed result is uniquely related to the gradient at that point. Thus quantitative information *is* available in this new kind of map overlay. Further, ambiguities present in black and white presentations disappear. By positioning the light sources properly, one can avoid problems occasioned by the accidental alignment of ridge or stream lines with the direction of incident light. Thus the need for *ad hoc* adjustments of the azimuth of the assumed light source is removed.

Colored shading is easy to interpret in terms of surface shape and effective in portraying surface form. It is unlikely however that it will be widely used because of the added expense of printing and conflict with existing uses of color in cartography to distinguish various kinds of planimetric information. Amongst other things, color is now used to code height and surface cover. Further, yellow is used in ordinary shading for sun-facing slopes, while violet is used for shaded regions [152]. This is thought to simulate the increased sky illumination component in areas turned away from the sun.

Summary and Conclusions

After a brief review of the history of hill-shading an efficient method for providing shaded overlays was described. It depends on a lookup table containing sampled values of the reflectance

map. Traditional, manual methods were explored in terms of their equivalent reflectance maps, as were phenomenonlogical models used in the computer graphics community. Methods that have been proposed for mechanizing the generation of relief shading were also treated. The automated method described here is very flexible, since it can use any reflectance map.

Nine of the reflectance maps described were plotted as contour diagrams (see Fig. 19 and Fig. 21). The first one (A) is independent of the direction of the gradient, depending only on the slope. This gives rise to a rotationally symmetric diagram. Three other diagrams (F, H, and I) show parallel straight lines. These correspond to reflectance maps which depend only on the slope in the direction away from the source. Reflectance maps for perfectly diffusing (C) and glossy (D) surfaces are included too. Tanaka's two methods (B and H), Peucker's approximation (G), Brassel's source adjustment (E), Marsik's method (F), and one of the particularly simple methods (I) complete the set.

Shaded images of five mathematically defined surfaces, cone, circular wall with triangular cross section, sphere, torus and 'volcano shape', were then created using these reflectance maps (see Fig. 19). Several of the subfigures give one a good appreciation for the shape of the objects. Assumption of a perfectly diffusing surface (C) and Peucker's approximation (G) lead to good results, while the image corresponding to a glossy surfaces (D) is perhaps the most vivid.

Information from digital terrain models of Lake Louise, Gulf Islands, Dent de Morcles and Les Diablerets, is presented in Fig. 20. Histograms of terrain elevation (A) are followed by scattergrams of surface gradient (B). Elevation is shown as brightness in another series of subfigures (C). Contours are shown at two densities (D and E). Finally, the surfaces are shown with brightness decreasing with slope (F).

The nine reflectance maps were then used to make shaded images of the four regions (see Fig. 21). Some reflectance maps appear much better than others in conveying an immediate impression of surface shape. The rotationally symmetric reflectance map (A) corresponding to overhead illumination of the terrain, is not very good, for example. Perfectly diffuse reflectance (C) is not optimal either. In fact, an approximation to the formula for a Lambertian reflector (G) seems to produce better results. Glossy reflectance components (D), while very useful in the portrayal of regular objects, result in tones that are too dark to be useful in a map overlay. We may also not be used to seeing a geographical surface presented in this form.

Marsik's method (F), in which half of the surface is a featureless white, is clearly not very effective. Several of the other methods require careful scrutiny before conclusions about their adequacy can be made. Amongst the best are Wiechel's modified brightness method and the modification of Brassel's method presented here. The methods depending on the slope in the direction away from the light source appear to be quite adequate (H and I). These are to be recommended unless there are good reasons to prefer one of the other methods.

Shaded images were created from several other digital terrain models (see Fig. 22) using one of these simple methods (I). The terrain models differ widely in their quality, resolution and origin. They do show the utility of the methods described here in presenting the information in a digital terrain model to a human observer.

Shading is an important depth cue. The choice of reflectance map should not be based on some *ad hoc* model of surface behavior, experimental measurement of reflectance of some material, or formulas that happen to be easy to calculate. Instead, one should use a reflectance map that gives rise to an immediate, accurate perception of surface shape.

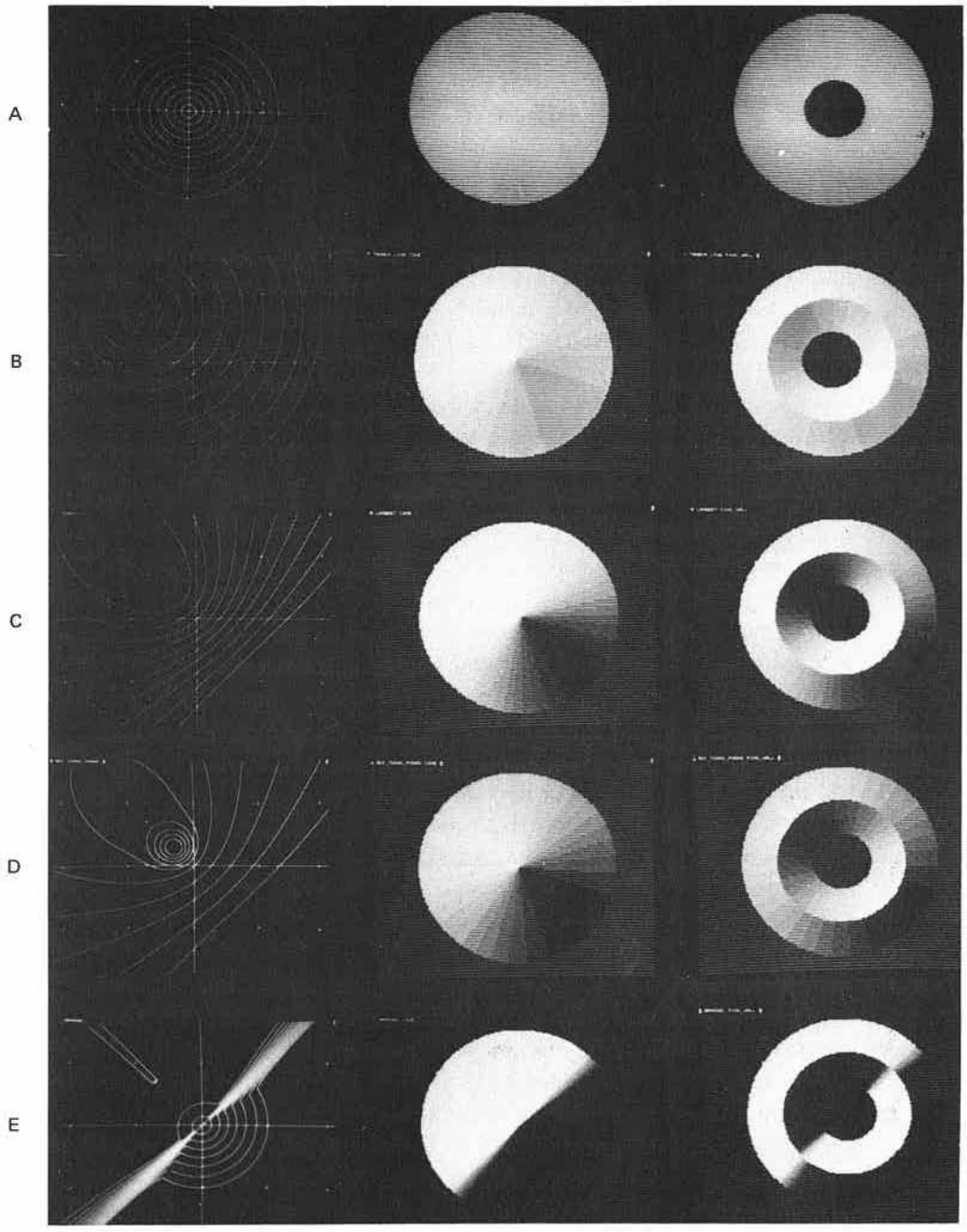

Figure 19

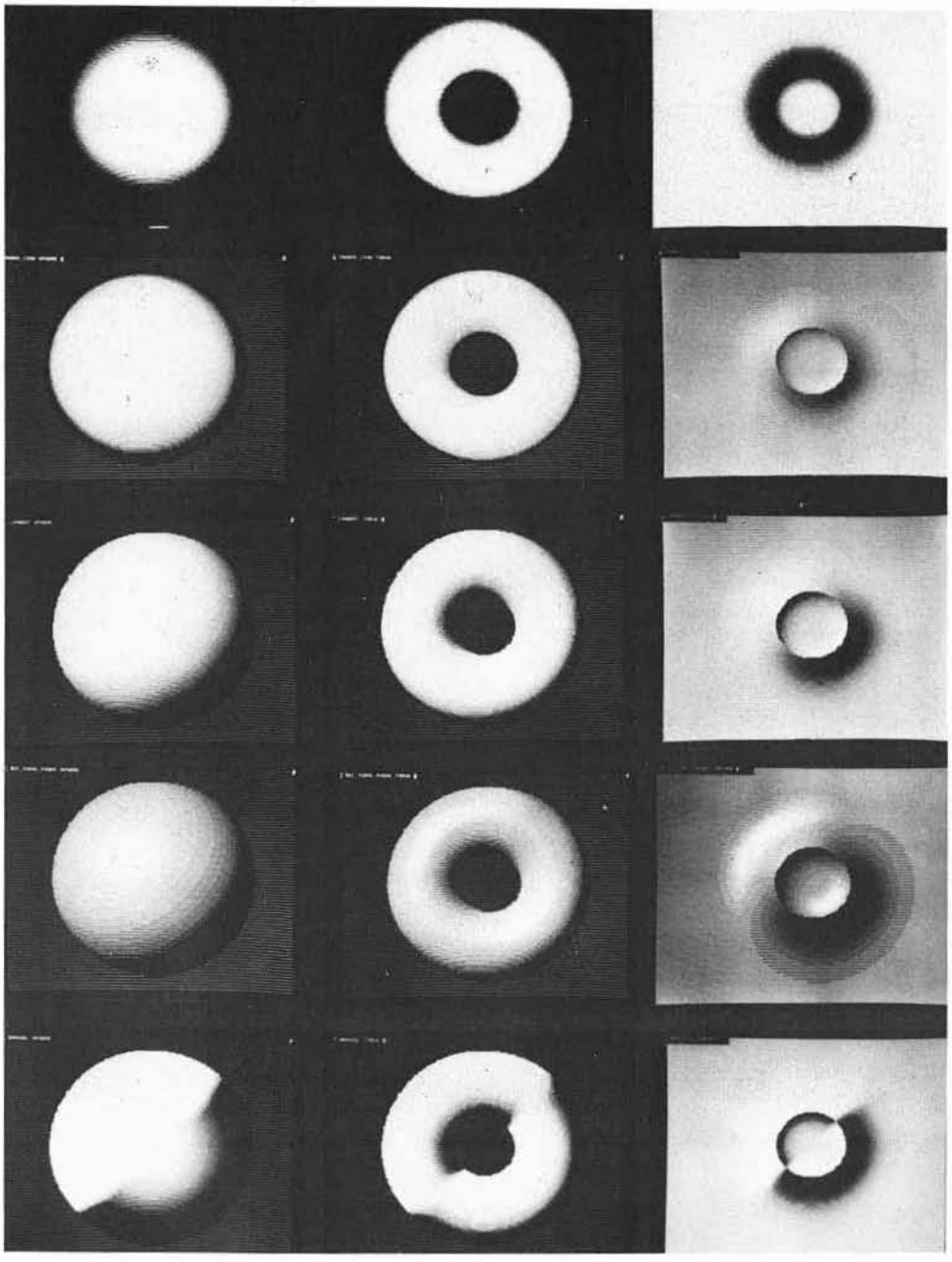

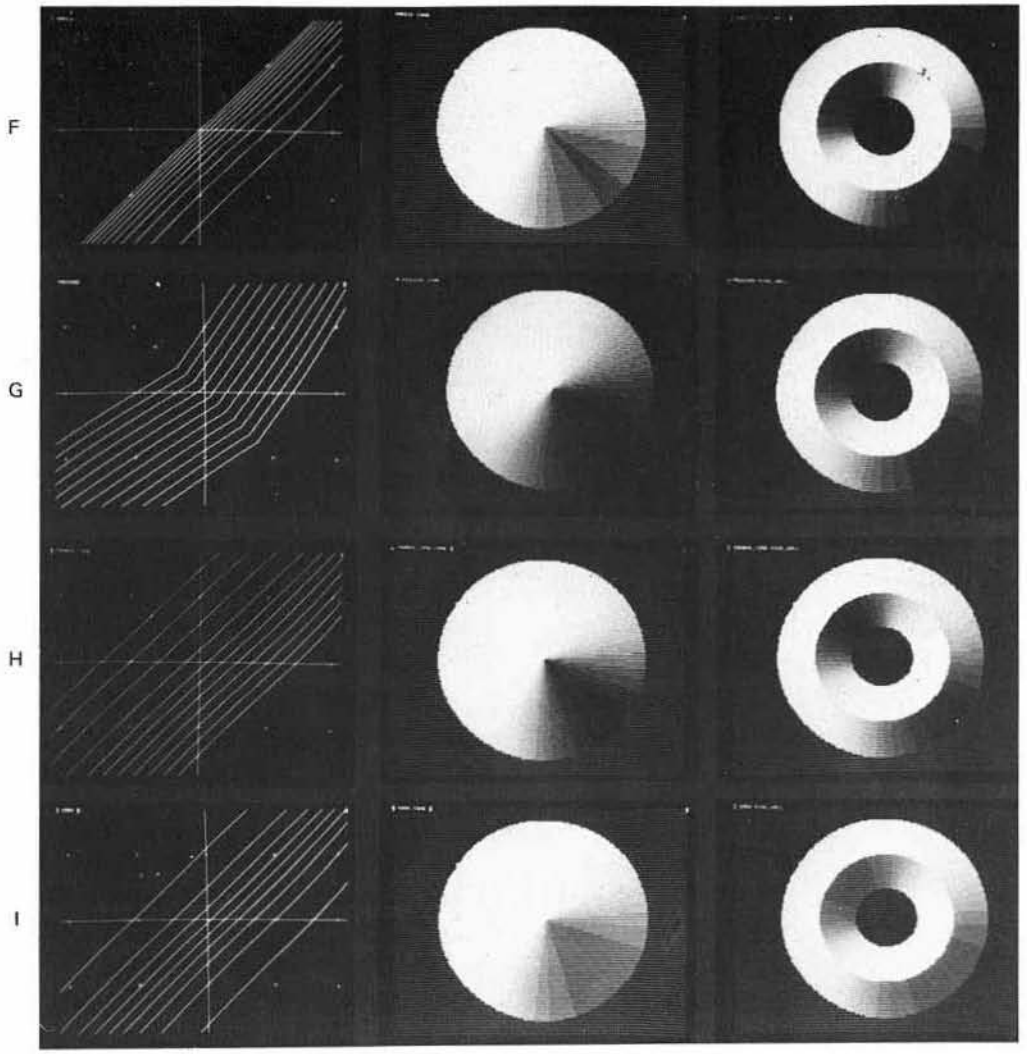
F
G
H
I

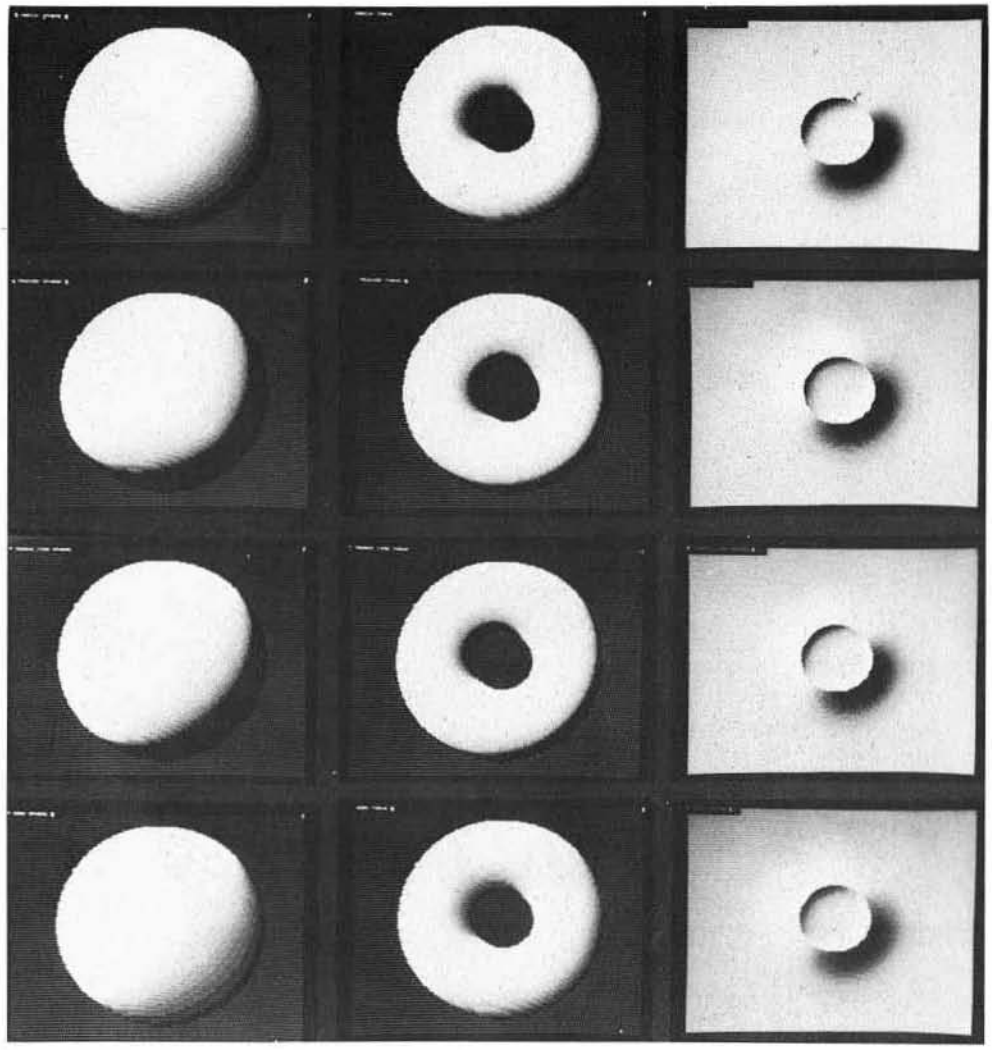

Figure 19: Five geometric figures displayed using nine reflectance maps. Shown in the leftmost column are contour diagrams of the reflectance maps. The remaining five columns show the method applied to a cone, a circular wall with triangular cross section, a sphere, a torus and a 'volcanoe' shape. The reflectance maps are: (A) Lehmann's method, (B) Tanaka's first method, (C) Lambertian, (D) Glossy, (E) Brassel's method, (F) Marsik's method, (G) Peucker's approximation, (H) Tanaka's second method, (I) and a particularly simple method.

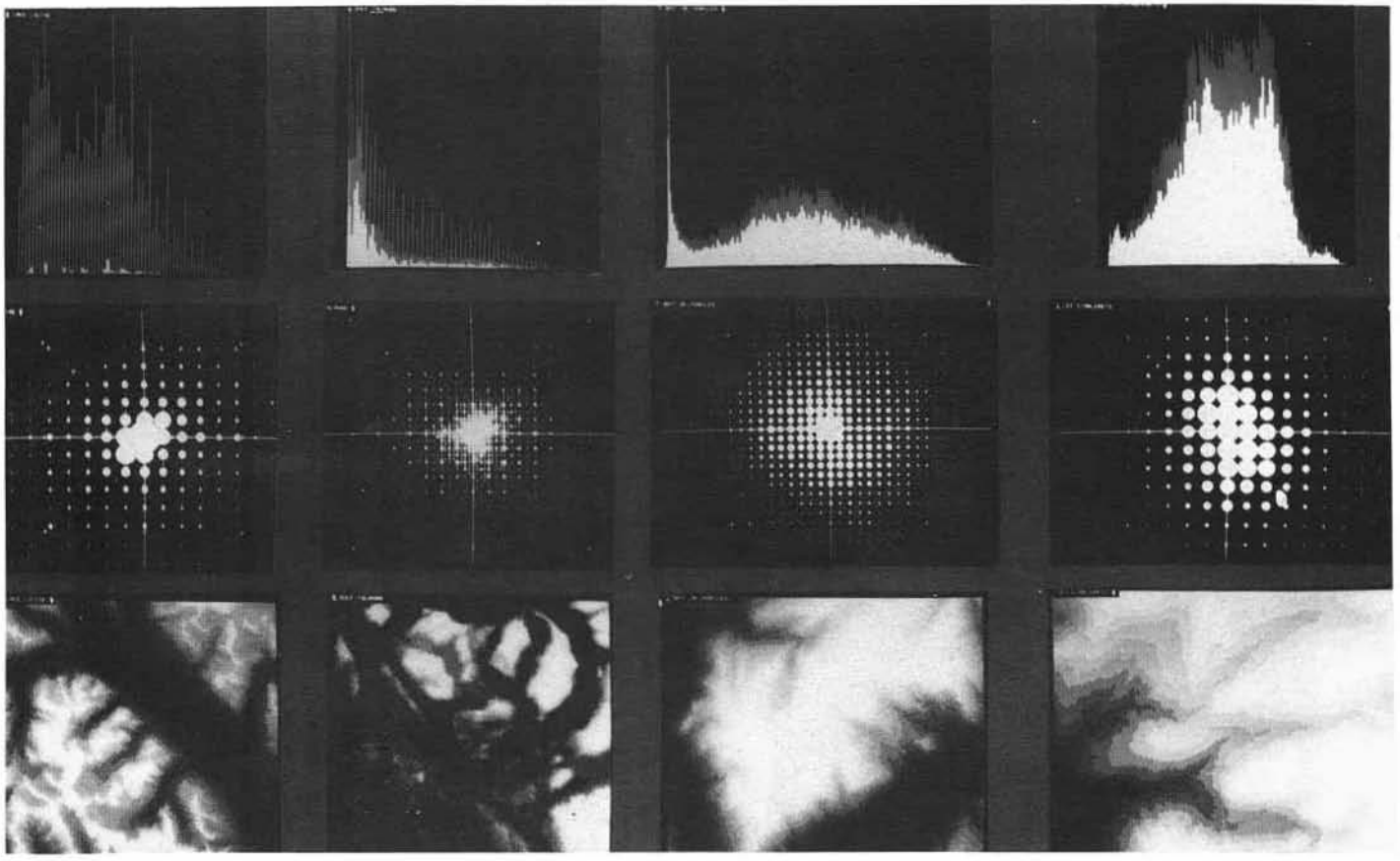

Figure 20: Information about four digital terrain models. The top row shows histograms of elevation, the second row a scattergram of surface gradient. In the third row elevation is coded as brightness, while the next two rows present contour maps. The last row

shows brightness decreasing with increasing slope. The digital terrain models are from left to right: (A) Lake Louise, (B) Gulf Islands, (C) Dent des Morcles, and (D) Les Diablerets.

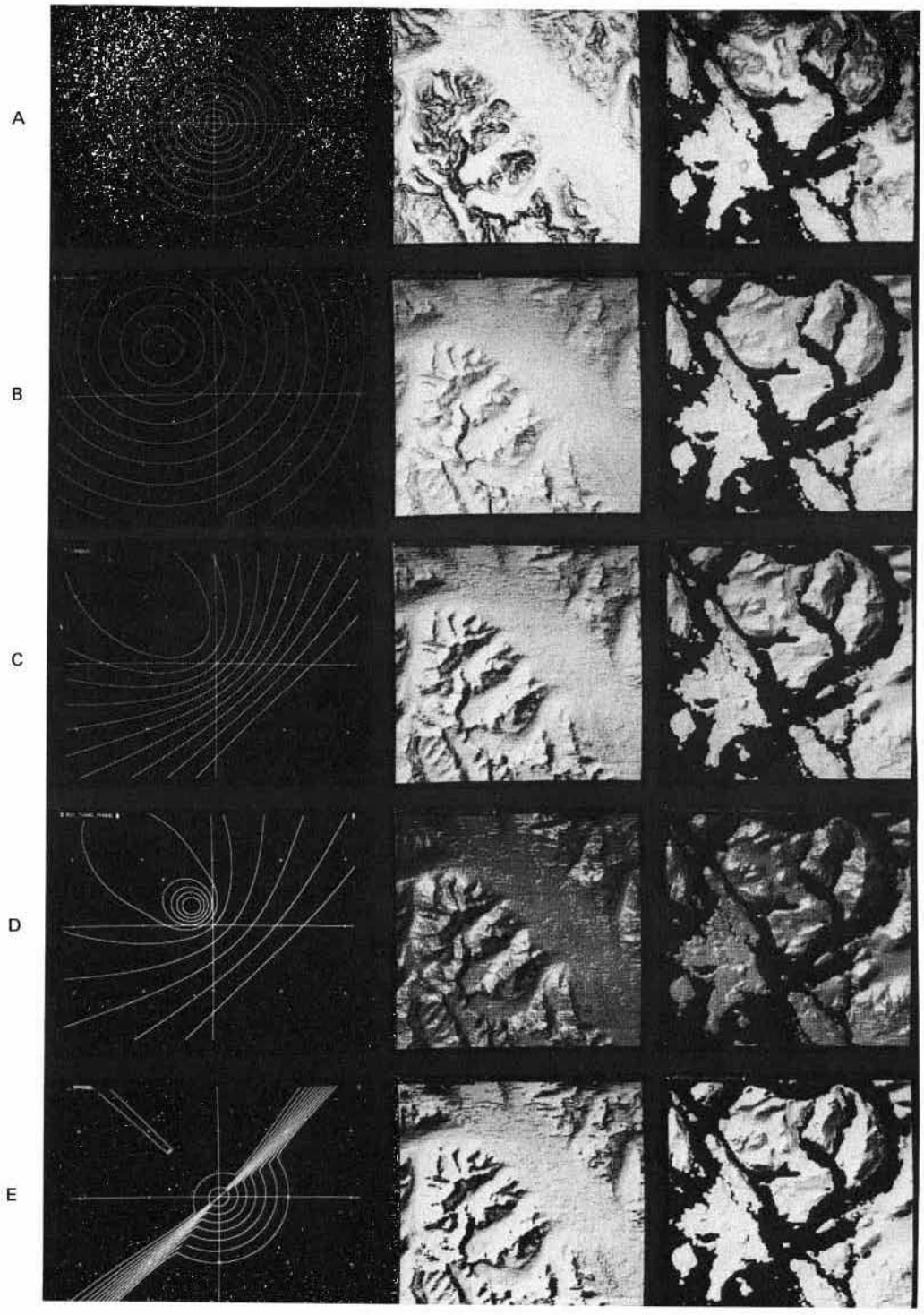

Figure 21

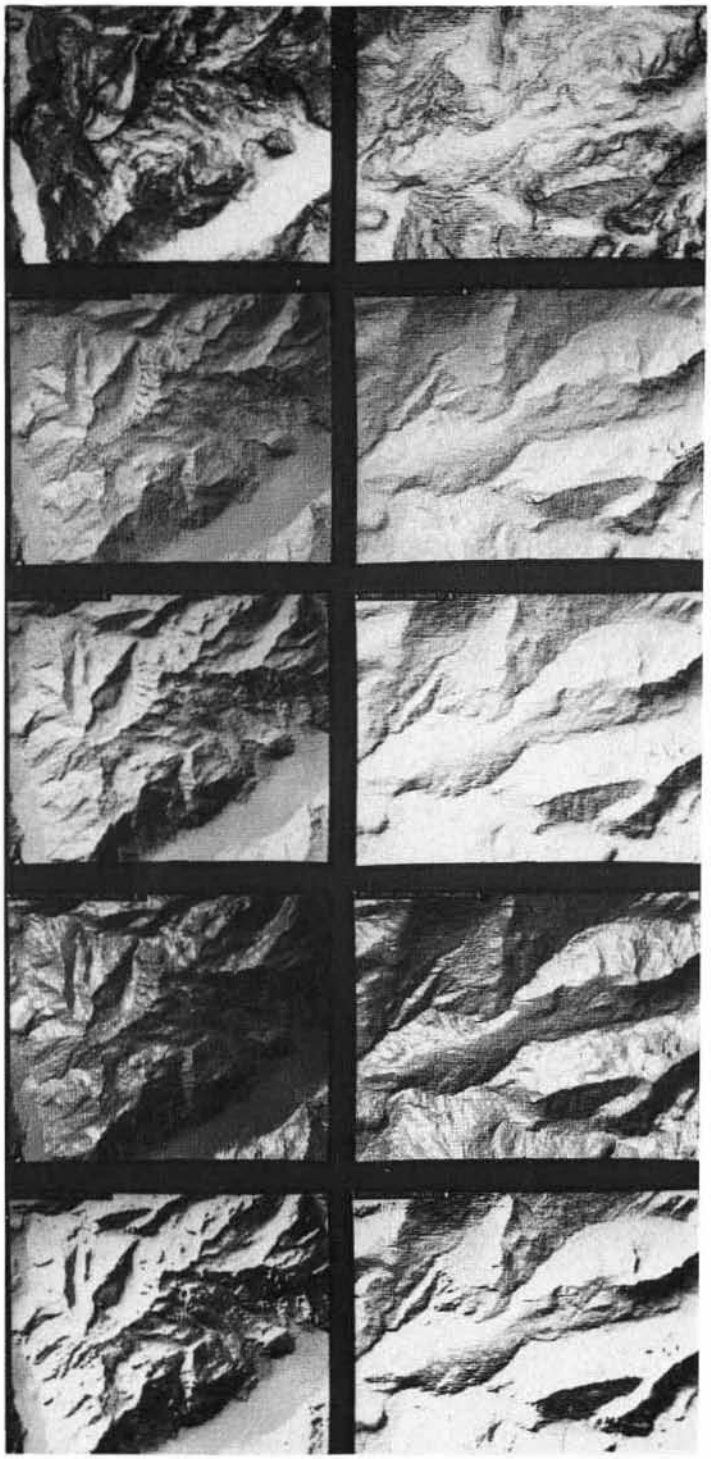

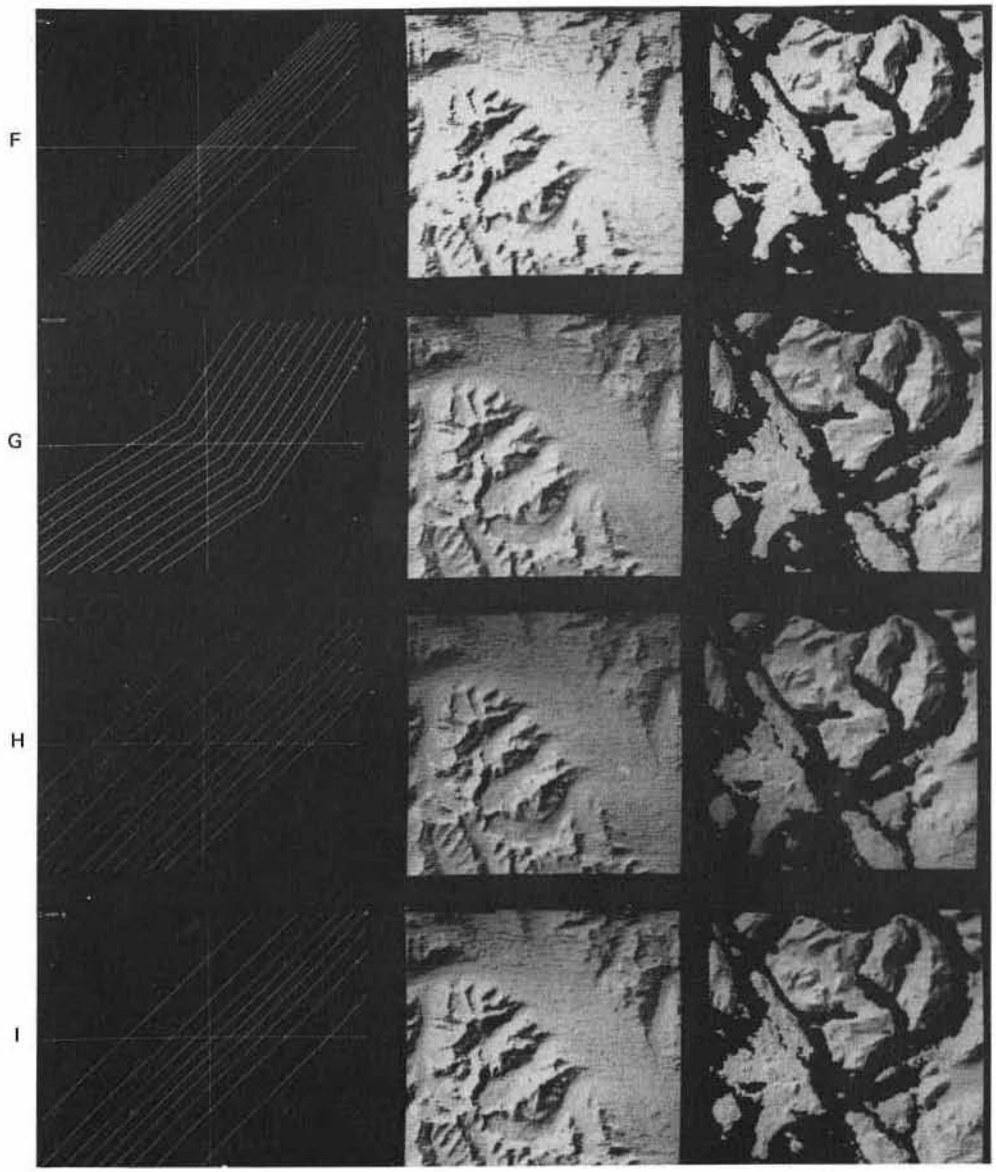
F
G
H
I

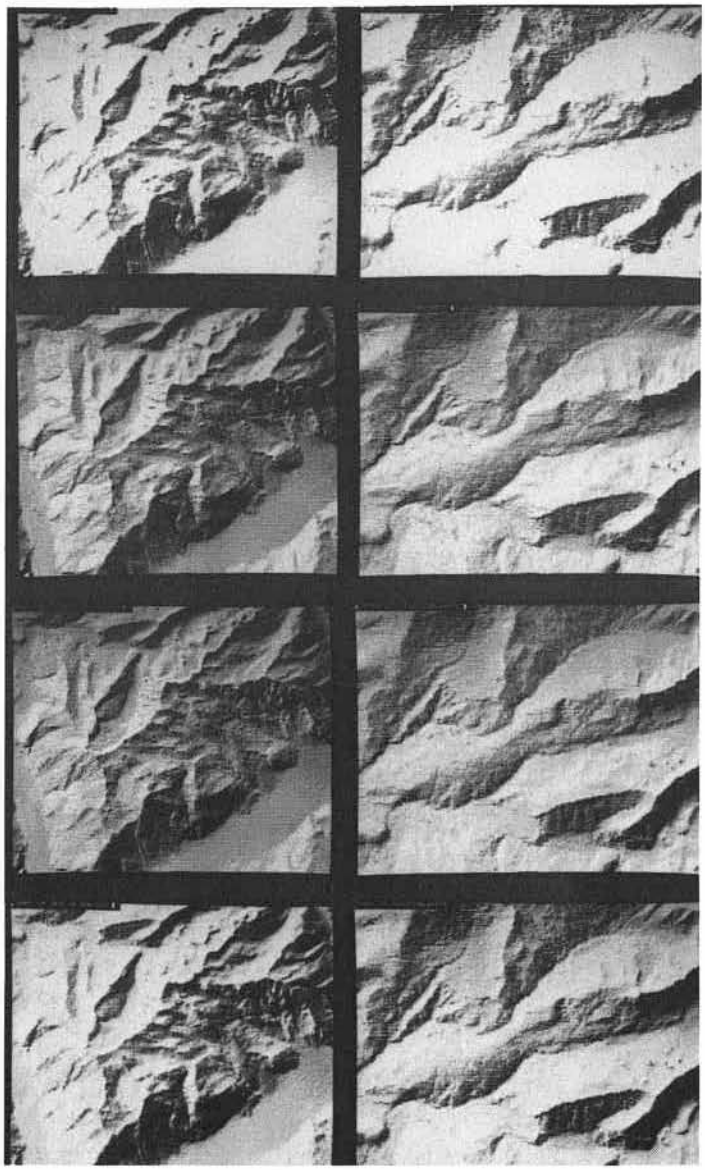

Figure 21: Shaded images of the four digital terrain models. The subfigures were made using the same reflectance maps as those used in Figure 19. The nine reflectance maps are again shown in the leftmost column. Small crosses mark points in gradient space where slope-components are integer multiplies of one. Where approriate, a small square marks the gradient of a surface element that is perpendicular to the rays from the assumed light-source.

It is important to arrange for the range of gray tones in the shaded overlays to be limited so as to avoid obscuring planimetric detail [153]. This is an area that has not received much attention so far. Another important issue relates to the appropriate scale for shaded overlays. Shaded overlays are useful for large scale maps. For small scale maps it is necessary to generalize the surface to avoid the appearance of complex textures that may be difficult to interpret [1],[48],[73],[74],[154],[155]. This nonlinear process of removing small hills, ridges and valleys has not yet been satisfactorily automated.

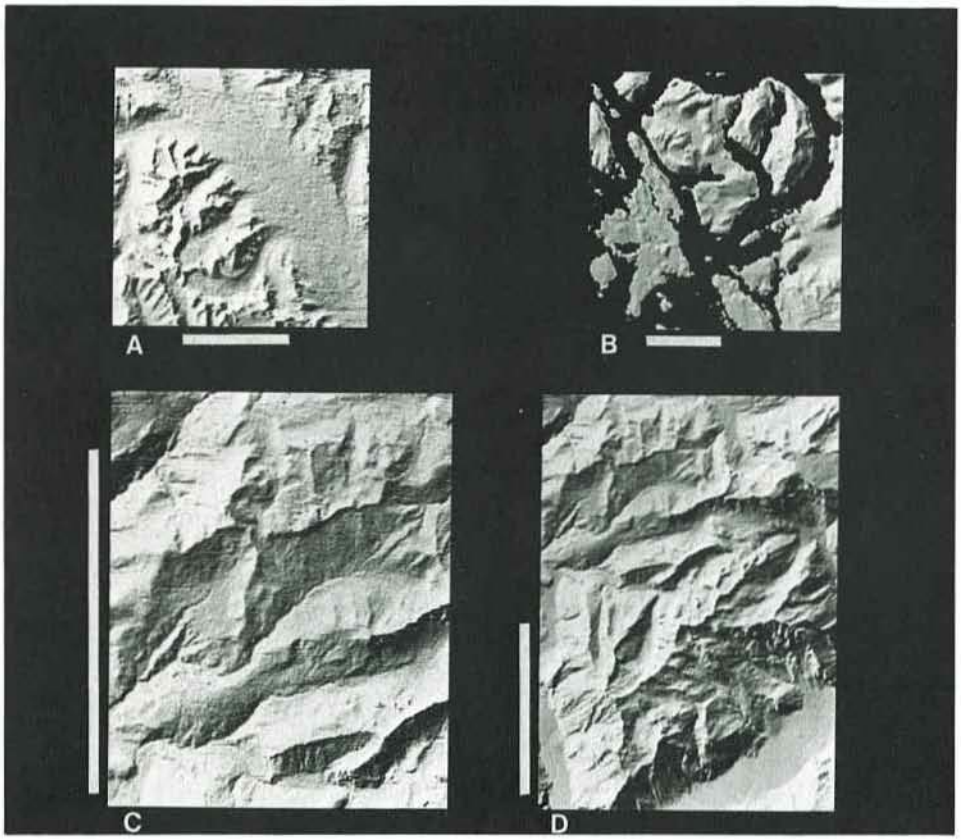

Figure 22: Shaded images of ten digital terrain models. A particularly simple reflectance map was used. (A) Lake Louise, Alberta, Canada (B) Gulf Islands, British Columbia, Canada (C) Les Diablerets, Switzerland (D) Dent de Morcles, Switzerland (E) Mexico City, Mexico (F) Jewell Ridge, Virginia (G) White Tail Butte, Wyoming (H) Tehachapi Mountains, California (I) Mount Index, Washington and (J) Mauritius, Indian Ocean. The lines in the subfigures correspond to a length of 10 km on the surface.

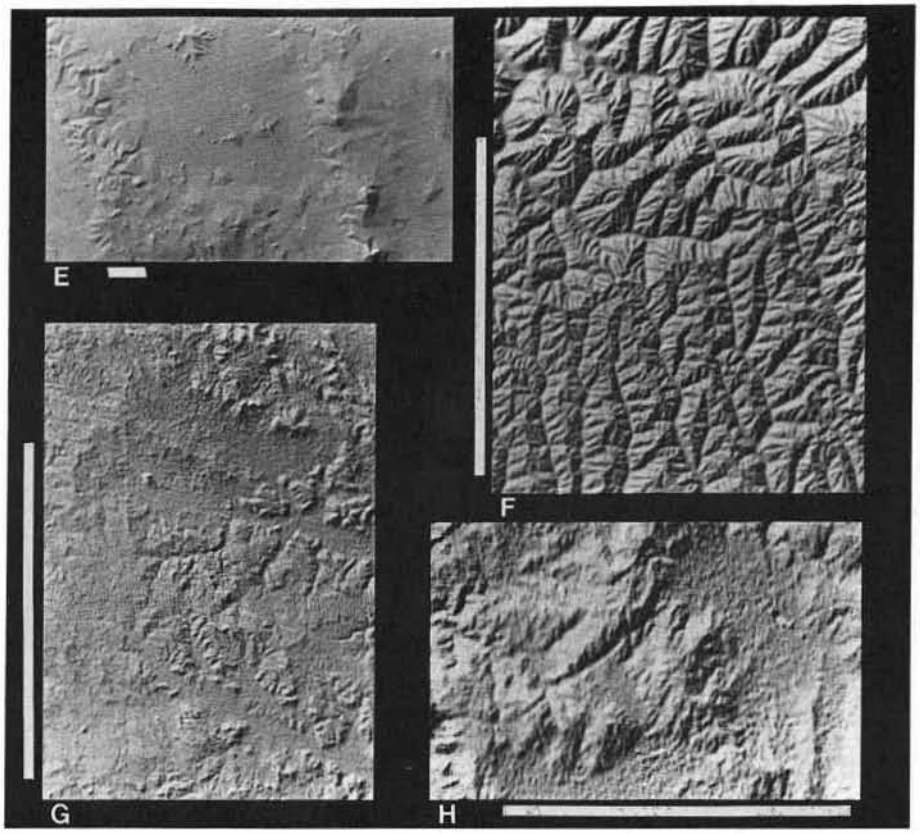

An as yet unexplored possibility depends on finely sampled terrain elevations. This is the ability of shading to show fine detail. Contour maps have to be carefully generalized or smoothed to avoid showing confusing detail on a scale smaller than the contour interval. This is not the case with shading, although historically the manually produced maps have always shown only quite coarse features. We do not yet know whether the textures produced by the shading method when working from really fine terrain models will be confusing, or of great value in identifying different types of terrain.

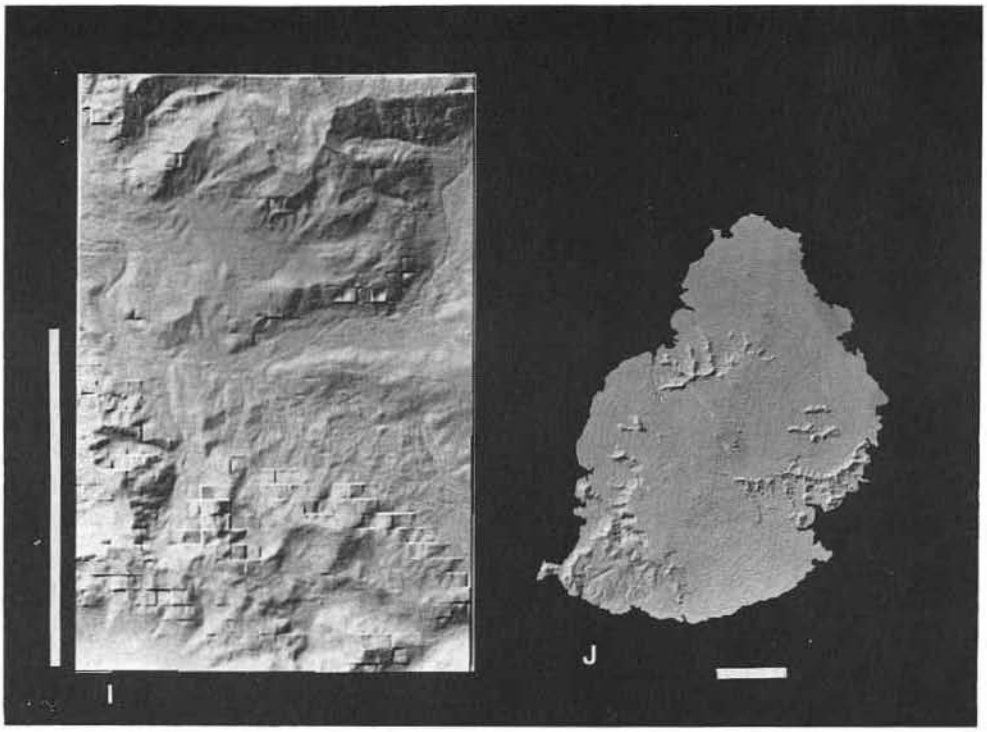

Acknowledgments

I would like to thank Kurt Brassel, Thomas Peucker, George Lukes, Robert McEwen, Marsha Jo Hannah and James Mahoney for generously supplying digital terrain model. Blenda Horn helped in the preparation of the text and Karen Prendergast created the figures. Helpful comments were provided by Robert Sjoberg, Katsushi Ikeuchi, and William Silver. Encouragment by Thomas Peucker, Kitiro Tanaka, and Kurt Brassel was instrumental in the generation of this paper.

This report describes research done at the Artificial Intelligence Laboratory of the Massachusetts Institute of Technology. Support for the laboratory's artificial intelligence research is provided in part by the Advanced Research Projects Agency of the Department of Defense under Office of Naval Research contract N00014-75-C-0643.

Appendix A: Rotated Gradients

It has been cartographic practice to assume a light source in the north-west at a 45° elevation above the horizon. It is helpful in this case to introduce a rotated coordinate system (see Fig. 23)

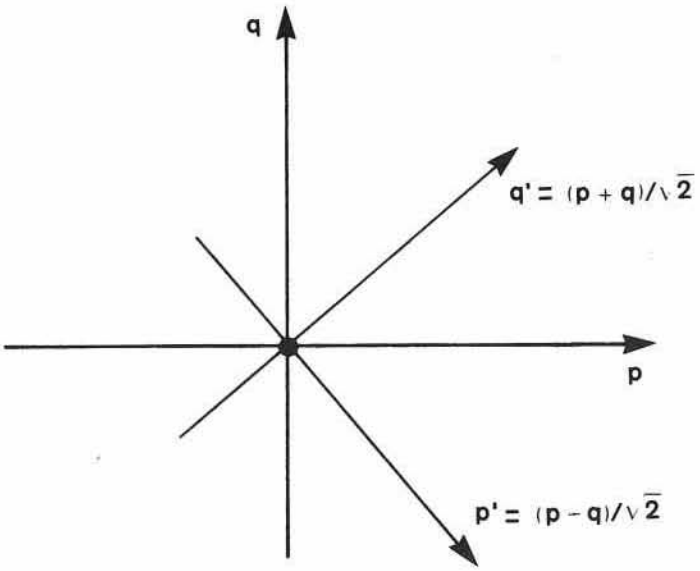

Figure 23: Rotated coordinate system that may be convenient when the assumed light-source is in the north-west. The reflectance map is symmetrical about the p'-axis.

with

$$p' = \frac{p - q}{\sqrt{2}} \quad \text{and} \quad q' = \frac{p + q}{\sqrt{2}}. \tag{137}$$

If $\Delta x = \Delta y = \Delta$ say, then the slopes in the north-west to south-east and in the south-west to north-east direction, can be estimated particularly easily by combining the formulas for p_w and q_w,

$$p'_w = \frac{(z_{+o} + z_{+-} + z_{o-}) - (z_{-o} + z_{-+} + z_{o+})}{4\sqrt{2}\,\Delta}, \tag{138}$$

$$q'_w = \frac{(z_{o+} + z_{++} + z_{+o}) - (z_{o-} + z_{--} + z_{-o})}{4\sqrt{2}\,\Delta}. \tag{139}$$

If one wishes to estimate the slopes for the center of the top-right quadrant (in the unrotated coordinate system) rather than the central point one may combine the expressions for $p_{1/2}$ and $q_{1/2}$ to get the simple formulas,

$$p'_{1/2} = \frac{z_{+o} - z_{o+}}{\sqrt{2}\,\Delta} \quad \text{and} \quad q'_{1/2} = \frac{z_{++} - z_{oo}}{\sqrt{2}\,\Delta}. \tag{140}$$

One advantage of the rotated coordinate system stems from the fact that models of surface reflectance considered here are symmetric with respect to a line pointing towards the source. That is, a surface element with slopes $p' = p'_o$ and $q' = q'_o$ say, has the same apparent brightness as one

with slopes $p' = p'_0$ and $q' = -q'_0$. Thus a lookup table based on the rotated coordinate system can be smaller, since only that half of the table corresponding to $q' > 0$ need be stored.

So far we have assumed that the grid of the terrain model is aligned with the geographical coordinates. If instead the whole model is rotated anti-clockwise by an angle θ, then slopes p'' and q'' can first be estimated from the model as described and then transformed as follows:

$$p = p'' \cos\theta - q'' \sin\theta \quad \text{and} \quad q = p'' \sin\theta + q'' \cos\theta \,. \tag{141}$$

Alternatively, the model can be resampled to produce a new version on a grid aligned with the axes.

Appendix B: Shading Apparent in Block Diagrams

We can analyze the shading apparent in block diagrams by calculating the spacing between lines as a function of the surface orientation. Let a local surface normal be $\mathbf{n}=(-p, -q, 1)$. A series of parallel planes, with common normal $\mathbf{s}$, cuts the terrain surface. The intersections of these planes with the surface are viewed from a direction specified by the vector $\mathbf{v}$. It is assumed that the viewer is at a great distance so that the profiles are projected orthographically along lines parallel to $\mathbf{v}$ (see Fig. 24).

The line of intersection of one of the cutting planes with the local tangent plane will be parallel to the vector $\mathbf{n} \times \mathbf{s}$, since the line lies in both planes and is therefore perpendicular to the normals, $\mathbf{n}$ and $\mathbf{s}$. Now construct a plane through the line of intersection and the viewer. This plane, called the viewing plane, contains both $\mathbf{n} \times \mathbf{s}$ and $\mathbf{v}$. The normal $\mathbf{e}$ of the viewing plane must therefore be perpendicular to both and can be defined as,

$$\mathbf{e} = (\mathbf{n} \times \mathbf{s}) \times \mathbf{v} \tag{142}$$

or,

$$\mathbf{e} = (\mathbf{n} \cdot \mathbf{v})\,\mathbf{s} - (\mathbf{s} \cdot \mathbf{v})\,\mathbf{n} \,. \tag{143}$$

If we let $\mathbf{p}=(x, y, z)$, then the equation for the local tangent plane can be written,

$$\mathbf{n} \cdot \mathbf{p} = c_n \tag{144}$$

for some value of the constant c_n. Similarly, the equation of a particular cutting plane is,

$$\mathbf{s} \cdot \mathbf{p} = c_s \,. \tag{145}$$

Different values of c_s correspond to different cutting planes. The plane corresponding to the value $c_s + dc_s$ is separated from the plane corresponding to the value c_s by a distance dc_s / s, where s is the magnitude of the vector $\mathbf{s}$. The equation for the viewing plane is just,

$$\mathbf{e} \cdot \mathbf{p} = c_e \,. \tag{146}$$

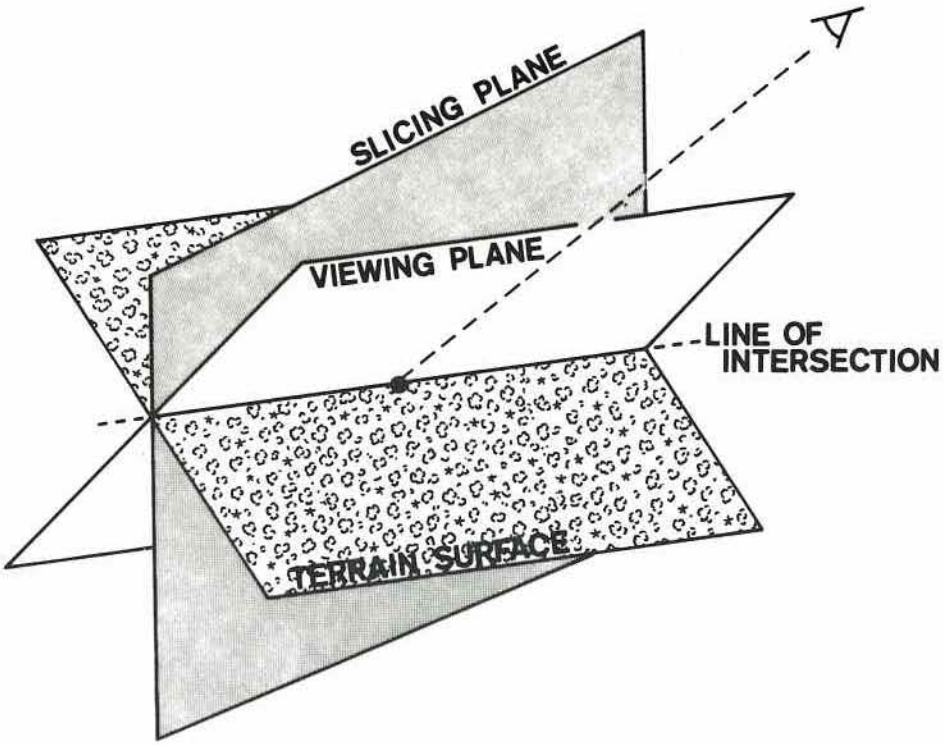

Figure 24: The viewing plane contains the viewer and the line of intersection of the slicing plane with the terrain surface. Line spacing in the block-diagram equals the spacing between successive viewing planes. The dotted line is parallel to the vector **v**.

Successive cutting planes will intersect the tangent plane in parallel lines. These give rise to parallel viewing planes corresponding to different values of the constant c_e. The spacing of these viewing planes is of interest, since it equals the spacing of the lines in the orthographic projection. The plane corresponding to the value $c_e + dc_e$ is separated from the plane corresponding to the value c_e by a distance of dc_e / e, where e is the magnitude of the vector **e**. In order to relate the spacing of lines in the block diagram to the spacing of the cutting planes we need to find the relationship between dc_e and dc_s.

A point **p** on the line of intersection lies in all three planes and therefore simultaneously satisfies the three equations given above for these planes. Expanding the last one of these, $\mathbf{e} \cdot \mathbf{p} = c_e$, we obtain,

$$(\mathbf{n} \cdot \mathbf{v})(\mathbf{s} \cdot \mathbf{p}) - (\mathbf{s} \cdot \mathbf{v})(\mathbf{n} \cdot \mathbf{p}) = c_e \tag{147}$$

or,

$$(\mathbf{n} \cdot \mathbf{v})\, c_s - (\mathbf{s} \cdot \mathbf{v})\, c_n = c_e \,. \tag{148}$$

Here, c_n is fixed and so the relationship between changes in c_e and c_s is simply

$$dc_e = (\mathbf{n} \cdot \mathbf{v})\, dc_s \,. \tag{149}$$

If the interval between cutting planes is δ and the map scale is k, then $dc_s / s = k\delta$. Consequently the spacing between lines in the block diagram, dc_e / e is,

$$d = k\delta\, (\mathbf{n} \cdot \mathbf{v})\, \frac{s}{e}, \tag{150}$$

where e is the magnitude of the vector $\mathbf{e} = (\mathbf{n} \cdot \mathbf{v})\, \mathbf{s} - (\mathbf{s} \cdot \mathbf{v})\, \mathbf{n}$. Finally, we remember that

$$R(p, q) = r_w - (r_w - r_b)\, \frac{b}{d} \tag{151}$$

where b is the thickness of the lines. Thus,

$$R(p, q) = r_w - \frac{b}{k\delta} (r_w - r_b)\, \frac{e}{s}\, \frac{1}{\mathbf{n} \cdot \mathbf{v}}. \tag{152}$$

The view vector is tangent to the surface when $\mathbf{n} \cdot \mathbf{v} = 0$. When this dot product becomes negative, the surface is turned *away* from the viewer and should not be visible. Also note that $d = k\delta$, when $\mathbf{s} \cdot \mathbf{v} = 0$. One should therefore choose $\mathbf{s}$ and $\mathbf{v}$ so that they are not orthogonal, to avoid getting only evenly spaced parallel lines.

In the case of perspective projection, line density will increase with distance, and the resulting reflectance will be lowered because of a change in the effective scale factor k. If the projected profiles are plotted on a raster device, one has to also take into account the fact that the number of dots per unit line length is not constant. The dot density varies as max [| cos θ | , | sin θ |], where θ is the angle between the line and the direction of the raster. This variation should be included if an accurate reflectance map is to be derived for output of this form.

Appendix C: Isometric Views of Vertical Profiles.

The transformation between the terrain coordinate system and that of an observer viewing the terrain obliquely can be found by multiplying a rotation matrix corresponding to rotation by θ_v about the x-axis with a matrix corresponding to rotation by $(\pi/2 + \varphi_v)$ about the z-axis, where φ_v is the azimuth and θ_v is the zenith angle of the direction specified by the vector $\mathbf{v}$. If the coordinates in the observer's system are x', y', and z', one finds,

$$x' = -\sin \varphi_v\, x + \cos \varphi_v\, y, \tag{153}$$

$$y' = -\cos \varphi_v \cos \theta_v\, x - \sin \varphi_v \cos \theta_v\, y + \sin \theta_v\, z, \tag{154}$$

$$z' = +\cos \varphi_v \sin \theta_v\, x + \sin \varphi_v \sin \theta_v\, y + \cos \theta_v\, z. \tag{155}$$

In the case of orthographic projection, the values of x' and y' are simply multiplied by the map scale k, to determine coordinates in the block diagram.

The general formula derived in Appendix B applies to all combinations of viewpoint and cutting plane orientation. It is interesting to look at a few special cases however. We can, for example, check our result for the contour interval in an ordinary contour map. Here $\mathbf{n}=(-p, -q, 1)$, as always, and $\mathbf{s}=(0, 0, 1)$, since we are considering the intersection of the surface with horizontal planes. Further, $\mathbf{v}=(0, 0, 1)$ since the viewer is vertically above the surface. Here then $s=1$, $\mathbf{n} \bullet \mathbf{v}=1$, and $\mathbf{e}=(p, q, 0)$ The line interval is therefore,

$$d = \frac{k\delta}{\sqrt{p^2+q^2}}. \tag{156}$$

The same reflectance map is obtained as before. Slightly more complicated is the case of Tanaka's inclined contours, where $\mathbf{s}=(-p_o, -q_o, 1)$. Here, again, $\mathbf{n} \bullet \mathbf{v}=1$, while,

$$\mathbf{e} = (p-p_o, q-q_o, 0) \tag{157}$$

and

$$s = \sqrt{1+p_o^2+q_o^2}. \tag{158}$$

The line interval is therefore,

$$d = k\delta \frac{\sqrt{1+p_o^2+q_o^2}}{\sqrt{(p-p_o)^2+(q-q_o)^2}}. \tag{159}$$

A result leading to the same reflectance map as the one derived before.

Finally, consider profiles running west to east, that is, $\mathbf{s}=(0, 1, 0)$. The resulting traces may be viewed isometrically from the south-east, a fairly common arrangment for a block diagram. Then $\mathbf{v}=(1, -1, 1)$. Consequently, $\mathbf{n} \bullet \mathbf{v}=(1-p+q)$ and $\mathbf{s} \bullet \mathbf{v}=-1$. Further, $\mathbf{e}=(-p, 1-p, 1)$ and hence,

$$d = k\delta \frac{1-p+q}{\sqrt{2}\sqrt{1-p+p^2}}. \tag{160}$$

So, if $r_b=0$ and $r_w=1$,

$$R(p, q) = 1 - \sqrt{2}\frac{b}{k\delta} \frac{\sqrt{1-p+p^2}}{1-p+q}. \tag{161}$$

Similarly, for profiles running south to north, $\mathbf{s}=(1, 0, 0)$, and,

$$R(p, q) = 1 - \sqrt{2}\frac{b}{k\delta} \frac{\sqrt{1+q+q^2}}{1-p+q}. \tag{162}$$

At times two orthogonal sets of slicing planes will be used, producing a mesh on the surface. The reflectance map corresponding to this case can be found by adding the last two formulas and subtracting one from the result.

Appendix D: Luminance Longitude and Luminance Latitude.

A convention for specifying the orientation of the surface element relative to the direction of a

light source and the viewer has become established in the work on planetary and lunar photometry. Imagine a sphere illuminated by a light source above the point S, viewed by an observer above the point V (see Fig. 25). These two points define a great circle which is called the luminance equator. Points on the sphere can be referenced using the longitude α measured from the point V along the equator, and the latitude β.

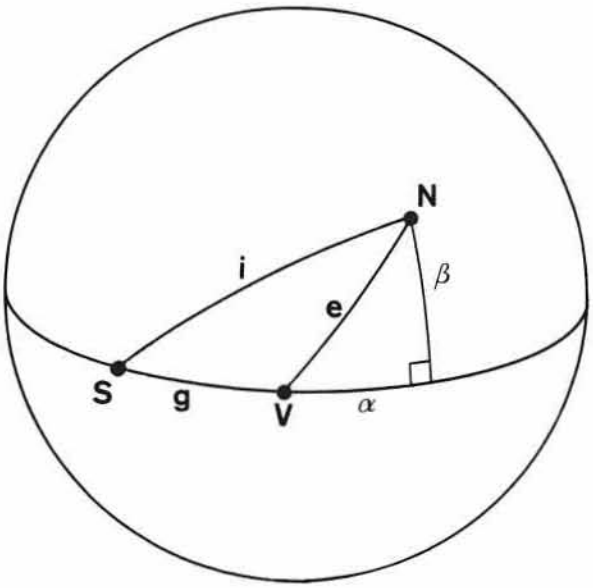

Figure 25: Luminance longitude α and luminance latitude β of a surface element are defined as the longitude and latitude of a patch on a sphere with the same orientation. Longitude and latitude are measured relative to the luminance equator through the light source S and the viewer V.

All possible surface orientations can be found on the sphere, and each surface orientation can be identified with some point N say. The luminance longitude and luminance latitude corresponding to a particular surface orientation are the longitude and latitude of N. It is not difficult to show that,

$$\cos e = \cos\beta \cos\alpha \quad \text{and} \quad \cos i = \cos\beta \cos(\alpha + g). \tag{163}$$

Conversely,

$$\tan\alpha = \frac{\cos e \cos g - \cos i}{\cos e \sin g} \tag{164}$$

and,

$$\tan^2\beta = \frac{[1 + 2\,IEG - (I^2 + E^2 + G^2)]}{[I^2 - 2\,IEG + E^2]} \tag{165}$$

where we have used the shorthand notation, $I=\cos i$, $E=\cos e$, and $G=\cos g$. These results can also be expressed in terms of the components of the gradient:

$$\tan \alpha = \frac{p_o p + q_o q}{\sqrt{p_o^2+q_o^2}}. \tag{166}$$

So $\tan \alpha$ is simply the slope in the direction away from the source. Now,

$$1 + 2\,IEG - (I^2+E^2+G^2) = \frac{(q_o p - p_o q)^2}{(1+p^2+q^2)(1+p_o^2+q_o^2)} \tag{167}$$

$$I^2 - 2\,IEG + E^2 = \frac{(p_o p+q_o q)^2 + (p_o^2+q_o^2)}{(1+p^2+q^2)(1+p_o^2+q_o^2)} \tag{168}$$

so,

$$\tan \beta = \frac{q_o p - p_o q}{\sqrt{(p_o p+q_o q)^2 + (p_o^2+q_o^2)}}. \tag{169}$$

The Lommel-Seeliger law can be expressed in terms of luminance longitude and luminance latitude as,

$$\frac{\cos(\alpha+g)}{\cos \alpha + \cos(\alpha+g)} \tag{170}$$

and it is clear from this form that scene radiance is independent of luminance *latitude*.

References

[1] E. Imhof, 1965. *Kartographische Geländedarstellung*, Berlin: W. de Gruyter & Co.

[2] J. G. Lehmann, 1799. *Darstellung einer neuen Theorie der Bezeichnung der schiefen Flächen im Grundriss oder der Situationzeichnung der Berge*, Leipzig.

[3] J. G. Lehmann, 1816. *Die Lehre der Situations-Zeichnung oder Anweisung zum richtigen Erkennen und genauen Abbilden der Erd-Oberfläche in topographischen Charten und Situation-Planen*, Dresden: Arnoldische Buch- und Kunsthandlung.

[4] F. Chauvin, 1852. *Die Darstellung der Berge in Karten und Plänen, mit besonderer Rücksicht auf ihre Anwendbarkeit im Felde*, Berlin: Nauck'sche Buchhandlung.

[5] F. Chauvin, 1854. *Das Bergzeichnen rationell entwickelt*, Berlin: Nauck'sche Buchhandlung.

[6] C. Vogel, 1893. "Die Terraindarstellung auf Landkarten mittels Schraffierung," *Petermanns Geogr. Mitt.*, Vol. 39, pg. 148.

[7] H. Bach, 1853. *Die Theorie der Bergzeichnung in Verbindung mit Geognosie*, Stuttgart.

[8] H. Wiechel, 1878. "Theorie und Darstellung der Beleuchtung von nicht gesetzmässig gebildeten Flächen mit Rücksicht auf die Bergzeichnung", *Civilingenieur*, Vol. 24, pp. 335-364.

[9] L. Burmester, 1875. *Theorie und Darstellung gesetzmässig gestalteter Flächen*, Leipzig.

[10] Kitirô Tanaka, 1930. "A New Method of Topographical Hill Delineation," Memoirs of the College of Engineering, Kyushu Imperial University, Fukuoka, Japan, Vol. 5, No. 3. pp. 121-143.

[11] Kitirô Tanaka, March 1932. "The orthographical relief method of representing hill features on a topographical map", *Geographical Journal*, Vol. 79, No. 3, pp. 213-219.

[12] H. StJ. L. Winterbotham, 1932. "Note on Professor Kitiro's Method of Orthographical Relief", *Geographical Journal*, Vol. 80, pp. 518-520.

[13] P. Wilski, 1934. "Eine neue Japanische Darstellung der Höhen auf Landkarten," *Petermanns Geogr. Mitt.*, Vol. 80, pg. 359.

[14] Jadwiga Remiszewska, 1955. "Metoda cieć pochylych w kartograficznym obrazie urzeźbienia" [The Method of Inclined Cut in the Cartographic Presentation of the Form of the Land], *Polish Geographical Review*, Vol. 27, pp. 125-134.

[15] A. H. Robinson, and N. J. W. Thrower, 1957. "A New Method for Terrain Representation," *Geographical Review*, Vol. 47, No. 4, October, pp. 507-520.

[16] A. H. Robinson, 1961. "The Cartographic Representation of the Statistical Surface," *International Yearbook of Cartography*, Vol. 1, pp. 53-63.

[17] N. J. W. Thrower, 1963. "Extended uses of the method of orthogonal mapping of traces of parallel, inclined planes with a surface, especially terrain," *International Yearbook of Cartography*, Vol. 3, pp. 26-28.

[18] C. M. King, 1966. *Techniques in Geomorphology*, New York: St. Martin's Press, pp. 255-256.

[19] T. K. Peucker, M. Tichenor, and W.-D. Rase, 1972. "Die Automatisierung der Methode der schrägen Schnittflächen," *Kartographische Nachrichten*, Vol. 22, No. 4, pp. 143-148.

[20] T. M. Oberlander, 1968. "A Critical Appraisal of the Inclined Contour Technique of Surface Representation", *Annals, Association of American Geographers*, Vol. 58, No. 4, pp. 802-813.

[21] A. H. Robinson, and R. D. Sale, 1969. *Elements of Cartography*, 3rd edition, New York: John Wiley. pp. 189-196.

[22] A. H. Robinson, and N. J. W. Thrower, 1969. "On surface representation using traces of parallel inclined planes," *Annals, Association of American Geographers*, Vol. 59, No. 3. pp. 600-603.

[23] T. M. Oberlander, 1969. "Reply to Robinson-Thrower Commentary," *Annals, Association of American Geographers*, Vol. 59, No. 3, pp. 603-605.

[24] Kitirô Tanaka, 1939. "The Relief Contour Method of Representing Topography on Maps," *The Geographical Review of Japan*, Vol. 15, No. 9 & 10, pp. 655-671, 784-796 (Japanese) pg. 797 (English abstract).

[25] Kitirô Tanaka, 1950. "The Relief Contour Method of Representing Topography on Maps," *Geographical Review*, Vol. 40, No. 3, pp. 444-456.

[26] Kitirô Tanaka, 1951. "The Relief Contour Method of Representing Topography on Maps," *Surveying and Mapping*, Vol. 11, pg. 27.

[27] C. Köpcke, 1885. "Ueber Reliefs und Relief-Photogramme," *Civilingenieur*, Vol. 31.

[28] Y. Pauliny, 1895. "Memoire über eine neue Situations Pläne- und Landkartendarstellungsmethode," *Streffen's Oesterreichischer Militärische Zeitschrift*, Vol. 36, pg. 177.

[29] Erwin Raisz, 1938. *General Cartography*, New York and London.

[30] W. Pillewizer, 1957. "Geländedarstellung durch Reliefphotographie," *Kartographische Nachrichten*, Vol. 7, pg. 141.

[31] O. C. Stoessel, 1959. "Photomechanische Reliefschummerung," *Nachrichten aus dem Karten- und Vermessungswesen*, Vol. 1, No. 10, pp. 53-55.

[32] A. A. Noma, and M. G. Misulia, 1959. "Programming Topographic Maps for Automatic Terrain Model Construction," *Surveying and Mapping*, Vol. 19, No. 3, September, pg. 335.

[33] H. R. Wilkerson, 1959. "Reliefschummerung durch Photographie von Geländemodellen, *Nachrichten aus dem Karten- und Vermessungswesen*, Vol. 1, No. 10, pp. 60-62.

[34] H. Friedemann, 1962. "Von neuen Erfindungen: Anordnung und Verfahren zur Herstellung von Schummerungen für kartographische Zwecke," *Kartographische Nachrichten*, Vol. 12, pg. 150.

[35] P. Richarme, 1963. "L'estompage photographique," *Bulletin du comité francais de cartographie*, Vol. 17, pg. 188.

[36] P. Richarme, 1963. "The Photographic Hill Shading of Maps", *Surveying and Mapping*, Vol. 23, No. 1, pp. 47-59.

[37] C. R. Gilman, 1971. "Photomechanical Experiments in Automated Cartography," in *Proceedings ASM Fall Meeting*, San Fransisco.

[38] H. G. Lyons, 1909. *The Representation of Reliefs on Maps*, Ministry of Finance, National Printing Department, Egypt.

[39] L. J. Harris, 1959. *Hill-shading for Relief-depiction in Topographical Maps*, London.

[40] E. Imhof, 1947. "Geländedarstellung in Karten grosser und mittlerer Massstäbe," *Vortrag Natf. Ges. Zürich* January.

[41] B. Carlberg, 1954. "Schweizer Manier und wirklichkeitsnahe Karte, Probleme der Farbgebung," *Kartographische Nachrichten*, Vol. 4, pp. 8-14.

[42] G. Pöhlmann, 1958. "Heutige Methoden und Verfahren der Geländedarstellung," *Kartographische Nachrichten*, Vol. 8, No. 3, pp. 71-78.

[43] H. Mietzner, 1959. "Die Schummerung unter Annahme einer naturgemässen Beleuchtung," *Kartographische Nachrichten*, Vol. 9, No. 3, pp. 73-79.

[44] E. Imhof, 1959. "Probleme der Kartographischen Geländedarstellung," *Nachrichten aus dem Karten- und Vermessungswesen*, Vol. 1, No. 10, pg. 9-31, 1959.

[45] J. S. Keates, 1961. "Techniques of Relief Representation," *Surveying and Mapping*, Vol. 21, No. 4, December, pp. 459-463.

[46] F. Hölzel, 1962. "Die Geländeschummerung in der Krise?", *Kartographische Nachrichten*, Vol. 12, No. 1, February, pp. 17-21.

[47] E. Imhof, (Editor) 1963. *International yearbook of cartography*, London: George Philip and Son.

[48] F. Hölzel, 1963. "Generalization Problems in Hill Shading," *Nachrichten aus dem Karten- und Vermessungswesen*, Vol. 5, No. 5, pp. 23-33.

[49] P. Yoéli, 1959. "Relief Shading," *Surveying and Mapping*, Vol. 19, pg. 229.

[50] P. Yoéli, 1965. "Analytische Schattierung," *Kartographische Nachrichten.*, Vol. 14, No. 4, pp. 142-148.

[51] P. Yoéli, 1965. "Analytical Hill Shading," *Surveying and Mapping*, Vol. 25, No. 4, December, pp. 573-579.

[52] P. Yoéli, 1966. "Analytische Schattierung und Dichte," *Kartographische Nachrichten*, Vol. 16, No. 1, pp. 17-23.

[53] P. Yoéli, June 1966. "Analytical Hill Shading and Density, *Surveying and Mapping*, Vol. 26, No. 2, pp. 253-259.

[54] P. Yoéli, 1966. "Die Mechanisierung der Analytischen Schattierung," *Kartographische Nachrichten*, Vol. 16, No. 3, pp. 103-107.

[55] P. Yoéli, 1967. "The Mechanisation of Analytical Hill Shading," *The Cartographic Journal*, December, Vol. 4, No. 2.

[56] P. Yoéli, 1967. "Die Richtung des Lichtes bei analytischer Schattierung," *Kartographische Nachrichten*, Vol. 17, No. 2, pp. 37-44.

[57] P. Yoéli, 1971. "An Experimental Electronic System for Converting Contours into Hill-shaded Relief," *International Yearbook of Cartography*, Vol. 11, pp. 111-114.

[58] T. J. Blachut, Z. Marsik, and D. Makow, 1969. "Relief shading process," Canada Patent No. 051-814.

[59] Z. Marsik, 1971. "Automatic Relief Shading," *Photogrammetrica*, Vol. 27, No. 2, pp. 57-70.

[60] T. K. Peucker, 1972. "Computer Cartography," Association of American Geographers, Washington, D. C., Commission on College Geography. *Resource Paper No. 17*, pp. 41-54.

[61] T. K. Peucker, and D. Cochrane, 1974. "Die Automation der Reliefdarstellung - Theorie und Praxis," *International Yearbook of Cartography*, Vol. 14, pp. 128-139.

[62] T. K. Peucker, M. Tichenor, and W.-D. Rase, 1974. "The Computer Version of Three Relief Representations," in *Display and Analysis of Spatial Data*, J. C. Davis, and M. McCullagh, Eds. New York: John Wiley.

[63] M. Eckert, 1962. *Die Kartenwissenschaft: Forschung und Grundlagen zu einer Kartographie als Wissenschaft - Vol. 1*, Berlin: Walter de Gruyt,

[64] L. D. Carmichael, 1964. "Experiments in Relief Portrayal," *Cartographic Journal*, Vol. 1, pp. 11-17.

[65] M. Eckert, 1965. *Die Kartenwissenschaft: Forschung und Grundlagen zu einer Kartographie als Wissenschaft - Vol. 2*, Berlin: Walter de Gruyt,

[66] M. S. Monmonier, 1965. "The Production of Shaded Maps on the Digital Computer," *The Professional Cartographer*, Vol. 17, No. 5, September, pp. 13-14.

[67] P. K. Koldayev, 1967. "Plastic Colour and Shadow Relief Representation," *Academy of Sciences of the USSR*, Council of Soviet Cartographers, Moscow.

[68] B. F. Sprunt, 1969. "Computer-generated halftone images from digital terrain models," M. Sc. Dissertation, Department of Mathematics, Univ. Southampton.

[69] B. Anda, 1974. "Automatic Hill-Shading using an Automatic Flatbed Drafting Machine with a Standard Photohead," *ITC Journal*, Enschede, No. 2, pp. 212-216.

[70] R. M. Batson, E. Edwards, and E. M. Eliason, 1975. "Computer Generated Relief Images," *Journal of Research, U. S. Geological Survey*, Vol. 3, No. 4, July-August, pp. 401-408.

[71] K. Brassel, 1973. *Modelle und Versuche zur automatischen Schräglichtschattierung*," Ph. D. dissertation, Geography Department, University of Zurich, Klosters, Switzerland.

[72] K. Brassel, 1973. "Ein- und mehrfarbige Printerdarstellungen," *Kartographische Nachrichten*, No. 5, pp. 177-183.

[73] K. Brassel, 1974. "Ein Modell zur Automatischen Schräglichtschattierung," *International Yearbook of Cartography*, pp. 66-77.

[74] K. Brassel 1974. "A Model for Automated Hill Shading," *The American Cartographer*, Vol. 1, No. 1, April, pp. 15-27.

[75] W. Blascke, 1967. "Le Modele Digital M.I.T.," *Societe Francaise de Photogrammetrie*, Bulletin 27, July, pp. 37-40.

[76] B. W. Boehm, 1967. "Tabular representations of multi-variate functions - with applications to topographic modelling," in *Association for Computing Machinery, 22nd National Conference Proceedings*, pp. 403-415.

[77] W. Aumen, 1970. "A New Map Form: Numbers," *International Yearbook of Cartography*, Vol. 10, pp. 80-84.

[78] M. W. Grist, 1972. "Digital Ground Models: An Account of Recent Research," *Photogrammetric Record*, Vol. 70, No. 4, October, pp. 424-441.

[79] F. Silar, 1972. "Das digitale Geländemodell - Theorie und Praxis," *Vermessungstechnik*, Vol. 20, No. 9, pp. 327-329.

[80] K. Torlegard, 1972. "Digital Terrain Models - General Survey and Swedish Experiences," *Bildmessung und Luftbildwesen*, Vol. 40, No. 1, pp. 21-30.

[81] American Society of Photogrammetry, 1978. *Proc. of the Digital Terrain Models (DTM) Symposium*, St. Louis, Missouri May 9-11.

[82] Wild Heerburg and Raytheon, 1968. "B8 Stereomat Automated Plotter," Company sales literature.

[83] S. Bertram, 1969. "The UNIMACE and the Automatic Photomapper," *Photogrammetric Engineering*, Vol. 35, pp. 569-576.

[84] R. H. Seymour, and A. E. Whiteside, 1972. "A new Computer-Assisted Stereocomparator," *Bendix Technical Journal*, Spring, pp. 1-5.

[85] B. G. Crawley, 1974. "Gestalt Contours," *Canadian Surveyor*, Vol. 28, No. 3, September, pp. 237-246.

[86] Bendix Research Laboratories, 1976. "AS-11B-X Automatic Stereo Mapper," RADC-TR-76-100, Rome Air Development Center, Griffiss Air Force Base, New York, April. ".

[87] D. J. Panton, 1976. "Digital Stereo Mapping," *Countermeasures*, May, pg. 12.

[88] W. Loscher, 1967. "Some aspects of orthophoto technology," *Photogrammetric Record*, Vol. 6, No. 30, pp. 419-432.

[89] T. J. Blachut, 1968. "Further extension of the orthophoto technique," *Canadian Surveyor*, Vol. 22, No. 1, pp. 206-220.

[90] T. J. Blachut, and M. C. Van Wijk, 1970. "3-D Information from Orthophotos," *Photogrammetric Engineering*, April, pp. 365-376.

[91] T. A. Hughes, A. R. Shope, and F. S. Baxter, 1971. "USGS Automatic Orthophoto System," *Photogrammetric Engineering*, Vol. 37, pp. 1055-1062.

[92] A. Beyer, 1972. "Zur Erfassung flächen Geländes durch willkürlich verteilte Höhenpunkte," *Vermessungstechnik*, Vol. 20, No. 6, pp. 204-207.

[93] T. K. Peucker, and N. Chrisman, 1975. "Cartographic Data Structures," *The American Cartographer*, Vol. 2, No. 1, April, pp. 55-69.

[94] E. Keppel, 1975. "Approximating complex surfaces by triangulation of contour lines," *IBM Journal of Research and Development*, January.

[95] T. K. Peucker, R. J. Fowler, J. J. Little, and D. M. Mark, 1976. "Digital Representation of Three-Dimensional Surfaces by Triangulated Irregular Networks (TIN)," Technical Report No. 10 (Revised), Department of Geography, Simon Fraser University, Barnaby, B. C., Canada.

[96] A. K. Lobeck, 1924. *Block Diagrams*, New York: John Wiley. Reprinted by Emerson-Trussell, Amherst, Mass. in 1958.

[97] M. Schuster, 1954. *Das Geographische und Geologische Blockbild*, Berlin: Akademie Verlag.

[98] D. A. Goosen, 1962. "Blockdiagrams," *ITC Information*, Delft, Netherlands, No. 3, Spring.

[99] G. F. Jenks, and D. A. Brown, 1966. "Three-Dimensional Map Construction," *Science*, Vol. 154, No. 3750, 18 November, pp. 857-864.

[100] B. Kubert, J. Szabo, and S. Giulieri, April 1968. "The Perspective Representation of Functions of Two Variables," *Journal of the A Vol. 15, No. 2, pp. 193*-204.

[101] D. Douglas, 1971. "VIEWBLOK: A computer program for constructing perspective view block diagrams," *Revué de Geographie de Montreal*, Vol. 26, pp. 102-104.

[102] T. J. Wright, 1973. "A Two-Space Solution to the Hidden Line Problem for Plotting Functions of Two Variables," *IEEE Trans. on Computers*, Vol. C-22, No. 1, January, pp. 28-33.

[103] C. Wylie, G. Romney, and D. Evans, 1967. "Half-tone Perspective Drawings by Computer," in *Fall Joint Computer Conference*, pp. 49-58.

[104] A. Appel, 1968. "Some Techniques for Shaded Machine Rendering of Solids," in *Spring Joint Computer Conference*, pp. 37-45.

[105] J. E. Warnock, 1969 "A Hidden-surface Algorithm for Computer Generated Half-tone Pictures," TR 4-15, Dept. of Computer Science, University of Utah, Salt Lake City, Utah.

[106] G. S. Watkins, 1970. "A Real-time Visible Surface Algorithm," Report UTEC-CSC-70-101, June, Dept. of Computer Science, University of Utah, Salt Lake City, Utah.

[107] W. J. Bouknight, September 1970. "A Procedure for Generation of Three-Dimensional Half-toned Computer Graphics Presentations," *Communications of the A.C.M.*, Vol. 13, No. 9, pp. 527-536.

[108] R. A. Goldstein, and R. Nagel, 1971. "3-D Visual Simulation," *Simulation*, Vol. 16, pp. 25-31.

[109] H. Gouraud, June 1971. "Computer Display of Curved Surfaces," *IEEE Trans. on Computers*, Vol. C-20, pp. 623-629.

[110] M. E. Newell, R. G. Newell, and T. L. Sancha, 1973. "A New Approach to the Shaded Picture Problem," in *Proceedings of the ACM National Conference*, Boston, Mass. Vol. 1, pp. 443-450.

[111] J. Staudhammer, and D. J. Odgen 1975. "Computer Graphics for Half-tone three-dimensional Object Images," *Computers and Graphics*, Vol. 1, No. 1, pp. 109-114.

[112] E. A. Catmull, 1975. "Computer display of curved surfaces," in *Proc. IEEE Conf. Computer Graphics, May, Pattern Recognition and Data Structures*, Los Angeles, (IEEE Cat. No. 75CH0981-1C), pp. 11-17.

[113] Phong Bui-Tuong, 1975. "Illumination for Computer-generated Images," *Communications of the A.C.M.*, Vol. 18, No. 6, June, pp. 311-317.

[114] J. F. Blinn, and M. E. Newell, 1976. "Texture and Reflection in Computer Generated Images," *Communications of the A.C.M.*, Vol. 19, No. 10, October, pp. 542-547.

[115] J. F. Blinn, 1977. "Models of Light Reflection for Computer Synthesized Pictures," in *SIGGRAPH '77, Proceedings of the 4th Conference on Computer Graphics and Interactive Techniques, A.C.M.*, pp. 192-198.

[116] J. F. Blinn, 1978. "A Scan Line Algorithm for Displaying Parametrically Defined Surfaces," in *SIGGRAPH '78, Proceedings of the 5th Conference on Computer Graphics and Interactive Techniques, A.C.M.*.

[117] J. H. Lambert, 1892. *Photometria sive de mensura de gratibus luminis, colorum et umbrae*, Eberhard Klett, Augsburg, 1760. Translated by W. Engelman "Lambert's Photometrie," *Ostwald's Klassiker der exacten Wissenschaften*, No. 31-33, Leipzig.

[118] l'Abbé de Lacaille 1961. *Traite d'optique sur la gradation de la lumière*, (Ouvrage posthume de M. Bouguer), L. F. Delatour, A Paris. Translated by W. E. K. Middleton *Optical treatise on the gradation of light*, University of Toronto Press, 1961.

[119] E. Lommel, 1880. "Ueber Flourescence," *Annalen der Physik*, Leipzig, Vol. 10, pp. 449-472.

[120] H. Seeliger, 1888. "Die Photometrie von diffus reflektierenden Flächen," *S.-B. Bayer. Akad. Wiss.*, Vol. 18, pg. 20.

[121] A. Markov, 1924. "Les particularités dans le réflexion de la lumière par la surface de la lune," *Astronomische Nachrichten*, Vol. 221, pp. 65-78.

[122] E. Schönberg, 1925. "Untersuchungen zur Theorie der Beleuchtung des Mondes auf Grund photometrischer Messungen," *Acta Soc. Sci. Fennicae*, Vol. 50, pp. 1-70.

[123] V. G. Fesenkov, 1929. "Photometric Investigations of the Lunar Surface," *Astronomicheskii Zhurnal*, Vol. 5, pp. 219-234. Translated by Redstone Scientific Information Center, April 1968.

[124] M. Minnaert, 1941. "The Reciprocity Principle in Lunar Photometry," *Astrophysical Journal*, Vol. 93, pp. 403-410.

[125] V. A. Fedoretz, 1952. "Photographic Photometry of the Lunar Surface," *Publ. Kharkov Obs.*, Vol. 2, pp. 49-172.

[126] M. Minnaert, 1961. "Photometry of the Moon," in *Planets and Satellites*, G. P. Kuiper, and B. M. Middlehurst, (Editors) Univ. Chicago Press. Vol. 3, ch. 6, pp. 213-248.

[127] V. Fesenkov, 1962. "Photometry of the Moon," in *Physics and Astronomy of the Moon*, Z. Kopal, Ed. New York: Academic Press. pp. 99-130.

[128] B. W. Hapke, 1963. "A Theoretical Photometric Function for the Lunar Surface," *Journal of Geophysical Research*, Vol. 68, No. 15, August, pp. 4571-4586.

[129] B. Hapke, and H. Van Horn, 1963. "Photometric Studies of Complex Surfaces, with Applications to the Moon," *Journal of Geographical Research*, Vol. 68, No. 15, August, pp. 4545-4570.

[130] B. Hapke, 1966. "An Improved Theoretical Lunar Photometric Function," *The Astronomical Journal*, Vol. 71, No. 5, June, pp. 333-339.

[131] W. E. Middleton, and A. G. Mungall, 1952. "The Luminous Directional Reflectance of Snow," *Journal of the Optical Society of America*, Vol. 42, No. 3, pp. 572-579.

[132] M. Planck, 1959. *The Theory of Heat Radiation*, New York: Dover.

[133] P. Beckmann, and A. Spizzichnio, 1963. *The Scattering of Electromagnetic Waves from Rough Surfaces*, New York: Pergamon Press.

[134] K. E. Torrance, E. M. Sparrow, and R. C. Birkebak, 1966. "Polarization, Directional Distribution, and Off-specular Peak Phenomena in Light Reflected from Roughened Surfaces," *Journal of the Optical Society of America*, Vol. 56, No. 7, July, pp. 916-925.

[135] K. E. Torrance, and E. M. Sparrow, 1967. "Theory for Off-specular Reflection from Roughened Surfaces," *Journal of the Optical Society of America*, Vol. 57, No. 9, September, pp. 1105-1114.

[136] T. S. Trowbridge, and K. P. Reitz, 1965. "Average irregularity representation of a rough surface for ray reflection," *Journal of the Optical Society of America*, Vol. 65, No. 5, May, pp. 531-536.

[137] B. K. P. Horn, 1975. "Determining Shape from Shading," in *The Psychology of Computer Vision*, P. H. Winston, Ed. New York: McGraw-Hill, ch. 4.

[138] B. K. P. Horn, 1977. "Understanding Image Intensities," *Artificial Intelligence*, Vol. 8, No. 11, pp. 201-231.

[139] B. K. P. Horn, and B. L. Bachman, 1978. "Using Synthetic Images to Register Real Images with Surface Models," *Communications of the A.C.M.*, Vol. 21, No. 11, November, pp. 914-924.

[140] B. K. P. Horn, and R. W. Sjoberg, 1979. "Calculating the Reflectance Map," *Applied Optics*, Vol. 18, No. 11, June, pp. 1770-1779.

[141] R. J. Woodham, 1978. "Photometric Stereo: A reflectance map technique for determining surface orientation from image intensity," *Image Understanding Systems and Industrial Applications*, in *Proc. S.P.I.E.*, Vol. 155 August.

[142] F. E. Nicodemus, J. C. Richmond, and J. J. Hsia, I. W. Ginsberg, T. Limperis, 1977. "Geometrical Considerations and Nomenclature for Reflectance," *NBS Monograph 160*, National Bureau of Standards, U. S. Department of Commerce, Washington, D. C., October.

[143] F. E. Nicodemus, (Editor) 1976, 1977 & 1978. "Self-Study Manual on Optical Radiation Measurements," *NBS Technical Notes 910-1, 910-2 & 910-3*, National Bureau of Standards, U. S. Department of Commerce, Washington, D. C.

[144] H. C. Babcock, 1970. "Evaluation of a Stereocompilation Digitizer," in *Congress on Surveying and Mapping*, 30th Annual Meeting, pp. 338-347.

[145] E. J. McCartney, 1976. *Optics of the Atmosphere: Scattering by Molecules and Particles*, New York: John Wiley.

[146] S. D. Conte, and C. de Boor, 1972. *Elementary Numerical Analysis*, New York: McGraw-Hill.

[147] R. W. Hamming, 1962. *Numerical Methods for Scientists and Engineers*, New York: McGraw-Hill.

[148] R. D. Richtmeyer, and K. W. Morton, 1967. *Difference Methods for Initial-Value Problems*, New York: John Wiley, pp. 136-143.

[149] F. B. Hildebrand, 1956, 1974. *Introduction to Numerical Analysis*, New York: McGraw-Hill.

[150] P. M. Bridge, and J. L. Inge, 1972. "Shaded Relief of Mars," Atlas of Mars, MH 25 M IR, JPL Contract WO-8122, USGS, Department of the Interior.

[151] T. Rindfleisch, 1966. "Photometric Method for Lunar Topography," *Photogrammetric Engineering*, Vol. 32, pp. 262-276.

[152] W. Bantel, 1973. "Der Reproduktionsweg vom einfarbigen Relieforiginal zur mehrfarbigen Reliefkarte," *International Yearbook of Cartography*, Vol. 13, pp. 134-136.

[153] A. DeLucis, 1971. "The effect of shaded relief terrain representation on map information accessibility," in *American Congress on Surveying and Mapping*, 31st Annual Meeting, Washington, D.C., pp. 641-657.

[154] J. Neumann, 1973. "Begriffsgeschichte und Definition des Begriffes 'Kartographische Generalisierung'," *International Yearbook of Cartography*, Vol. 13, pp. 59-67.

[155] F. Topfer, (Editor) 1974. *Kartographische Generalisierung*, Geographisch-Kartographische Anstalt, Gotha, Leipzig.